

TARGET PARAMETER ESTIMATION IN MIMO RADARS

BY

HUSSAIN ALI

A Dissertation Presented to the
DEANSHIP OF GRADUATE STUDIES

KING FAHD UNIVERSITY OF PETROLEUM & MINERALS

DHAHRAN, SAUDI ARABIA

In Partial Fulfillment of the
Requirements for the Degree of

DOCTOR OF PHILOSOPHY

In

ELECTRICAL ENGINEERING

DECEMBER 2017


KING FAHD UNIVERSITY OF PETROLEUM & MINERALS
DHAHRAN 31261, SAUDI ARABIA

DEANSHIP OF GRADUATE STUDIES

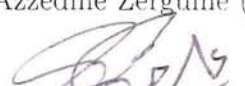
This thesis, written by **HUSSAIN ALI** under the direction of his thesis adviser and approved by his thesis committee, has been presented to and accepted by the Dean of Graduate Studies, in partial fulfillment of the requirements for the degree of **DOCTOR OF PHILOSOPHY IN ELECTRICAL ENGINEERING**.

Dissertation Committee



Dr. Mohammiad S. Sharawi (Adviser)



Dr. Tareq Y. Al-Naffouri (Co-adviser)


Dr. Azzedine Zerguine (Member)


Dr. Ali Muqaibel (Member)


Dr. Samir Al-Ghathban (Member)


Dr. Ali A. Al-Shaikhi
Department Chairman


Dr. Salam A. Zummo
Dean of Graduate Studies


Date 8/1/13



©Hussain Ali
2017

To the loving memories of my Father, Mother, Wife and Taha

ACKNOWLEDGMENTS

In the name of Allah (the One and the Only Creator of everything), the most Gracious and the most Merciful. All praise be to Allah for his guidance and limitless blessings. I pray to Allah to guide me on the right path.

First and foremost gratitude to my adviser, Prof. Tareq Y. Al-Naffouri at King Abdullah University of Sciences and Technology (KAUST). His mentorship and guidance will serve as a life experience and a beacon for my future. His patience and understanding are the key factors in my accomplishments. The learning that I accomplished from his theoretical experience is priceless.

I would like to express my gratitude to Prof. Sajid Ahmed at KAUST for his supervision in the majority of this work. There is no doubt that without his help this task could not be accomplished. His guidance throughout this work was an excellent and fruitful learning experience.

My gratitude also goes to Prof. Mohammad S. Sharawi at KFUPM for reviewing and improving all of my work. I would like to thank his research group (Antennas and Microwave Structure Design) for their useful discussions and valuable comments.

I will never forget to mention my gratitude to Prof. Maan A. Kousa at KFUPM

who is my thesis adviser in master's degree. His mentorship provided me a solid platform to expand my research. I enjoyed his company throughout my stay at KFUPM. His guidance and help improved my teaching skills and provided me with direction in hard times during the complete academic phase.

I would also like to thank Dr. Tarig Ahmed and Prof. Slim Alouini, my collaborators at KAUST for valuable comments.

My appreciation goes to the committee members for reading my dissertation in a short time.

I would like to thank the Deanship of Graduate Studies at KFUPM for granting me scholarship for graduate studies at KFUPM. I would like to appreciate the faculty at Electrical Engineering Department, KFUPM for imparting quality learning.

There are always times that one needs friends who also add a memorable experience to life. No matter what is the work load, my friends always helped me and I always found their company. I would like to thank Umar Khan, Omer Bin Sohail, Noman Zafar, Waqas Afzal, Naveed Iqbal, Ali Qureshi, Asim Ghalib and many more I forgot to mention.

Finally, I thank my father and mother who are always there to provide help, guidance and pray for my success. I cannot express my gratitude to them in words. Also, I would like to thank my wife for the moral support she provided and my loving son, Taha.

TABLE OF CONTENTS

ACKNOWLEDGEMENT	iii
LIST OF TABLES	ix
LIST OF FIGURES	x
LIST OF SYMBOLS	xiii
ABSTRACT (ENGLISH)	xv
ABSTRACT (ARABIC)	xviii
CHAPTER 1 INTRODUCTION	1
1.1 MIMO Radar	2
1.1.1 Monostatic MIMO Radar	3
1.1.2 Bistatic MIMO Radar	4
1.2 Compressive Sensing	6
1.2.1 On-grid CS	7
1.2.2 Off-grid CS	8
1.3 Compressive Sensing in MIMO Radar	10
1.3.1 On-grid targets	10
1.3.2 Off-grid targets	11
1.4 Thesis Statement	11
1.5 Overview of Contributions	11

CHAPTER 2	TARGET PARAMETER ESTIMATION IN MIMO	
	RADARS USING COMPRESSIVE SENSING	14
2.1	Introduction	15
2.1.1	Organization of the Chapter	17
2.1.2	Support Agnostic Bayesian Matching Pursuit	18
2.2	Signal Model	20
2.3	CS for Target Parameter Estimation	22
2.3.1	Spatial Formulation	22
2.3.2	Temporal Formulation	26
2.4	Cramér Rao Lower Bound	28
2.4.1	CRLB for known ϕ_k	28
2.4.2	CRLB for unknown ϕ_k	30
2.5	Simulation Results	31
2.5.1	CS Spatial Formulation	32
2.5.2	CS Temporal Formulation	37
2.6	Conclusion	44
CHAPTER 3	MPDR-BASED REDUCED COMPLEXITY DOA	
	AND DOD ESTIMATION FOR MOVING TARGET IN BISTATIC	
	MIMO RADAR	45
3.1	Introduction	46
3.1.1	Organization of the Chapter	50
3.2	Signal Model	51
3.3	MPDR-based Reduced Dimension Estimation	53
3.4	Reduced Complexity FFT-based Solution	59
3.4.1	Evaluation of Three-Dimensional Terms by FFT	60
3.4.2	Evaluation of Two-Dimensional Terms by FFT	63
3.4.3	Evaluation of One-Dimensional Terms by FFT	63
3.4.4	Algorithms	63
3.5	Complexity Analysis	64

3.6	Simulation Results and Discussion	66
3.6.1	Static Target Comparison	67
3.6.2	MSE Performance of ϕ_k Estimation	67
3.6.3	MSE Performance of θ_k Estimation	69
3.6.4	MSE Performance of f_{d_k} Estimation	69
3.6.5	Complexity Comparison	70
3.7	Concluding Remarks	71
3.8	APPENDIX A: Proof of Equation (3.18)	72
3.9	APPENDIX B: Proof of Equation (3.38)	73

CHAPTER 4 APES-BASED REDUCED COMPLEXITY DOA AND DOD ESTIMATION FOR MOVING TARGET IN BISTATIC MIMO RADAR 76

4.1	Introduction	76
4.1.1	Organization of the Chapter	77
4.2	APES-based Reduced Dimension Estimation	78
4.3	Reduced Complexity FFT-based Solution	83
4.3.1	Evaluation of Three-Dimensional Terms by FFT	83
4.3.2	Evaluation of two-dimensional terms by FFT	86
4.3.3	Evaluation of one-dimensional terms by FFT	86
4.3.4	Algorithms	87
4.4	Complexity Analysis	87
4.5	Cramér-Rao Lower Bound	89
4.5.1	CRLB for Static Target	90
4.5.2	CRLB for Moving Target	92
4.6	Simulation Results and Discussion	93
4.6.1	MSE Performance of ϕ_k Estimation	94
4.6.2	MSE Performance of θ_k Estimation	95
4.6.3	MSE Performance of f_{d_k} Estimation	95
4.6.4	Complexity Comparison	96

4.7	Concluding Remarks	98
CHAPTER 5 DOA ESTIMATION BY REGULARIZED LEAST-		
	SQUARES	99
5.1	Introduction	100
5.1.1	Organization of the Chapter	101
5.1.2	Regularized Least-Squares	101
5.2	Problem Formulation	103
5.3	DOA estimation by RLS	106
5.4	Simulation Results	108
5.5	Concluding Remarks	111
CHAPTER 6 CONCLUSIONS AND FUTURE WORK		112
6.1	Concluding Remarks	112
6.2	Future Work	113
REFERENCES		115
VITAE		129
LIST OF PUBLICATIONS		130

LIST OF TABLES

3.1	MPDR-based low complexity proposed algorithms	65
3.2	Complexity comparison.	71
4.1	APES-based Low complexity proposed algorithm	88
4.2	Complexity comparison	97
5.1	DOA estimation by RLS	108
5.2	Complexity comparison.	110

LIST OF FIGURES

2.1	Colocated MIMO radar setup.	20
2.2	MSE performance for β_k estimation. Simulation parameters: $L = 20$, $n_T = 16$, $n_R = 16$, $N = 512$, $\phi_k \sim \mathcal{U}(-60^\circ, 60^\circ)$ but on-grid, $\beta_k = e^{j\varphi_k}$ where $\varphi_k \sim \mathcal{U}(0, 1)$	32
2.3	MSE performance for ϕ_k estimation. Simulation parameters: $L = 20$, $n_T = 16$, $n_R = 16$, $N = 512$, $\phi_k \sim \mathcal{U}(-60^\circ, 60^\circ)$ but falling off-grid, $\beta_k = e^{j\varphi_k}$ where $\varphi_k \sim \mathcal{U}(0, 1)$	33
2.4	MSE performance for β_k estimation. Simulation parameters: $L = 10$, $n_T = 128$, $n_R = 128$, $N = 512$, $\phi_k \sim \mathcal{U}(-60^\circ, 60^\circ)$ but on-grid, $\beta_k = e^{j\varphi_k}$ where $\varphi_k \sim \mathcal{U}(0, 1)$. No recovery for Capon and APES methods.	35
2.5	MSE performance for ϕ_k estimation. Simulation parameters: $L = 10$, $n_T = 128$, $n_R = 128$, $N = 512$, $\phi_k \sim \mathcal{U}(-60^\circ, 60^\circ)$ but falling off-grid, $\beta_k = e^{j\varphi_k}$ where $\varphi_k \sim \mathcal{U}(0, 1)$. No recovery for Capon and APES methods.	35
2.6	Complexity comparison. Simulation parameters: $n_T = n_R$, SNR = 20 dB, $\phi_k \sim \mathcal{U}(-60^\circ, 60^\circ)$ but on-grid, $\beta_k = e^{j\varphi_k}$ where $\varphi_k \sim \mathcal{U}(0, 1)$	36
2.7	Resolution comparison. Simulation parameters: $L = 256$, $n_T = 10$, $n_R = 10$, SNR = 0 dB (left), SNR = 25 dB (right). CS algorithm used is SABMP.	37
2.8	MSE performance for β_k estimation. Simulation parameters: $L = 256$, $n_T = 10$, $n_R = 10$, $N = 512$, $\phi_k \sim \mathcal{U}(-60^\circ, 60^\circ)$ but on-grid, $\beta_k = e^{j\varphi_k}$ where $\varphi_k \sim \mathcal{U}(0, 1)$	38

2.9	MSE performance for ϕ_k estimation. Simulation parameters: $L = 256$, $n_T = 10$, $n_R = 10$, $N = 512$, $\phi_k \sim \mathcal{U}(-60^\circ, 60^\circ)$ but falling off-grid, $\beta_k = e^{j\varphi_k}$ where $\varphi_k \sim \mathcal{U}(0, 1)$	39
2.10	MSE performance for β_k estimation. Simulation parameters: $L = 8$, $n_T = 10$, $n_R = 10$, $N = 512$, $\phi_k \sim \mathcal{U}(-60^\circ, 60^\circ)$ but on-grid, $\beta_k = e^{j\varphi_k}$ where $\varphi_k \sim \mathcal{U}(0, 1)$. No recovery for Capon and APES methods.	40
2.11	MSE performance for ϕ_k estimation. Simulation parameters: $L = 8$, $n_T = 10$, $n_R = 10$, $N = 512$, $\phi_k \sim \mathcal{U}(-60^\circ, 60^\circ)$ but falling off-grid, $\beta_k = e^{j\varphi_k}$ where $\varphi_k \sim \mathcal{U}(0, 1)$. No recovery for Capon and APES methods.	41
2.12	MSE performance for β_k estimation. Simulation parameters: $L = 256$, $n_T = 10$, $n_R = 10$, $N = 512$, $\phi_k = 5^\circ$ (solid lines) & $\phi_k = 70^\circ$ (dashed lines) but on-grid, $\beta_k = e^{j\varphi_k}$ where $\varphi_k \sim \mathcal{U}(0, 1)$ and is same for all iterations.	42
2.13	MSE performance for ϕ_k estimation. Simulation parameters: $L = 256$, $n_T = 10$, $n_R = 10$, $N = 512$, $\phi_k = 5^\circ$ (solid lines) & $\phi_k = 70^\circ$ (dashed lines) but falling off-grid, $\beta_k = e^{j\varphi_k}$ where $\varphi_k \sim \mathcal{U}(0, 1)$ and is same for all iterations.	43
2.14	Complexity comparison. Simulation parameters: $L = 256$, $n_T = 10$, $n_R = 10$, $\text{SNR} = 20$ dB, $\phi_k \sim \mathcal{U}(-60^\circ, 60^\circ)$ but on-grid, $\beta_k = e^{j\varphi_k}$ where $\varphi_k \sim \mathcal{U}(0, 1)$	43
2.15	ROC comparison. Simulation parameters: $n_T = 10$, $n_R = 10$, $\text{SNR} = -12$ dB, $\phi_k \sim \mathcal{U}(-60^\circ, 60^\circ)$ but on-grid, $\beta_k = e^{j\varphi_k}$ where $\varphi_k \sim \mathcal{U}(0, 1)$. (Markers are added in this plot only for the purpose of identification of different curves.)	44
3.1	Bistatic radar geometry.	52
3.2	MSE performance for DOA estimation ($\hat{\phi}_k$) using $J_1(\phi_k, \theta_k)$. Simulation parameters: $L = 256$, $n_T = 10$, $n_R = 10$	68

3.3	MSE performance for DOD estimation ($\hat{\theta}_k$) using $J_1(\phi_k, \theta_k)$. Simulation parameters: $L = 256, n_T = 10, n_R = 10$	68
3.4	MSE performance of DOA ϕ_k for moving target. Simulation parameters: $L = 64, n_T = 8, n_R = 8, K = 3$	69
3.5	MSE performance of DOD θ_k for moving target. Simulation parameters: $L = 64, n_T = 8, n_R = 8, K = 3$	70
3.6	MSE performance of Doppler f_{d_k} for moving target. Simulation parameters: $L = 64, n_T = 8, n_R = 8, K = 3$	70
4.1	MSE performance of DOA ϕ_k for moving target. Simulation parameters: $L = 64, n_T = 8, n_R = 8, K = 3$	95
4.2	MSE performance of DOD θ_k for moving target. Simulation parameters: $L = 64, n_T = 8, n_R = 8, K = 3$	96
4.3	MSE performance of Doppler f_{d_k} for moving target. Simulation parameters: $L = 64, n_T = 8, n_R = 8, K = 3$	96
5.1	RMSE performance. Simulation parameters: $N = 8, n_R = 10, K = 2$ uncorrelated sources.	109
5.2	RMSE performance. Simulation parameters: $N = 8, n_R = 10, K = 2$ coherent sources.	110

LIST OF SYMBOLS

\mathbf{x}	:	bold lower case letters denote vectors
\mathbf{X}	:	bold upper case letters denote matrices
\mathbf{x}^\top	:	transpose of a vector \mathbf{x}
\mathbf{X}^\top	:	transpose of a matrix \mathbf{X}
\mathbf{x}^*	:	complex conjugate of a vector \mathbf{x}
\mathbf{X}^*	:	complex conjugate of a matrix \mathbf{X}
\mathbf{x}^H	:	complex conjugate transpose of a vector \mathbf{x}
\mathbf{X}^H	:	complex conjugate transpose of a matrix \mathbf{X}
$x_m(n)$:	element of m -th row and n -th column in a matrix \mathbf{X}
$\ \cdot\ _2^2$:	squared two-norm of a vector
$\ \cdot\ _F^2$:	Frobenius norm of a matrix
$\mathbb{E}\{\cdot\}$:	statistical expectation
$\text{diag}\{a, b\}$:	diagonal matrix with diagonal entries a and b
$\text{diag}\{\mathbf{X}\}$:	vector with the diagonal entries of \mathbf{X}
$\text{diag}\{\mathbf{x}\}$:	a diagonal matrix with entries read from the vector \mathbf{x}
$\mathcal{F}\{\cdot\}$:	fast-Fourier-transform of a vector
$\mathcal{F}_r\{\cdot\}$:	row-by-row fast-Fourier-transform of a matrix
$\mathcal{F}_c\{\cdot\}$:	column-by-column fast-Fourier-transform of a matrix

\circ	: Hadamard product
\otimes	: Kronecker product
\circledast	: Khatri-Rao product
$\mathbf{X}^{\circ 2}$: Hadamard square
$\mathcal{O}(X)$: order of X
\mathfrak{X}	: bold calligraphic letters denote tensors of third-order
$\mathcal{R}(x)$: real part of x
$\mathcal{I}(x)$: imaginary part of x
β_k	: is the reflection coefficient or the path gain of k -th target
ϕ_k	: direction of arrival of k -th target at the receiver
θ_k	: direction of departure of k -th target at the transmitter
f_{d_k}	: is the Doppler shift of k -th target
L	: number of snapshots

THESIS ABSTRACT

NAME: Hussain Ali
TITLE OF STUDY: Target Parameter Estimation for MIMO Radars
MAJOR FIELD: Electrical Engineering
DATE OF DEGREE: DECEMBER 2017

Accurate target parameter estimation and localization with fine resolution is important in radar systems. In this thesis, target parameter estimation methods are proposed for multiple-input multiple-output (MIMO) radars. The two different categories of radars, monostatic and bistatic radars from signal processing perspective are addressed. The proposed algorithms are developed to reduce the computational complexity while keeping low mean-square error.

In the first part of the thesis, target parameter estimation methods in colocated MIMO radar are discussed. Conventional algorithms used for parameter estimation in colocated MIMO radars require the inversion of the covariance matrix of the received spatial samples. In these algorithms, the number of received snapshots should be at least equal to the size of the covariance matrix. For large size MIMO antenna arrays, the inversion of the covariance matrix becomes com-

putationally very expensive. Compressive sensing (CS) algorithms which do not require the inversion of the complete covariance matrix can be used for parameter estimation with fewer number of received snapshots. In this work, it is shown that the spatial formulation is best suitable for large MIMO arrays when CS algorithms are used. A temporal formulation is proposed which fits the CS algorithms framework, especially for small size MIMO arrays. The simulation results show the advantage of CS algorithm utilizing low number of snapshots and better parameter estimation for both small and large number of antenna elements.

In the second part of the thesis, we propose a reduced dimension and low complexity algorithm to estimate direction-of-arrival (DOA), direction-of-departure (DOD) and the Doppler shift of a moving target for a MIMO radar. We derive two cost functions based on two different objective functions. First, we solve each cost function with a low complexity FFT-based solution in three dimensions. We further carry out a derivation to reduce the three-dimensional search to two-dimensional search and solve it with a 2D-FFT. Another reduced dimension algorithm is derived using the generalized eigen value method which finds the estimate of unknown parameters in one dimension with less memory constraints. This way, we propose three algorithms based on the first cost function and another three algorithms based on the second. We show simulation results for a static target case and a moving target case. We compare the mean-square-error (MSE) performance and computational complexity of our proposed algorithms with existing algorithms as well. We show that our proposed algorithms have

better MSE performance than existing algorithms and achieves the Cramér-Rao lower bound (CRLB) for all unknown target parameters. The proposed algorithms exhibit lower computational complexity than the existing ones and also provide an estimate for the Doppler shift.

Finally, in the last part of the thesis, we discuss the application of regularized least-squares in DOA estimation. If the covariance matrix of received signal is rank deficient, then we cannot find the inverse of the covariance matrix. Regularized least-squares algorithms deal with ill-conditioned matrices and rank deficient matrices. In this part of the thesis, we solve the DOA problem by using regularized least-squares algorithms when the covariance matrix of received signal is rank deficient. The simulation results show that it can recover the unknown target locations when the covariance matrix of received signal is rank deficient.

مُلخّص الرسالة

الاسم الكامل: حسين علي

عنوان الدراسة: تقدير معامل الهدف في الرادارات متعددة المدخلات متعددة المخرجات

التخصص: هندسة كهربائية

تاريخ الدرجة العلمية: ديسمبر 2017

يعتبر التقدير الدقيق لمعامل الهدف وتحديد مكانه بجودة عالية من الاولويات المهمة في أنظمة الرادارات. في هذه الأطروحة، تم إقتراح أساليب لتقدير معامل الهدف للرادارات متعددة المدخلات متعددة المخرجات (MIMO-radars). وقد تم تناول نوعين من الرادارات من منظور معالجة الإشارات، هما الرادارات الأحادية والإزدواجية. ومن ثم طورت الخوارزميات المقترحة لتقليل التعقيد الحسابي مع الحفاظ على متوسط مربع خطأ منخفض.

في الجزء الأول من الأطروحة، يتم مناقشة أساليب تقدير معامل الهدف في رادارات MIMO المتحددة الموقع. في الواقع تتطلب الخوارزميات التقليدية المستخدمة لتقدير المعامل في هذه الرادارات عكس مصفوفة تباين العينات المكانية المستقبلية. في هذه الخوارزميات، يجب أن يكون عدد اللقطات المستقبلية مساويا على الأقل لحجم مصفوفة التباين. وبالنسبة لمصفوفات هوائيات MIMO الكبيرة الحجم، يصبح عكس مصفوفة التباين مكلفا جدا حسابيا. في المقابل فإن خوارزميات الاستشعار المقلص -التي لا تتطلب عكس كل مصفوفة التباين- يمكن استخدامها لتقدير معامل الهدف بعدد أقل من اللقطات المستقبلية. في هذا العمل، تم توضيح ان الصيغة المكانية هي أكثر موائمة لمصفوفات MIMO الكبيرة عند استخدام خوارزميات الاستشعار المقلص. وتم إقتراح صيغة زمانية تتواءم مع إطار خوارزميات الاستشعار المقلص، لا سيما لمصفوفات MIMO الصغيرة الحجم. وتظهر نتائج المحاكاة ميزة خوارزمية الاستشعار المقلص باستعمال عدد قليل من اللقطات وتقدير أفضل للمعامل لكل من العدد الصغير والكبير لعناصر الهوائي.

في الجزء الثاني من الرسالة نقتراح خوارزمية قليلة التعقيد والأبعاد لتقدير اتجاهي الذهاب والوصول ومقدار إزاحة (Doppler shift) هدف متحرك لرادار متعدد هوائيات الارسل والاستقبال. هذه الخوارزمية مبنية على استنتاج دالتي تكلفة تعتمدان على دالتي هدف مختلفتين. تم حل كل من دالتي التكلفة باستخدام طريقة (FFT-based) قليلة التعقيد حلا ثلاثي الأبعاد. ومن ثم تم تخفيض مجال البحث من ثلاثي الأبعاد لآخر ثنائي الأبعاد باستخدام (2D-FFT) و (generalized eigen value). تم اجراء المحاكاة للخوارزمية المقترحة لهدف ثابت وآخر متحرك وتم تقييم

أدائه وكفائته بحساب معدل الخطأ ومقارنته بالخوارزميات الموجودة. أظهرت نتائج البحث كفاءة الخوارزمية المقترحة من حيث معدل الخطأ وكفائته علاوة على قلة تعقيده مقارنة بالخوارزميات الأخرى.

وأخيراً، في الجزء الأخير من الرسالة، نناقش استخدام خوارزمية (regularized least-squares) في تقدير اتجاه الوصول (DOA) لقدرته على التعامل مع مصفوفة التباين للإشارة المستقبلية إذا كانت رتبته غير مكتملة و لا يمكن إيجاد معكوسها. وتبين النتائج أنه باستخدام هذا الخوارزمية يمكن تعيين موقع الهدف بدقة في حالة كون مصفوفة التباين غير مرنة (رتبته غير مكتملة).

CHAPTER 1

INTRODUCTION

Radars have both civilian and military applications and are used for the purpose of surveillance, collision avoidance of vehicles, earth resources monitoring and tracking of aircrafts and vehicles. The challenges in radar design is to reduce the data size, the operational complexity, the power consumption and the weight of radar equipment for ease of mobility. The key functions of a radar is to detect, localize, identify and track a possible target. In localizing a target, a radar engineer will be interested in finding its range, velocity (Doppler), direction of arrival (DOA) and maybe direction of departure (DOD). Interference introduced in the received signal of a radar include echos from the environment (also known as clutter), noise at the receiver, electromagnetic interference and possibly electronic counter measures or jamming signals.

Radars can be classified as active radars or passive radars based on the availability/non-availability of control on the transmitter, also termed as cooperative/non-cooperative transmitters in literature. In an active radar, the transmitted waveform is known a

priori at the receiver whereas no prior knowledge of transmitted signal is available in the passive radar receiver. Radars can also be classified based on the receiver location as monostatic radar in which the transmitter/receiver pair are colocated and bistatic radar where we have wide separation between the transmitter and the receiver. In this dissertation, our focus is mainly on the categories of monostatic MIMO radar and bistatic MIMO radar parameter estimation for target localization. The unknown parameters that need to be estimated are reflection coefficient, direction of arrival, direction of departure and Doppler shift associated with the target.

1.1 MIMO Radar

The theory of multiple-input multiple-output (MIMO) radars was motivated by MIMO antennas in wireless communication. Similar to MIMO communication systems, MIMO radars are equipped with antenna arrays at the transmitter and the receiver. MIMO radars are shown to have improved degrees of freedom and better resolution as compared to phased array ones [1]. MIMO radars also provide better target localization and flexibility of transmit beampattern designs [2], [3]. The antenna elements in the transmitter/receiver array can be closely spaced [4] allowing coherent processing of the received signals at the receiver array. MIMO radar can also be designed with widely separated transmitter/receiver antennas [5], also known as non-coherent MIMO radar.

1.1.1 Monostatic MIMO Radar

Colocated (monostatic) MIMO radars have been extensively studied in literature for surveillance applications [1], [2], [4], [6], [7] and references therein. The conventional phased array radar consists of a phased array antenna or electronically scanned antenna at the front end with each antenna element transmitting the phase shifted version of the same waveform to steer the transmit beam. Therefore, in phased array radar, the transmitted waveforms are fully correlated. In contrast, MIMO radar can be seen as an extension of phased array radar, where transmitted waveforms can be independent or partially correlated. Such waveforms yield extra degrees of freedom that can be exploited for better detection performance and resolution [4]. The received signal is processed coherently when the array elements are closely spaced at the receiver.

For monostatic MIMO radar, many parameter estimation algorithms have been studied to estimate the direction of arrival (DOA) and reflection coefficient which is proportional to the radar cross section, such as Capon [8], amplitude-and-phase estimation (APES) [9], Capon and APES (CAPES) [10], approximate maximum likelihood (AML) [11], Capon and approximate maximum likelihood (CAML) [6], iterative adaptive approach (IAA) [12] and its efficient implementation in [13] (further details can be found in [7], [14] and the references therein). Almost all of these algorithms require the inverse of the received samples covariance matrix. Therefore, for these algorithms to work, a reasonable number of snapshots are required so that the covariance matrix of the received signal matrix is full rank.

Furthermore, for large size antenna arrays, to invert the covariance matrix, large number of snapshots will be required and it will be computationally expensive. Moreover, MIMO radar beamforming has been addressed in [15], [16]. A low complexity algorithm is recently proposed for DOA estimation for colocated MIMO for moving target in [17], [18] where the Doppler and DOA are jointly estimated for both on and off-grid targets but it cannot work with rank deficient covariance matrices.

1.1.2 Bistatic MIMO Radar

Bistatic MIMO radar has the transmitter and receiver separated by large distances. Bistatic radar has some additional advantages over monostatic radar, such as better performance for target detection and covert operation [5]. The target localization in bistatic MIMO radar can be achieved by finding its DOA and DOD. The DOA and DOD are the same in colocated MIMO radar whereas in bistatic MIMO radar they are two different unknown parameters. Several algorithms have been proposed in literature for the estimation of these two unknown parameters in bistatic MIMO radars.

The DOA and DOD parameter estimation is a two-dimension search problem for static targets. The conventional estimation method of signal parameters via rotational invariance technique (ESPRIT) [19] for DOA and DOD estimation have been presented in [20]. The ESPRIT algorithm exploits the invariance property to convert the two-dimension search problem into two independent one-dimension

search problems but it requires pair matching between the estimates of transmit and receive angles. A low complexity ESPRIT algorithm which automatically performs the pair matching is proposed in [21]. Another scheme based on ESPRIT has been proposed in [22] for three transmitters only which is extended and generalized in [23] for any number of transmitters. The Cramér-Rao Bound (CRB) found in [22] was not derived completely in closed form rather it was found by finding and inverting the Fisher information matrix (FIM) and it was restricted to three transmitters.

The two-dimension multiple signal classification (2D-MUSIC) algorithm has better estimation performance for DOA and DOD estimation than ESPRIT methods but it is computationally expensive because it requires a two-dimensional search. In [24], a reduced-complexity multiple signal classification (RD-MUSIC) algorithm has been proposed which requires one-dimension search and its performance is very close to 2D-MUSIC with lower complexity. A joint DOA and DOD estimation by polynomial root finding technique was proposed in [25] which is shown to have lower computational complexity than 2D-MUSIC. Another estimation algorithm based on properties of Kronecker product is discussed in [26] whereas in [27] the DOA and DOD estimation problem for coherent targets was investigated. In [28], the Capon beamformer is used to improve parameter estimation but the presented method required two-dimensional computationally expensive search.

Another method for direction finding in bistatic MIMO radar was presented

in [29] that was based on the solution of a constrained minimization problem to find the directions which is a computationally expensive method. In [30], the non-circular characteristics of transmitted signals were exploited for DOA and DOD estimation in bistatic MIMO radar. Maximum likelihood estimation for DOA and DOD was discussed in [31]. CRB was also derived for two parameters, i.e. DOA and DOD, but assuming the target reflection coefficients as deterministic. In [32], a joint diagonalization based method for DOA and DOD has been proposed. CRB was also derived for DOA and DOD but assuming the target reflection coefficients as deterministic. The signal model used in most of the existing works was based on matched filtering with the transmitted signal and assumed that the covariance matrix of the transmitted signal is identity. The performance of DOA and DOD estimation using velocity sensors were investigated in [33], [34] and reduced complexity algorithms based on MUSIC were derived. The estimation problem for non-uniform array was investigated in [35]. The algorithm proposed in [36] was also based on ESPRIT and MUSIC. The joint 4-dimensional angle and Doppler shift estimation via tensor decomposition for MIMO array was proposed in [37].

1.2 Compressive Sensing

Compressive sensing (CS) is a technique that is used to recover information from sparse signals. The signal with incomplete information can be reconstructed by CS techniques. CS techniques can be classified as *on-grid CS* where the locations

of sparse entries are restricted to a finite grid and *off-grid CS* where the locations of sparse entries lie on a continuous interval. These two categories are discussed briefly as follows.

1.2.1 On-grid CS

CS [38], [39] is a technique that is used to recover information from signals that are sparse in some domain, using fewer measurements than required by Nyquist theory. According to the classical approach, a large number of samples are required to reconstruct a signal completely from a received version (Nyquist criteria). For higher data resolution, this constraint puts all the pressure on signal processing part and storage. Compressive sensing provides a solution to compress data and then reconstruct from under sampled signals.

Some efficient algorithms proposed, that fall in the category of greedy algorithms, include orthogonal matching pursuit(OMP) [40], regularized orthogonal matching pursuit (ROMP) [41], stagewise orthogonal matching pursuit (StOMP) [42] and compressive sampling matching pursuit (CoSaMP) [43]. There is another category of CS algorithms called Bayesian algorithms that assume the a priori statistics are known. These algorithms include sparse Bayes [44], Bayesian compressive sensing (BCS) [45] and the fast Bayesian matching pursuit (FBMP) [46]. Another reduced complexity algorithm based on the structure of sensing matrix is proposed in [47]. In addition to these algorithms, support agnostic Bayesian matching pursuit (SABMP) is proposed in [48] which assumes that the support

distribution is unknown and finds the Bayesian estimate for the sparse signal by utilizing noise statistics and sparsity rate.

1.2.2 Off-grid CS

The classical CS algorithms are discrete and require a grid. If there is any thing that is off-grid, the CS algorithms fails to recover. Recently, the problem of compressive off-grid has been solved in [49]–[51]. The work in [49], [51] is also called super resolution and is shown to recover the signal from sub-sampled measurements. Consider the following signal model

$$x = \sum_j a_j \delta_{t_j} \quad (1.1)$$

where $\{t_j\}$ are locations on a continuous interval $[0, 1]$ and δ_{t_j} is a spike at t_j with amplitude $a_j \in \mathcal{C}$. The measurements are $n = 2f_c + 1$ low-frequency coefficients given by

$$y(k) = \int_0^1 e^{-i2\pi kt} x(dt) \quad (1.2)$$

$$= \sum_j a_j e^{-i2\pi kt_j}, \quad k \in \mathcal{Z}, |k| \leq f_c \quad (1.3)$$

$$\mathbf{y} = \mathbf{F}_n \mathbf{x} \quad (1.4)$$

The equivalent problem of spectral estimation can be obtained by swapping time and frequency. Thus, for a signal $x(t)$

$$x(t) = \sum_j a_j e^{i2\pi\omega_j t}, \quad a_j \in \mathcal{C}, \omega_j \in [0, 1] \quad (1.5)$$

The problem is to recover the sparse \mathbf{x} from \mathbf{y} . The signal \mathbf{x} can be recovered by solving

$$\min \|\tilde{\mathbf{x}}\|_{\text{TV}} \quad \text{subject to} \quad \mathbf{F}_n \tilde{\mathbf{x}} = \mathbf{y} \quad (1.6)$$

The total variation norm is defined as

$$\|\mathbf{x}\|_{\text{TV}} = \int |\mathbf{x}(dt)| \quad (1.7)$$

which is the continuous analog of the ℓ_1 -norm. Equation (1.6) is the primal solution for which the solution is not straightforward. Therefore, the problem is solved by finding it's dual. The semidefinite program to solve the dual program is available along with [51].

Super resolution CS with prior information is presented in [52], [53]. To solve for more than one measurement vector with common sparse location, the multiple measurement vectors (MMV) version of the off-grid CS appeared in [54].

1.3 Compressive Sensing in MIMO Radar

1.3.1 On-grid targets

Generally, target detection in radars requires a finite grid and is assumed that the target lies on the grid. To lower the probability of miss, the grid should be fine enough. Most of the literature existing on MIMO radar assumes that the target lies on the grid. With this assumption, on-grid CS algorithms can be used with application to MIMO radar. To estimate the reflection coefficient and location angle of the target, the MIMO radar problem can be formulated as a sparse estimation problem, which allows us to use existing CS algorithms. It has been shown in [55]–[57] that the MIMO radar problem can be seen as an ℓ_1 -norm minimization problem. In DOA estimation, a discretized grid is selected to search all possible DOA estimates. The grid is equal to the search points in the angle domain of MIMO radar. The complexity of the CS method developed for MIMO radar in [56] grows with the size of the grid for higher resolution. In [57], the minimization problem is solved based on the covariance matrix estimation approach which requires large number of snapshots. The work published in [58] provides a CS based estimation but does not provide a fast parameter estimation algorithm and assumes that the number of targets, sparsity rate and noise variance are known.

1.3.2 Off-grid targets

As previously mentioned, most of the CS based parameter estimation methods discussed in literature assumes that the targets lie on the grid. Super resolution theory developed in [49] was extended to MIMO array in [59] which solves the off-grid estimation problem by convex optimization semi-definite programming (SDP) but are computationally expensive. Some recent work in off-grid CS includes [60]–[62]. The work proposed in [63] addresses the pulsed-Doppler radar parameter estimation using CS which has a different signal model than MIMO radar. In [64], off-grid DOA is estimated using sparse Bayesian inference where the number of sources or targets is assumed to be known.

1.4 Thesis Statement

The problem statement of this thesis is to address the problem of target parameter estimation, in particular MIMO radars. The main objective of the thesis is to address the target parameter estimation problem from signal processing perspective. Apart from the existing algorithms, we develop low complexity algorithms with near optimal performance.

1.5 Overview of Contributions

Several contributions have been achieved in this work, specifically

1. In Chapter 2, we present colocated MIMO radar setup. We use CS algo-

rithms to find the DOA. We discuss the performance of CS algorithms in temporal and spatial formulations. The proposed formulation works with low number of snapshots and have fine resolution.

2. In Chapter 3, we propose reduced complexity algorithms for DOA and DOD estimation for a moving target. In that Chapter, we develop algorithms based on minimum-power distortionless response of the received signal and derive the cost function to minimize the mean-square error (MSE). The three-dimensional problem obtained by solving the cost function is simplified to two-dimensional and one-dimensional problems. The proposed algorithms have low computational time because they are based on fast-Fourier transform.
3. In Chapter 4, we propose reduced complexity algorithm for DOA and DOD estimation for moving target with amplitude and phase estimation formulation. We also derive Cramer-Rao lower bound (CRLB) for the discussed signal model. The algorithms are compared against the existing algorithms as well as CRLB. It is shown that the proposed algorithms have near optimal performance close to CRLB. Their computational complexity is also shown to be lower than existing algorithms.
4. In Chapter 5, we address the rank deficiency problem of covariance matrix of received signal in DOA estimation problem. We discuss the use of regularized least-squares (RLS) algorithms for DOA problem with rank deficient covariance matrix. It is shown that the proposed method using RLS

algorithm can recover DOAs from multiple sources.

CHAPTER 2

TARGET PARAMETER ESTIMATION IN MIMO RADARS USING COMPRESSIVE SENSING

Conventional algorithms used for parameter estimation in colocated multiple-input-multiple-output (MIMO) radars require the inversion of the covariance matrix of the received spatial samples. In these algorithms, the number of received snapshots should be at least equal to the size of the covariance matrix. For large size MIMO antenna arrays, the inversion of the covariance matrix becomes computationally very expensive. Compressive sensing (CS) algorithms which do not require the inversion of the complete covariance matrix can be used for parameter estimation with fewer number of received snapshots. In this chapter, it is

shown that the spatial formulation is best suitable for large MIMO arrays when CS algorithms are used. A temporal formulation is proposed which fits the CS algorithms framework, especially for small size MIMO arrays. A recently proposed low-complexity CS algorithm named support agnostic Bayesian matching pursuit (SABMP) is used to estimate target parameters for both spatial and temporal formulations for the unknown number of targets. The simulation results show the advantage of SABMP algorithm utilizing low number of snapshots and better parameter estimation for both small and large number of antenna elements. Moreover, it is shown by simulations that SABMP is more effective than other existing algorithms at high signal-to-noise ratio (SNR).

2.1 Introduction

Colocated multiple-input-multiple-output (MIMO) radars have been extensively studied in literature for surveillance applications. In phased array radars, each antenna transmits the phase shifted version of the same waveform to steer the transmit beam. Therefore, in phased array radars, the transmitted waveforms at each antenna element are sufficiently correlated resulting in a single beamformed waveform. In contrast, MIMO radar can be seen as an extension of phased array radar, where transmitted waveforms can be independent or partially correlated. Such waveforms yield extra degrees of freedom that can be exploited for better detection performance and resolution and to achieve desired beam patterns achieving uniform transmit energy in the desired direction.

The target parameters to be estimated are the reflection coefficients (path gains) and location of the target. To estimate the reflection coefficient and the location angle of the target, existing CS algorithms can be utilized by formulating the MIMO radar parameter estimation problem as a sparse estimation one. It is shown in [55]–[57] that the MIMO radar problem can be seen as an ℓ_1 -norm minimization problem. In DOA estimation, a discretized grid is selected to search all possible DOA estimates. The grid is equal to the search points in the angle domain of MIMO radar. The complexity of the CS method developed in [56] grows with the size of the discretized grid. In [57], the minimization problem is solved based on the covariance matrix estimation approach which requires a large number of snapshots. The work in [58] does not provide a fast parameter estimation algorithm and assumes that the number of targets, sparsity rate, and noise variance are known. The authors in [65] have used CVX (a package to solve convex problems) to solve the minimization problem obtained by CS formulation of MIMO radar. The solution of CS problems by CVX is computationally expensive for large angle grids. In [64], off-grid DOA is estimated using sparse Bayesian inference where the number of sources or targets is assumed to be known. An off-grid CS algorithm called adaptive matching pursuit with constrained total least squares is proposed in [66] with application to DOA estimation. Another algorithm based on iterative recovery of off-grid target is proposed in [17], [18]. For recent developments that are useful in off-grid recovery, please see [67] and references therein.

In this chapter, our contribution is two-fold. First, we solve the spatial formulation for parameter estimation by SABMP for on-grid targets assuming that the number of targets and noise variance are unknown. Second, we solve an alternative temporal formulation to find estimates for the unknown parameters. We also make comparisons of mean-square error (MSE) and complexity of our work with the existing conventional algorithms. Specifically, the advantages of using a CS based algorithm are as follows:

1. The spatial formulation can recover the unknown parameters when the number of snapshots is less than the number of receiving antennas.
2. The proposed approach for parameter estimation is capable of estimating unknown parameters even away from the broadside of the beam pattern.
3. The recovery of the reflection coefficient in CS temporal formulation using SABMP is better than Capon, APES and CoSaMP algorithms.
4. The complexity of SABMP algorithm is not much effected by the number of receive antenna elements in the spatial formulation.

2.1.1 Organization of the Chapter

The rest of the chapter is organized as follows: In Section 2.2, the signal model for MIMO radar DOA problem is formulated. In Section 2.3, the system model is reformulated in a CS environment for on-grid parameter estimation along with the spatial and temporal formulations for large and small arrays (Section 2.3.1

& 2.3.2) respectively. In Section 2.4, we show the derivation for the Cramér Rao lower bound (CRLB). The simulation results are discussed in Section 2.5 and the chapter is concluded in Section 2.6.

2.1.2 Support Agnostic Bayesian Matching Pursuit

CS technique is used to recover information from signals that are sparse in some domain, using fewer measurements than required by Nyquist theory. Let $\mathbf{x} \in \mathcal{C}^N$ be a sparse signal which consists of K non-zero coefficients in an N -dimensional space where $K \ll N$. If $\mathbf{y} \in \mathcal{C}^M$ be the observation vector with $M \ll N$, then the CS problem can be formulated as

$$\mathbf{y} = \Phi \mathbf{x} + \mathbf{z} \quad (2.1)$$

where $\Phi \in \mathcal{C}^{M \times N}$ is referred to as sensing matrix and $\mathbf{z} \in \mathcal{C}^M$ is complex additive white Gaussian noise, $\mathcal{CN}(\mathbf{0}, \sigma_z^2 \mathbf{I}_M)$. The theoretical way to reconstruct \mathbf{x} is to solve an ℓ_0 -norm minimization problem when it is known a priori that the signal \mathbf{x} is sparse and measurements are noise free, i.e.,

$$\min \|\mathbf{x}\|_0, \quad \text{subject to} \quad \mathbf{y} = \Phi \mathbf{x}. \quad (2.2)$$

Solving the ℓ_0 -norm minimization problem is NP-hard problem and requires exhaustive search to find the solution. Therefore, a more tractable solution [68] is

to minimize the ℓ_1 -norm with a relaxed constraint, i.e.

$$\min \|\mathbf{x}\|_1, \quad \text{subject to} \quad \|\mathbf{y} - \Phi\mathbf{x}\|_2 \leq \delta, \quad (2.3)$$

where $\delta = \sqrt{\sigma_{\mathbf{z}}^2(M + \sqrt{2M})}$. ℓ_1 -norm minimization problem reduces to a linear program known as basis pursuit.

SABMP algorithm [48] is a Bayesian algorithm which provides robust sparse reconstruction. As discussed in [48], Bayesian estimation finds the estimate of \mathbf{x} by solving the conditional expectation

$$\hat{\mathbf{x}} = \mathbb{E} [\mathbf{x}|\mathbf{y}] = \sum_{\mathcal{S}} p(\mathcal{S}|\mathbf{y}) \mathbb{E} [\mathbf{x}|\mathbf{y}, \mathcal{S}] \quad (2.4)$$

where \mathcal{S} denotes the support set which contains the location of non-zero entries and $p(\mathcal{S}|\mathbf{y})$ is the probability of \mathcal{S} given \mathbf{y} which is found by evaluating Bayes rule. In SABMP algorithm, the support set \mathcal{S} is found by greedy approach. Once the support set \mathcal{S} is known, the best linear unbiased estimator is found using \mathbf{y} to estimate \mathbf{x} . SABMP algorithm, like other Bayesian algorithms, utilizes statistics of noise and sparsity rate. SABMP algorithm assumes prior Gaussian statistics of the additive noise and the sparsity rate. The estimates of noise variance and sparsity rate need not to be known rather SABMP algorithm estimates them in a robust manner. The statistics of locations of non-zero coefficients or signal support are assumed either non-Gaussian or unknown. Hence, it is agnostic to the support distribution. SABMP is a low complexity algorithm as it searches for the

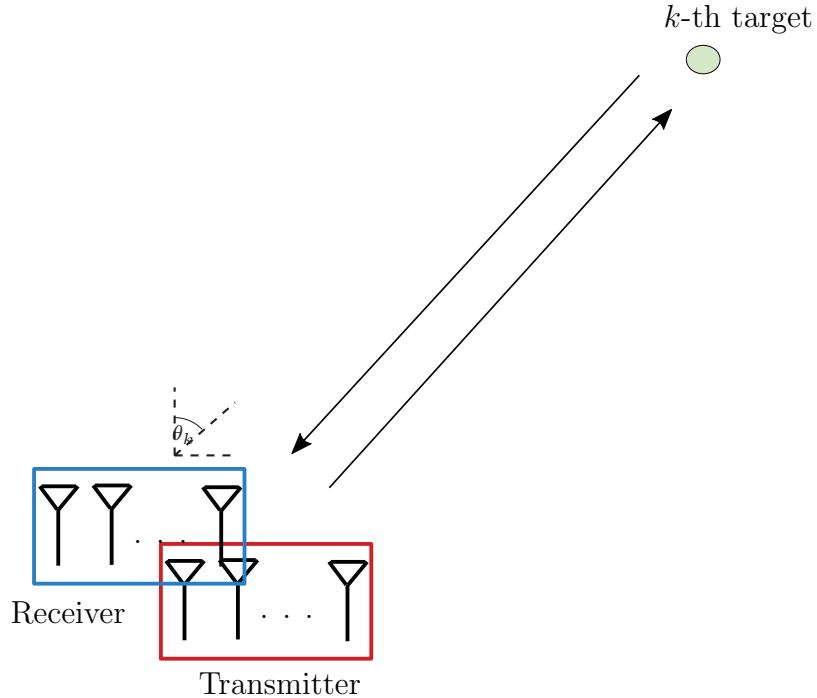


Figure 2.1: Colocated MIMO radar setup.

solution in a greedy manner. The matrix inversion involved in the calculations is done in an order-recursive manner which leads to further reduction in complexity.

2.2 Signal Model

We focus on a colocated MIMO radar setup as illustrated in Fig. 2.1. In colocated MIMO radar, the transmitting antenna elements in the transmitter and the receiving antenna elements in the receiver are closely spaced. Both the transmitter and receiver are closely spaced too in a monostatic configuration. In the monostatic configuration, the transmitter and receiver see the same aspects of a target. In other words, the distance between the target and transmitter/receiver is large enough that the distance between transmitter and receiver becomes insignif-

icant. Consider a MIMO radar system of n_T transmit and n_R receive antenna elements. The antenna arrays at the transmitter and receiver are uniform and linear, the inter-element-spacing between any two adjacent antennas is half of the transmitted signal wavelength, and there are K possible targets located at angles $\phi_k \in [\phi_1, \phi_2, \dots, \phi_K]$. Let $\mathbf{s}(n)$ denote the vector of transmitted symbols which are uncorrelated quadrature phase shift keying (QPSK) sequences. If $\mathbf{z}(n)$ denotes the vector of circularly symmetric white Gaussian noise samples at n_R receive antennas at time index n , the vector of baseband samples at all n_R receive antennas can be written as [4]

$$\mathbf{y}(n) = \sum_{k=1}^K \beta_k(\phi_k) \mathbf{a}_R(\phi_k) \mathbf{a}_T^T(\phi_k) \mathbf{s}(n) + \mathbf{z}(n), \quad (2.5)$$

where $(.)^T$ denotes the transpose, β_k denotes the reflection coefficient of the k -th target at location angle ϕ_k , while $\mathbf{a}_T(\phi_k) = [1, e^{i\pi \sin(\phi_k)}, \dots, e^{i\pi(n_T-1)\sin(\phi_k)}]^T$ and $\mathbf{a}_R(\phi_k) = [1, e^{i\pi \sin(\phi_k)}, \dots, e^{i\pi(n_R-1)\sin(\phi_k)}]^T$ respectively denote the transmit and receive steering vectors. We have assumed $\mathbf{z}(n)$ as uncorrelated noise. A correlated noise model can be found in [69]. We are interested in estimating the two parameters: DOA represented by ϕ_k and reflection coefficient β_k which is proportional to the radar cross section (RCS) of the target. It is assumed that the targets are in the same range bins.

The reflection coefficient gives us a measure of how much the energy is reflected back from the target. In the received signal model of (2.5), the reflection coefficient denoted by β_k for k -th target can be represented by a complex number. It is

observed that large size targets (such as ships) have high value of β whereas the small size target have low value of β_k . The value of β_k is proportional to RCS which characterizes the target. (In this Chapter, we assume $\beta_k = e^{i\varphi}$ where $\varphi \sim \mathcal{U}(0, 1)$ for simplicity of simulations. The amplitude of β_k is assumed to be 1 but for more practical scenarios it can be anything.)

2.3 CS for Target Parameter Estimation

CS formulation for target parameter estimation can be done in two different ways. First, via spatial formulation in which the samples at all antennas constitute a measurement vector. In the second approach, termed as temporal formulation, all snapshots in time at one antenna represent a measurement vector. These two methods are discussed next.

2.3.1 Spatial Formulation

Suppose each antenna transmit L uncorrelated symbols, the matrix of all received samples can be written as [6], [65]

$$\mathbf{Y} = \sum_{k=1}^K \beta_k(\phi_k) \mathbf{a}_R(\phi_k) \mathbf{a}_T^T(\phi_k) \mathbf{S} + \mathbf{Z}, \quad (2.6)$$

where

$$\mathbf{Y} = [\mathbf{y}(0), \mathbf{y}(1), \dots, \mathbf{y}(L-1)] \in \mathcal{C}^{n_R \times L} \quad (2.7)$$

and

$$\mathbf{S} = [\mathbf{s}(0), \mathbf{s}(1), \dots, \mathbf{s}(L-1)] \in \mathcal{C}^{n_T \times L} \quad (2.8)$$

is a matrix of all transmitted symbols from all antennas. For independent transmitted waveforms the rows of \mathbf{S} will be uncorrelated. It should be noted that (2.6) holds if and only if the targets fall in the same range bins which is a special case. The model in (2.6) can be generalized for delay by adding the delay parameter in the transmitted waveform \mathbf{S} . If the targets are in different range bin, there will be another parameter of delay or time of arrival associated with each target making the problem more complex. Since the targets are located at only finite discretized locations in the angle range $[-\pi/2, \pi/2]$, by dividing the region-of-interest into N grid points $\{\hat{\phi}_1, \hat{\phi}_2, \dots, \hat{\phi}_N\}$ and assuming $\mathbf{A}_R = [\mathbf{a}_R(\hat{\phi}_1), \mathbf{a}_R(\hat{\phi}_2), \dots, \mathbf{a}_R(\hat{\phi}_N)]$, $\mathbf{A}_T = [\mathbf{a}_T(\hat{\phi}_1), \mathbf{a}_T(\hat{\phi}_2), \dots, \mathbf{a}_T(\hat{\phi}_N)]$, and $\mathbf{B} = \text{diag}\{\beta_1, \beta_2, \dots, \beta_N\}$, we have

$$\mathbf{Y} = \mathbf{A}_R \mathbf{B} \mathbf{A}_T^T \mathbf{S} + \mathbf{Z} \quad (2.9)$$

It should be noted here that the diagonal elements of \mathbf{B} will be non-zero if and only if the target is present at the corresponding grid location. If $N \gg K$, the columns of the matrix $\mathbf{B} \mathbf{A}_T^T \mathbf{S}$ will be sparse. Therefore, (2.9) can be written as

$$\begin{aligned} [\mathbf{y}(0), \mathbf{y}(1), \dots, \mathbf{y}(L-1)] &= \mathbf{A}_R [\tilde{\mathbf{x}}(0), \tilde{\mathbf{x}}(1), \dots, \\ &\quad \tilde{\mathbf{x}}(L-1)] + \mathbf{Z}, \end{aligned} \quad (2.10)$$

where $\tilde{\mathbf{x}}(l) = \mathbf{B}\mathbf{A}_T^\top \mathbf{s}(l)$ for $l = 0, 1, \dots, L-1$ is a sparse vector. For a single snapshot, we can solve

$$\mathbf{y}(l) = \mathbf{A}_R \tilde{\mathbf{x}}(l) + \mathbf{z}(l) \quad (2.11)$$

by optimizing the cost function

$$\min_{\tilde{\mathbf{x}}(l)} \|\tilde{\mathbf{x}}(l)\|_1 \quad \text{subject to} \quad \|\mathbf{y} - \mathbf{A}_R \tilde{\mathbf{x}}(l)\|_2 \leq \eta \quad (2.12)$$

and assuming \mathbf{A}_R as the sensing matrix using convex optimization tools. The sensing matrix \mathbf{A}_R is a structured matrix similar to the Fourier matrix. For guaranteed sparse recovery, there are conditions on the sensing matrix. One such condition is called restricted isometry property (RIP) [70] which says a matrix Φ satisfies RIP with constant δ_k if

$$(1 - \delta_k) \|\mathbf{x}\|_2^2 \leq \|\Phi \mathbf{x}\|^2 \leq (1 + \delta_k) \|\mathbf{x}\|_2^2 \quad (2.13)$$

for every vector \mathbf{x} with sparsity k . For guaranteed sparse recovery in unbounded noise, δ_{2k} should be less than $\sqrt{2}-1$. To find the exact value of δ_k is a combinatorial problem which requires exhaustive search. For noiseless recovery of sparse vectors, the coherence criteria is more tractable. The coherence of a sensing matrix with column norms 1 is given by

$$\mu(\Phi) = \max_{i \neq j} |\langle \phi_i, \phi_j \rangle| \quad (2.14)$$

where $\{i, j\} = 1, 2, \dots, N$ and ϕ_i is the i -th column of Φ . In general for any matrix Φ , $0 < \mu \leq 1$ but for guaranteed sparse recovery, μ should be as small as possible and it must be less than one. The sensing matrix \mathbf{A}_R can be used for sparse reconstruction because it satisfies the coherence criteria with $\mu(\mathbf{A}_R) < 1$. Convex optimization methods require randomness in the sensing matrix. The structure in the sensing matrix deteriorates the performance of convex optimization methods due to high $\mu(\Phi)$. But the properties of the structured sensing matrix can be exploited for reduced complexity sparse reconstruction. It is shown in [47] that for a Toeplitz matrix exhibiting structure and $\mu(\Phi) \simeq 0.9$, Bayesian reconstruction is more efficient than convex optimization methods. Furthermore, the matrix \mathbf{A}_R has Vandermonde structure and its usage for sparse recovery with a similar matrix to \mathbf{A}_R is also discussed in [58]. Ref [71] analyzed Fourier-based structured matrices for CS.

Group sparsity algorithms were used to solve (2.10) for multiple snapshots and showed that the complexity grows with the number of measurement vectors as well as handling of the sensing matrix becomes difficult due to a Kronecker product involved in the construction of the group sensing matrix [72]. Since the column vectors $\tilde{\mathbf{x}}(l)$, for $l = 0, 1, \dots, L - 1$ in (2.12) are sparse, using \mathbf{A}_R as the sensing matrix, CS algorithms can be used to estimate the location and corresponding values of non-zero elements in $\tilde{\mathbf{x}}(l)$. Once they are known, the reflection coefficients and location angles of the targets can be easily found.

The formulation developed in (2.9) can be considered as block-sparse and can

be solved by SABMP for block sparse signals [73]. SABMP is a low complexity algorithm and provides an approximate minimum mean-square error (MMSE) estimate of the sparse vector with unknown support distribution. It should be emphasized that SABMP does not require the estimates of sparsity rate and noise variance rather it refines the initial estimates of these parameters in an iterative fashion. Therefore, it is assumed that the noise variance and the number of targets are unknown. Moreover, SABMP is a low complexity algorithm because it calculates the inverses by order-recursive updates. The undersampling ratio in CS environment is defined as the length of sparse vector divided by the number of measurements, i.e. N/M . As the undersampling ratio increases, the performance of CS algorithms deteriorates (please see [48] and the references therein). The results in [48] show that the best performance of SABMP algorithm can be achieved when the undersampling ratio is $1 < N/M < 7$. Since the number of measurements is n_R , it can be deduced for the number of receiving antennas that $N/7 < n_R < N$. For a given grid size and to maintain a low undersampling ratio, the spatial formulation is best suitable for large arrays.

2.3.2 Temporal Formulation

For smaller antenna arrays, where $n_R \ll N$, the formulation mentioned above can have a very high undersampling ratio which will lead to poor sparse recovery. To overcome this problem, by taking the transpose of (2.9) an alternate formulation

can be written as

$$\mathbf{Y}^\top = \mathbf{S}^\top \mathbf{A}_T \mathbf{B} \mathbf{A}_R^\top + \mathbf{Z}^\top \quad (2.15)$$

Since \mathbf{B} is sparse, $\bar{\mathbf{X}} = \mathbf{B} \mathbf{A}_R^\top$ will consist of sparse column vectors, the new sensing matrix will be

$$\boldsymbol{\Psi} = \mathbf{S}^\top \mathbf{A}_T \in \mathcal{C}^{L \times N}. \quad (2.16)$$

Similar to the argument of target range bins on (2.6), the model in (2.15) holds if and only if the targets fall in the same range bins. Moreover, if there is any delay in waveform \mathbf{S} , it will effect the RIP of $\boldsymbol{\Psi}$. Although the sensing matrix $\boldsymbol{\Psi}$ exhibits structure, the coherence of this sensing matrix is less than 1. Here, we are assuming that the transmitted waveforms matrix \mathbf{S} is known at the receiver and \mathbf{A}_T can be reconstructed at the receiver in the absence of any calibration error. Therefore, the second formulation for CS becomes

$$\bar{\mathbf{Y}} = \boldsymbol{\Psi} \bar{\mathbf{X}} + \bar{\mathbf{Z}}, \quad (2.17)$$

where $\bar{\mathbf{Y}} = \mathbf{Y}^\top$ and $\bar{\mathbf{Z}} = \mathbf{Z}^\top$. As long as $\mu(\boldsymbol{\Psi}) < 1$, the solution obtained for $\bar{\mathbf{X}}$ is the sparsest solution. More specifically, if any vector $\bar{\mathbf{x}}$ in $\bar{\mathbf{X}}$ satisfies the following inequality

$$\|\bar{\mathbf{x}}\|_0 < \frac{1}{2} (1 + \mu(\boldsymbol{\Psi})^{-1}) \quad (2.18)$$

then ℓ_1 -minimization recovers $\bar{\mathbf{x}}$ [74], [75].

With this new formulation, the advantage that we get is that the undersam-

pling ratio will become N/L . Using a similar argument for the undersampling ratio as made in the spatial formulation, it can be shown that $N/7 < L < N$ because the number of measurements is now L . Since the undersampling ratio is determined by the number of snapshots for a given grid size, this formulation is more suitable for small arrays. This formulation also has the additional advantage of increasing the number of grid points N for finer resolution by keeping a low undersampling ratio N/L by increasing the number of snapshots L at the same time.

2.4 Cramér Rao Lower Bound

In the following subsections, we discuss the CRLB for two cases, i.e. for known ϕ_k and for unknown ϕ_k respectively. Although both ϕ_k and β_k are unknown, yet we need to differentiate between the two cases of CRLB based on the assumption that either the target lies on-grid or off-grid. For CRLB, the error has to be consistent. In order to keep the consistency of error for CRLB, we will use the CRLB for known ϕ_k when the target is on-grid and we will use CRLB for unknown ϕ_k when the target is off-grid.

2.4.1 CRLB for known ϕ_k

Let's define:

$$\boldsymbol{\eta} = \begin{bmatrix} \mathcal{R}(\beta_k) & \mathcal{I}(\beta_k) \end{bmatrix}. \quad (2.19)$$

The Fisher information matrix (FIM) for the unknown parameters is given by the Slepian-Bang's formula assuming that the noise samples are uncorrelated [76].

$$\mathbf{F}(\boldsymbol{\eta}) = \frac{2}{\sigma_z^2} \mathcal{R} \left[\sum_{n=0}^{N-1} \left(\frac{\partial \mathbf{u}^H(n)}{\partial \boldsymbol{\eta}} \frac{\partial \mathbf{u}(n)}{\partial \boldsymbol{\eta}^T} \right) \right] \quad (2.20)$$

where

$$\frac{\partial \mathbf{u}^H(n)}{\partial \boldsymbol{\eta}} = \left[\begin{array}{c} \frac{\partial \mathbf{u}^H(n)}{\partial \mathcal{R}(\beta_k)} \\ \frac{\partial \mathbf{u}^H(n)}{\partial \mathcal{I}(\beta_k)} \end{array} \right]_{2 \times n_R}, \quad (2.21)$$

$$\frac{\partial \mathbf{u}(n)}{\partial \boldsymbol{\eta}^T} = \left[\begin{array}{cc} \frac{\partial \mathbf{u}}{\partial \mathcal{R}(\beta_k)} & \frac{\partial \mathbf{u}}{\partial \mathcal{I}(\beta_k)} \end{array} \right]_{n_R \times 2} \quad (2.22)$$

and

$$\mathbf{u}(n) = \beta_k(\phi_k) \mathbf{a}_R(\phi_k) \mathbf{a}_T^T(\phi_k) \mathbf{s}(n) \quad (2.23)$$

The two terms with partial derivatives in (2.22) are found to be:

$$\frac{\partial \mathbf{u}(n)}{\partial \mathcal{R}(\beta_k)} = \mathbf{a}_R(\phi_k) \mathbf{a}_T^T(\phi_k) \mathbf{s}(n) \quad (2.24)$$

and

$$\frac{\partial \mathbf{u}(n)}{\partial \mathcal{I}(\beta_k)} = j \mathbf{a}_R(\phi_k) \mathbf{a}_T^T(\phi_k) \mathbf{s}(n) \quad (2.25)$$

The other two partial derivatives in (2.21) can be found by using the identity $\partial \mathbf{x}^H = (\partial \mathbf{x})^H$. Thus, (2.20) can be solved by using (2.24) and (2.25). The CRLB is found by inverting $\mathbf{F}(\boldsymbol{\eta})$.

2.4.2 CRLB for unknown ϕ_k

Next, we derive CRLB for unknown ϕ_k . Let's define:

$$\boldsymbol{\alpha} = \begin{bmatrix} \mathcal{R}(\beta_k) & \mathcal{I}(\beta_k) & \phi_k \end{bmatrix} \quad (2.26)$$

The FIM for the unknown parameters is given by the Slepian-Bang's formula assuming that the noise samples are uncorrelated.

$$\mathbf{F}(\boldsymbol{\alpha}) = \frac{2}{\sigma_z^2} \mathcal{R} \left[\sum_{n=0}^{N-1} \left(\frac{\partial \mathbf{u}^H(n)}{\partial \boldsymbol{\alpha}} \frac{\partial \mathbf{u}(n)}{\partial \boldsymbol{\alpha}^T} \right) \right] \quad (2.27)$$

where

$$\frac{\partial \mathbf{u}^H(n)}{\partial \boldsymbol{\alpha}} = \begin{bmatrix} \frac{\partial \mathbf{u}^H(n)}{\partial \mathcal{R}(\beta_k)} \\ \frac{\partial \mathbf{u}^H(n)}{\partial \mathcal{I}(\beta_k)} \\ \frac{\partial \mathbf{u}^H(n)}{\partial \phi_k} \end{bmatrix}_{3 \times n_R} \quad (2.28)$$

and

$$\frac{\partial \mathbf{u}(n)}{\partial \boldsymbol{\alpha}^T} = \begin{bmatrix} \frac{\partial \mathbf{u}}{\partial \mathcal{R}(\beta_k)} & \frac{\partial \mathbf{u}}{\partial \mathcal{I}(\beta_k)} & \frac{\partial \mathbf{u}}{\partial \phi_k} \end{bmatrix}_{n_R \times 3} \quad (2.29)$$

The partial derivatives with respect to $\mathcal{R}(\beta_k)$ and $\mathcal{I}(\beta_k)$ are given in (2.24) and (2.25) respectively. The third partial derivative is found as follows by taking the second order derivative. Therefore,

$$\begin{aligned} \frac{\partial \mathbf{u}(n)}{\partial \phi_k} &= \beta_k (j\pi \cos(\phi_k)) \left(\mathbf{a}_T^\top(\phi_k) \mathbf{A}_T \mathbf{s}(n) \mathbf{a}_R(\phi_k) \right. \\ &\quad \left. + \mathbf{a}_T^\top(\phi_k) \mathbf{s}(n) \mathbf{A}_T \mathbf{a}_R(\phi_k) \right) \end{aligned} \quad (2.30)$$

where

$$\mathbf{A}_T = \text{diag}\{0, 1, \dots, n_T - 1\}$$

FIM can be found by above equation (2.30) along with (2.24) and (2.25) and the inversion of $\mathbf{F}(\boldsymbol{\alpha})$ leads to CRLB.

2.5 Simulation Results

We present here some simulation results to validate the methods discussed in this work. We assume a single target ($K = 1$) located at ϕ_k . The parameters to be estimated are the reflection coefficient β_k and DOA of the target ϕ_k . To assess the performance of the algorithms, the unknown parameters are generated randomly according to $\phi_k \sim \mathcal{U}(-60^\circ, 60^\circ)$ and $\beta_k = e^{i\varphi_k}$ of amplitude unity where $\varphi_k \sim \mathcal{U}(0, 1)$. The grid is uniformly discretized between -90° to $+90^\circ$ with N grid points. The number of grid points N is 512 in all the simulations. All

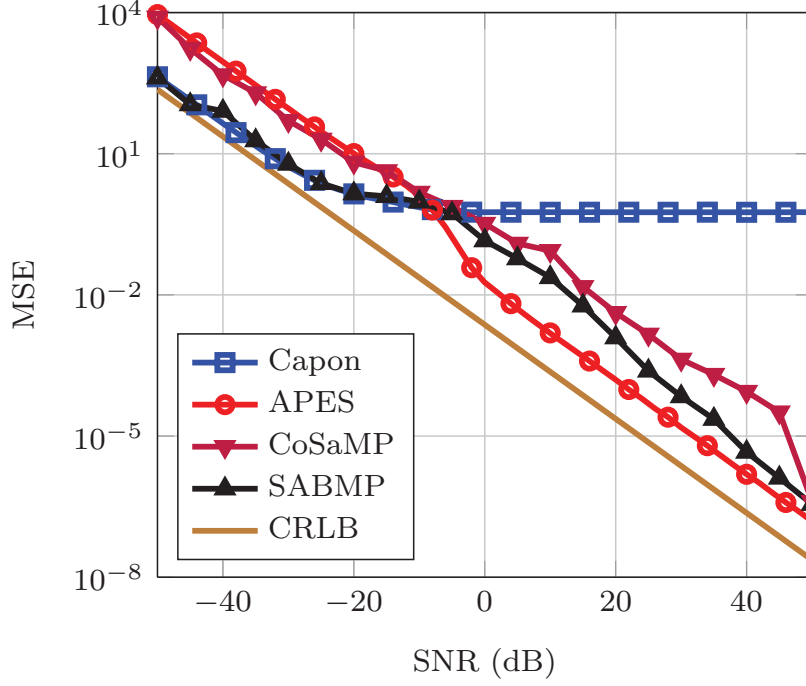


Figure 2.2: MSE performance for β_k estimation. Simulation parameters: $L = 20$, $n_T = 16$, $n_R = 16$, $N = 512$, $\phi_k \sim \mathcal{U}(-60^\circ, 60^\circ)$ but on-grid, $\beta_k = e^{j\varphi_k}$ where $\varphi_k \sim \mathcal{U}(0, 1)$.

algorithms are iterated for 10^4 iterations. The noise is assumed to be uncorrelated Gaussian with zero mean and variance σ_z^2 . The algorithms that are included for comparisons are Capon, APES and CoSaMP algorithms. In the simulation results, while referring to SABMP means the SABMP for block sparse signals. Also, for CoSaMP algorithm, its block-CoSaMP version is used as in [77].

2.5.1 CS Spatial Formulation

In this sub-section, we discuss the simulation results for the spatial formulation. Figs. 2.2 and 2.3 show the MSE performance for estimating β_k and ϕ_k respectively. The number of antenna elements n_T and n_R is 16 and the number of snapshots L is 20. This is the case where $L > n_R$. Both APES and Capon algorithms

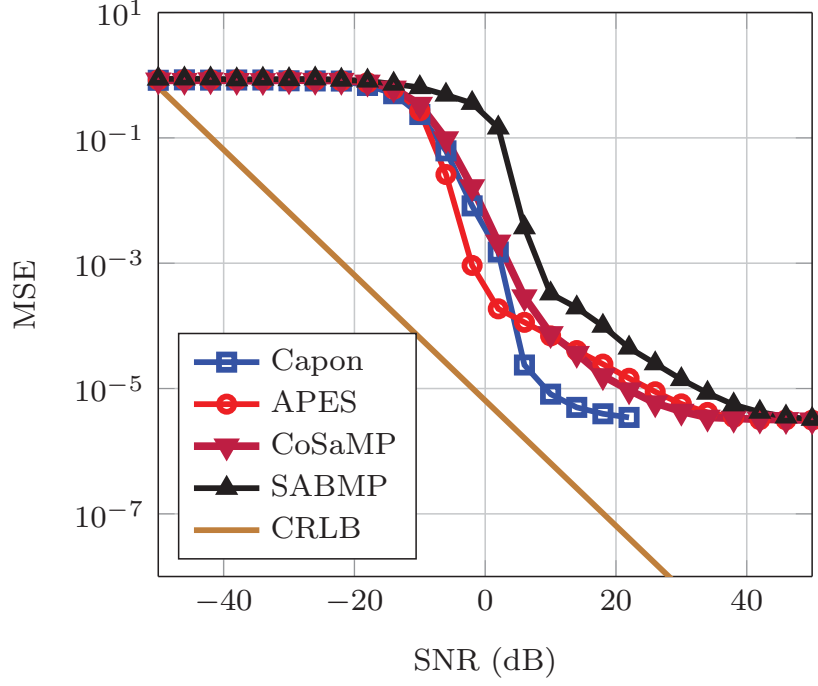


Figure 2.3: MSE performance for ϕ_k estimation. Simulation parameters: $L = 20$, $n_T = 16$, $n_R = 16$, $N = 512$, $\phi_k \sim \mathcal{U}(-60^\circ, 60^\circ)$ but falling off-grid, $\beta_k = e^{j\varphi_k}$ where $\varphi_k \sim \mathcal{U}(0, 1)$.

require $L > n_R$ to evaluate the correlation of the received signal. The estimation performance of β_k utilizing Capon reaches an error floor because Capon estimates are always biased [7]. APES algorithm shows the best estimation for β_k for SNR values greater than -8 dB. Both SABMP and CoSaMP algorithms do not perform well due to the high under-sampling ratios. But SABMP has better performance than CoSaMP algorithm for β_k estimation. For ϕ_k estimation, the results in Fig. 2.3 show that the Capon algorithm has the best performance at SNR levels greater than 3 dB. In Capon algorithm, at high SNR, the covariance matrix of received signals becomes close to singular causing poor estimation of ϕ_k . That is why, the results are not plotted after 22 dB. Nevertheless, the results available in Fig. 2.3 will serve the purpose of comparison. SABMP performs worse in

this scenario because it requires more measurements for better sparse recovery. All four algorithms reach an error floor because the grid is finite. In [78], this phenomenon is referred to as off-grid effect.

In Figs. 2.4 and 2.5, we discuss the case when $L < n_R$. To simulate this case, we choose n_T and n_R equal to 128 and L is kept to 10 only to keep a high under-sampling ratio for SABMP algorithm. In this case, both Capon and APES will fail to recover the estimates due to rank deficiency of the received signal covariance matrix. However, CoSaMP and SABMP algorithms will still be able to work for both β_k and ϕ_k estimation. For β_k estimation, SABMP algorithm has better estimation than CoSaMP algorithm up to SNR 22 dB. At high SNR, both CoSaMP and SABMP algorithms almost have the same performance for β_k estimation. Both CoSaMP and SABMP are not able to achieve the CRLB due to high under-sampling ratio. The results obtained in Fig. 2.5 show that SABMP algorithm has slightly better performance than CoSaMP algorithm for ϕ_k estimation.

We show the complexity comparison in Fig. 2.6. The plot is shown for processing time against n_R . For all cases of n_R , the number of snapshots L is 10 for CS. For both Capon and APES algorithms, if we keep $L = 10$, it will not recover the unknown parameters. However, the comparison remains fair if we assume L at least equal to n_R because the computational burden is on the inversion of the covariance matrix. It can be seen that as n_R increases, the processing time for Capon and APES algorithm increases significantly. Since the size of the

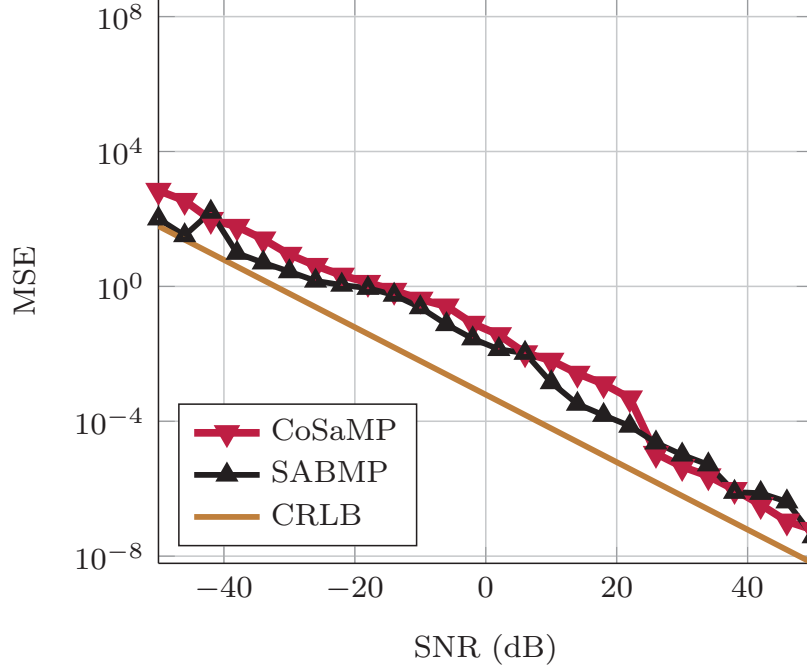


Figure 2.4: MSE performance for β_k estimation. Simulation parameters: $L = 10$, $n_T = 128$, $n_R = 128$, $N = 512$, $\phi_k \sim \mathcal{U}(-60^\circ, 60^\circ)$ but on-grid, $\beta_k = e^{j\varphi_k}$ where $\varphi_k \sim \mathcal{U}(0, 1)$. No recovery for Capon and APES methods.

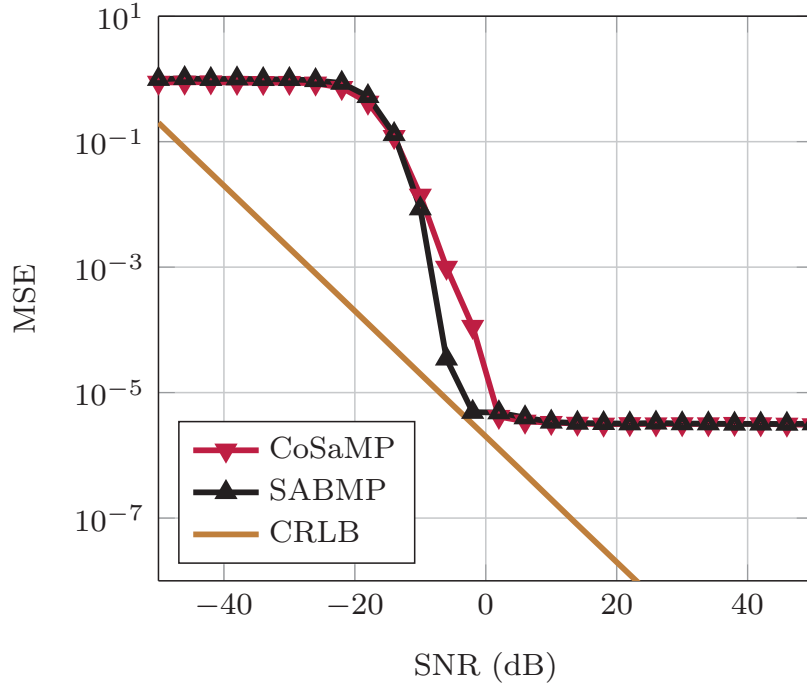


Figure 2.5: MSE performance for ϕ_k estimation. Simulation parameters: $L = 10$, $n_T = 128$, $n_R = 128$, $N = 512$, $\phi_k \sim \mathcal{U}(-60^\circ, 60^\circ)$ but falling off-grid, $\beta_k = e^{j\varphi_k}$ where $\varphi_k \sim \mathcal{U}(0, 1)$. No recovery for Capon and APES methods.

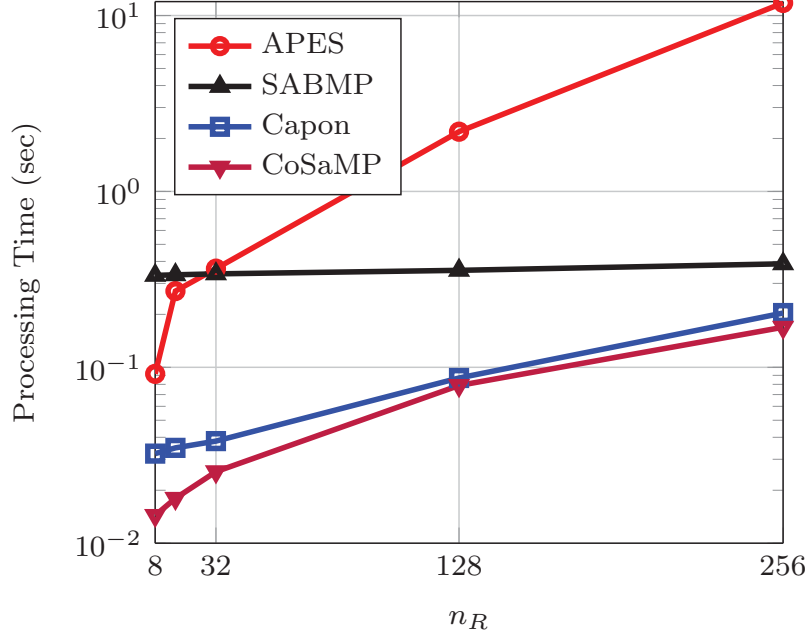


Figure 2.6: Complexity comparison. Simulation parameters: $n_T = n_R$, SNR = 20 dB, $\phi_k \sim \mathcal{U}(-60^\circ, 60^\circ)$ but on-grid, $\beta_k = e^{j\varphi_k}$ where $\varphi_k \sim \mathcal{U}(0, 1)$.

covariance matrix is equal to $n_R \times n_R$, the size of covariance matrix increases with n_R . Both Capon and APES need to invert the covariance matrix obtained from the received samples which increase the processing time with increased n_R . For SABMP, the increase in computation is mainly dependent on L in spatial formulation and is less dependent on n_R . That's why SABMP complexity does not change drastically with n_R . From Fig. 2.6, we can note that for n_R greater than or equal to 32, the complexity of SABMP algorithm is lower than APES but higher than Capon algorithm. CoSaMP algorithm has lower complexity than SABMP algorithm but is increasing significantly with n_R because its complexity is dependent on both the number of measurements n_R and the number of blocks L . Since it has lower complexity, a trade-off between performance and complexity exists between SABMP and CoSaMP with spatial formulation.

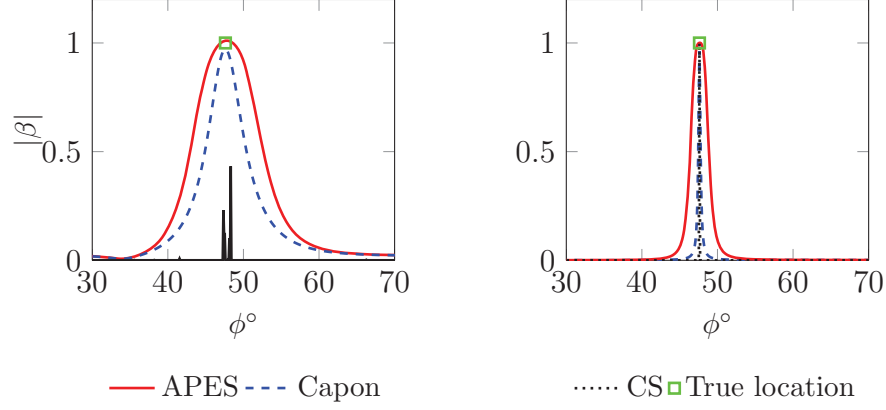


Figure 2.7: Resolution comparison. Simulation parameters: $L = 256$, $n_T = 10$, $n_R = 10$, $\text{SNR} = 0$ dB (left), $\text{SNR} = 25$ dB (right). CS algorithm used is SABMP.

2.5.2 CS Temporal Formulation

In this subsection, the simulation results for the temporal formulation as an alternative to the spatial one are presented. First, a comparison of resolution is made. Fig. 2.7 shows a comparison of resolution of the three algorithms. The plot shows ϕ° versus spectral estimates obtained by β . The true value of $|\beta_k|$ is 1 for the k -th source located at $\phi_k = 47.6^\circ$. The two figures are shown for two SNR levels, i.e. 0 dB (left) and 25 dB (right). APES has wider resolution than both Capon and SABMP algorithms. Capon has finer resolution, but its amplitude is biased downwards. SABMP algorithm gives the best resolution because on-grid CS algorithms are based on recovery of non-zero entries. That is why SABMP algorithm provides a single sample at the target location. A similar behavior can be anticipated for CoSaMP algorithm because it is also an on-grid CS algorithm.

The MSE is shown in Fig. 2.8 and 2.9 respectively for β_k and ϕ_k estimates. The number of snapshots $L = 256$ and the array size is kept small, i.e. $n_T = 10$ and $n_R = 10$. We plot the MSE obtained by using Capon, APES and CoSaMP

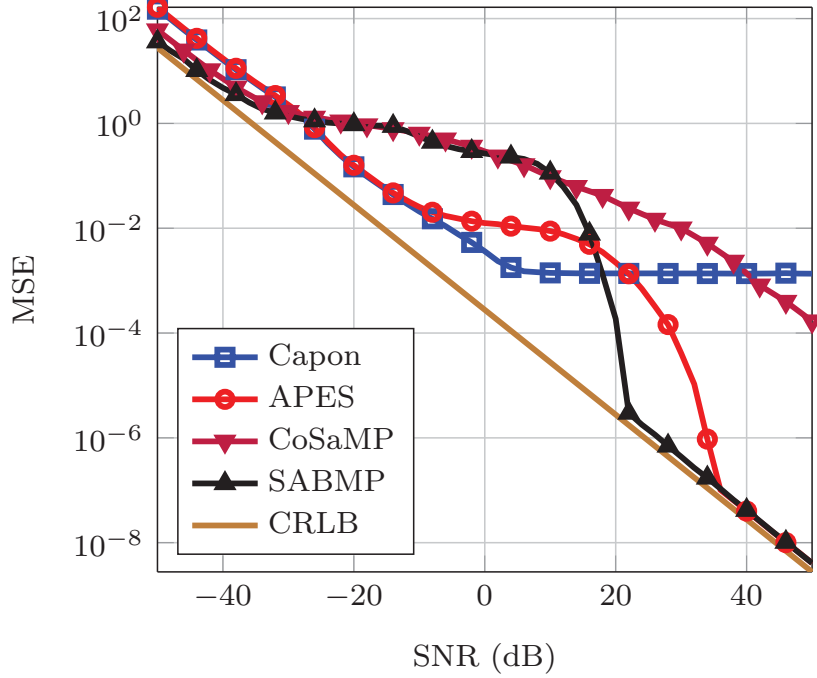


Figure 2.8: MSE performance for β_k estimation. Simulation parameters: $L = 256$, $n_T = 10$, $n_R = 10$, $N = 512$, $\phi_k \sim \mathcal{U}(-60^\circ, 60^\circ)$ but on-grid, $\beta_k = e^{j\varphi_k}$ where $\varphi_k \sim \mathcal{U}(0, 1)$.

along with SABMP for comparison versus SNR. CRLB is also plotted. In Fig 2.8, we assume that the target lie on the grid to plot MSE of β_k and to compare it with CRLB for known ϕ_k . Otherwise, we need infinite grid points to compare the performance of algorithms with CRLB. The simulation results show that SABMP performs better than all algorithms, i.e. Capon, APES and CoSaMP in estimating β_k at high SNR levels. This better performance of SABMP is due to its Bayesian approach and its robustness to noise. Moreover, the coherence of the sensing matrix is also less than 1 which guarantees sparse recovery at low noise. In Fig 2.9, we simulate the algorithms by generating ϕ_k anywhere randomly and not necessarily on the grid. Due to this reason, it can be seen that MSE of ϕ_k reached the error floor which is due to the discretized grid and depends on the difference

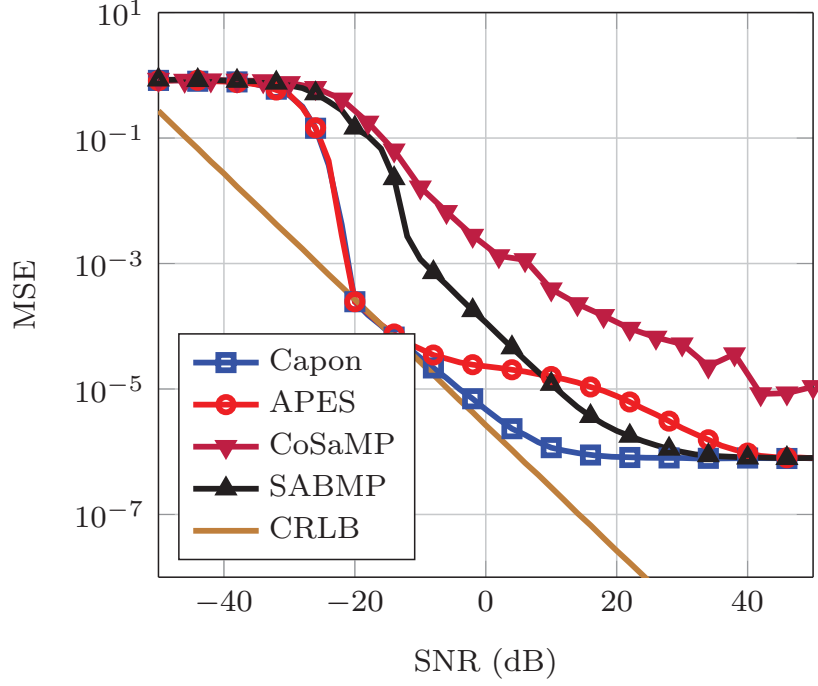


Figure 2.9: MSE performance for ϕ_k estimation. Simulation parameters: $L = 256$, $n_T = 10$, $n_R = 10$, $N = 512$, $\phi_k \sim \mathcal{U}(-60^\circ, 60^\circ)$ but falling off-grid, $\beta_k = e^{j\varphi_k}$ where $\varphi_k \sim \mathcal{U}(0, 1)$.

between the two consecutive grid points. For ϕ_k estimation, SABMP performs better than APES algorithm beyond 10 dB but worse than Capon algorithm. CoSaMP algorithm has the worst performance because it cannot work well with structured sensing matrices.

The above mentioned simulation results are obtained for $L > n_R$. Now, we discuss the case when $L < n_R$ and the number of snapshots is low. In the simulation results shown in Fig. 2.10 and 2.11, the number of snapshots L is 8 only. In this case, there will be no recovery by both Capon and APES methods due to rank deficiency of the covariance matrix. But both CS algorithms can work in this scenario. SABMP performs better than CoSaMP algorithm for both β_k and ϕ_k estimation. SABMP cannot achieve the CRLB because of very low number of

measurements in this case.

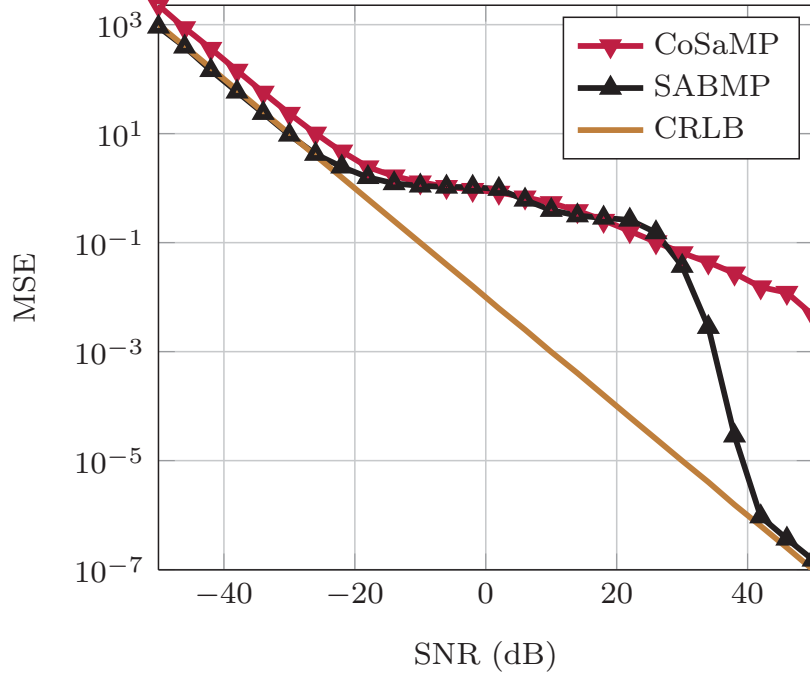


Figure 2.10: MSE performance for β_k estimation. Simulation parameters: $L = 8$, $n_T = 10$, $n_R = 10$, $N = 512$, $\phi_k \sim \mathcal{U}(-60^\circ, 60^\circ)$ but on-grid, $\beta_k = e^{j\varphi_k}$ where $\varphi_k \sim \mathcal{U}(0, 1)$. No recovery for Capon and APES methods.

Next, we compare the performance of algorithms at two different target locations. We choose one location at 5° and a second location at 70° . The simulation results in Fig. 2.12 and 2.13 show the estimation performance for ϕ_k and β_k respectively. The performance of all algorithms is degraded for $\phi_k = 70^\circ$ case because it comes in the low power region. For β_k estimation, the results show that for the $\phi_k = 5^\circ$, the APES and SABMP algorithms achieve the bound earlier than $\phi_k = 70^\circ$.

We compare the complexity of the discussed algorithms. Fig. 2.14 gives the processing time plotted against the number of grid points N . The runtime is calculated using a machine with Xeon E5-2680 2.8 GHz dual-processors with max-

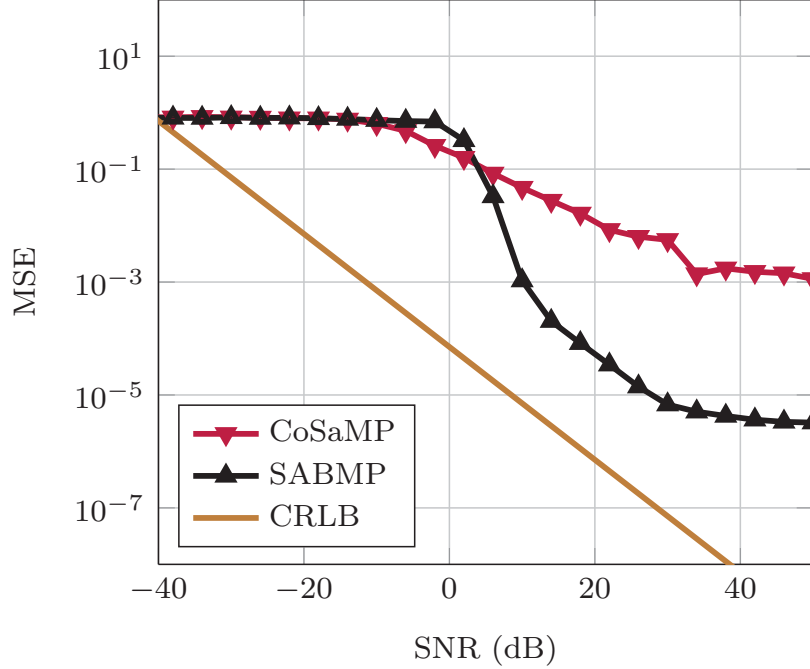


Figure 2.11: MSE performance for ϕ_k estimation. Simulation parameters: $L = 8$, $n_T = 10$, $n_R = 10$, $N = 512$, $\phi_k \sim \mathcal{U}(-60^\circ, 60^\circ)$ but falling off-grid, $\beta_k = e^{j\varphi_k}$ where $\varphi_k \sim \mathcal{U}(0, 1)$. No recovery for Capon and APES methods.

imum available RAM of 64 GB. The results show that SABMP algorithm has the higher complexity than Capon and APES algorithms but lower than CoSaMP algorithm. CoSaMP algorithm has the highest complexity due to a Kronecker product involved in the construction of its sensing matrix. The complexity of SABMP is dependent on the number of multiple-measurement-vectors. In this case the number of multiple-measurement-vectors is equal to number of receive antennas. Therefore, there exists a tradeoff between performance and complexity of Capon, APES, CoSaMP and SABMP algorithm.

Lastly, we show a comparison of receiver operating characteristic (ROC) curves. At high SNR, the probability of detection for all algorithms is 1 almost for all probabilities of false alarm. Therefore, MSE criteria is better to compare performance

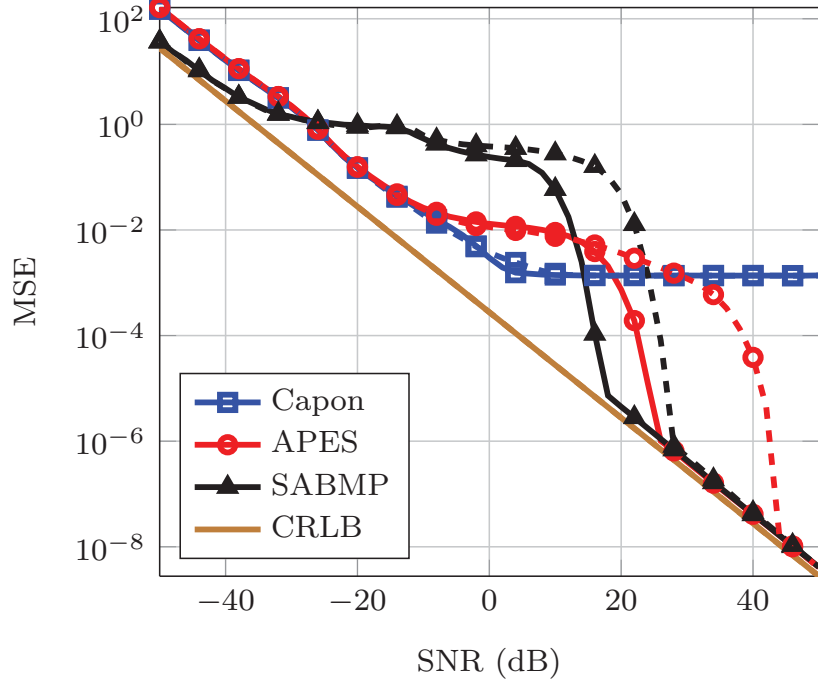


Figure 2.12: MSE performance for β_k estimation. Simulation parameters: $L = 256$, $n_T = 10$, $n_R = 10$, $N = 512$, $\phi_k = 5^\circ$ (solid lines) & $\phi_k = 70^\circ$ (dashed lines) but on-grid, $\beta_k = e^{j\varphi_k}$ where $\varphi_k \sim \mathcal{U}(0, 1)$ and is same for all iterations.

of different algorithms at high SNRs. However, we can choose small SNR value of -12 dB to plot ROCs for all four algorithms. Figure. 2.15 shows the ROC comparison of the four algorithms discussed. The probability of detection is close to one for both Capon and APES algorithms for a wide range of probabilities of false alarm. SABMP algorithm has a little worse performance than both Capon and APES algorithms because we have chosen a low SNR value of -12 dB but SABMP performance gains are at usually at high SNRs CoSaMP algorithm has slightly better performance than SABMP algorithm for low values of probability of false alarm but its performance deteriorates afterwards.

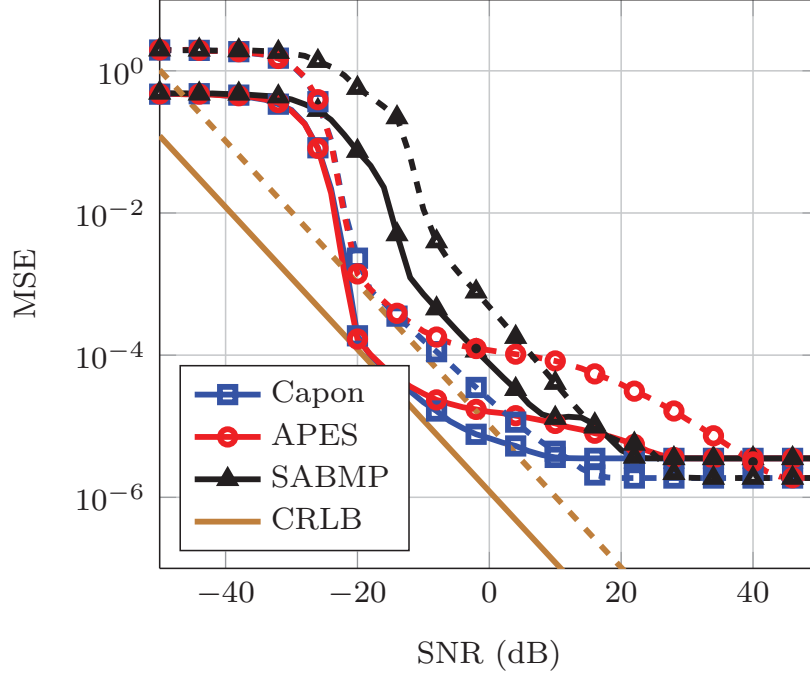


Figure 2.13: MSE performance for ϕ_k estimation. Simulation parameters: $L = 256$, $n_T = 10$, $n_R = 10$, $N = 512$, $\phi_k = 5^\circ$ (solid lines) & $\phi_k = 70^\circ$ (dashed lines) but falling off-grid, $\beta_k = e^{j\varphi_k}$ where $\varphi_k \sim \mathcal{U}(0, 1)$ and is same for all iterations.

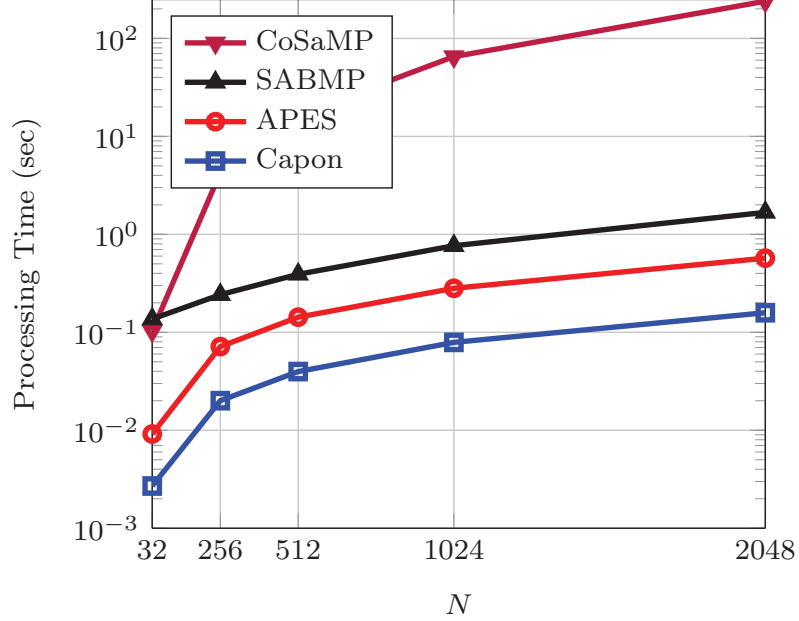


Figure 2.14: Complexity comparison. Simulation parameters: $L = 256$, $n_T = 10$, $n_R = 10$, SNR = 20 dB, $\phi_k \sim \mathcal{U}(-60^\circ, 60^\circ)$ but on-grid, $\beta_k = e^{j\varphi_k}$ where $\varphi_k \sim \mathcal{U}(0, 1)$.

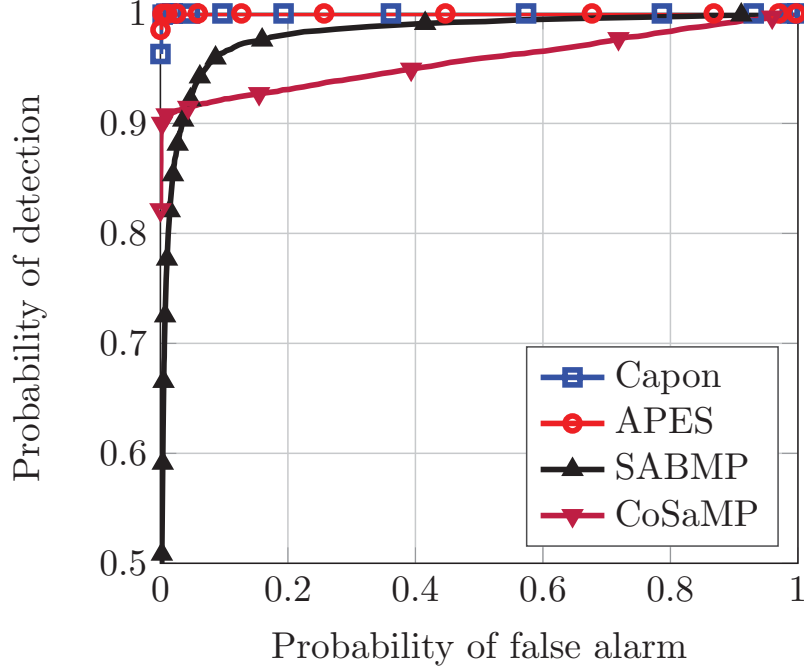


Figure 2.15: ROC comparison. Simulation parameters: $n_T = 10$, $n_R = 10$, $\text{SNR} = -12$ dB, $\phi_k \sim \mathcal{U}(-60^\circ, 60^\circ)$ but on-grid, $\beta_k = e^{j\varphi_k}$ where $\varphi_k \sim \mathcal{U}(0, 1)$. (Markers are added in this plot only for the purpose of identification of different curves.)

2.6 Conclusion

In this chapter, the MIMO radar parameter estimation problem was solved by two methods: the spatial method for large arrays and temporal method for small arrays by a fast and robust CS algorithm. It is shown that SABMP provides the best estimates for parameter estimation at high SNR even when the number of targets and noise variance are unknown. It is shown that SABMP has better resolution than both the Capon and APES algorithms. Furthermore, it is shown that the best estimation for reflection coefficient is obtained by SABMP algorithm. The complexity of SABMP algorithm is shown to be lower than CoSaMP but higher than Capon and APES algorithms.

CHAPTER 3

MPDR-BASED REDUCED COMPLEXITY DOA AND DOD ESTIMATION FOR MOVING TARGET IN BISTATIC MIMO RADAR

In this chapter, a reduced dimension and low complexity algorithm is proposed to estimate the DOA, direction-of-departure (DOD) and the Doppler shift of a moving target for a MIMO radar. We derive the cost function based on minimum power distortionless response (MPDR). First, we solve the cost function with a low complexity FFT-based solution in three dimensions. We further carry out a derivation to reduce the three-dimensional search to two-dimensional search and

solve it with a 2D-FFT. Another reduced dimension algorithm is derived using the generalized eigen value method which finds the estimate of unknown parameters in one dimension with less memory constraints. This way, we propose three algorithms based on the simplification of the derived cost function. The simulation results are presented for a static target case and a moving target case. Also, the scenarios of on-grid targets and off-grid targets are considered. We compare the MSE performance and computational complexity of our proposed algorithms with existing algorithms as well. The proposed algorithms exhibit lower computational complexity than the existing ones and also provide an estimate for the Doppler shift which was not accomplished in most of previous works.

3.1 Introduction

MIMO radars have been extensively investigated in literature for surveillance applications. A MIMO radar can be seen as an extension of a phased array radar, where the transmitted waveforms can be independent or partially correlated. Such waveforms yield extra degrees of freedom that can be exploited for better detection performance and resolution [4], [5], [79]. MIMO radars with colocated antennas can be classified into two categories; monostatic and bistatic radars. A bistatic radar has some additional advantages over the monostatic one, such as better performance for target detection and covert operation [5]. The target localization in bistatic MIMO radar can be achieved by finding its DOA and DOD. The DOA and DOD are the same in colocated MIMO radars whereas in bistatic MIMO

radars they are two different unknown parameters. Several algorithms have been proposed in literature for the estimation of these two unknown parameters in bistatic MIMO radars.

For a static target, the estimation of DOA and DOD is a two-dimensional search problem. To estimate DOA and DOD for a static target, a technique called estimation method of signal parameters via rotational invariance technique (ESPRIT) was presented in [20]. The ESPRIT algorithm exploits the invariance property to convert the two-dimensional search problem into two independent one-dimensional search problems but it requires pair matching between the estimates of transmit and receive angles. A low complexity ESPRIT algorithm which automatically performs the pair matching was proposed in [21]. Another scheme based on ESPRIT has been proposed in [22] for three transmitters only which is extended and generalized in [23] for any number of transmitters. The drawback of ESPRIT based algorithms is the poor estimation performance.

The two-dimensional multiple signal classification (2D-MUSIC) algorithm has better estimation performance for DOA and DOD estimation than ESPRIT but it is computationally expensive [80]. In [24], a reduced-complexity MUSIC (RD-MUSIC) algorithm was proposed which requires one-dimensional search and its performance is very close to 2D-MUSIC with less complexity. A joint DOA and DOD estimation via polynomial root finding technique was proposed in [25] which was shown to have less computational complexity than 2D-MUSIC. Another estimation algorithm that is simplified based on the properties of the Kronecker

product was discussed in [26] whereas in [27] the DOA and DOD estimation problem for coherent targets were investigated. In [28], a Capon beamformer is used to improve parameter estimation but the presented method required two-dimensional computationally expensive search.

The work in [81] outperforms 2D-Capon of [28] in both estimation performance and complexity but is based on coarse grid and then iterative grid refinement which is considered a trivial approach. This algorithm will be computationally expensive for a finer grid.

Another method for direction finding in bistatic MIMO radar was presented in [29] that is based on the solution of a constrained minimization problem to find the directions which is again a computationally expensive method. In [30], the non-circular characteristics of transmitted signals are exploited for DOA and DOD estimation in bistatic MIMO radar but the estimation performance of the proposed algorithm in [30] did not achieve the CRLB. Maximum likelihood estimation for DOA and DOD was discussed in [31]. The algorithm developed in [31] to solve the maximum likelihood estimation is an iterative search method which is computationally expensive. The signal models presented in [27], [28], [30], [31], [80], [81] did not consider a Doppler shift.

In [32], a joint diagonalization based method for DOA and DOD was proposed. The signal model used in most of the existing work is based on matched filtering with the transmitted signal and assume that the covariance matrix of transmitted signal is identity. The performance of DOA and DOD estimation using velocity

sensors are investigated in [33], [34] and reduced complexity algorithms based on MUSIC were derived. The DOA and DOD estimation problems for non-uniform array were investigated in [35]. The algorithm proposed in [36] is also based on ESPRIT and MUSIC. The algorithm presented in [82] did not estimate the Doppler shift, its angle estimation performance does not achieve the CRLB and it has heavier computational load than ESPRIT [20]. Also, [69] and [83] did not estimate the Doppler shift. In all of the aforementioned algorithms for DOA and DOD estimation, the Doppler shift was not estimated.

The algorithm presented in [84] provides an estimate of the Doppler shift but the algorithm is based on a computationally expensive exhaustive search. The algorithm exhibited better estimation performance than [20]–[22] for three transmit and four receive antennas but showed close performance for eight transmit and six receive antennas when compared to [20], [21]. The algorithm developed in [85] showed better estimation performance than some existing algorithms but it estimates the Doppler shift by three-dimensional ESPRIT. The method is also computationally expensive than two-dimensional (2D) ESPRIT for angles search. The tensor decomposition based algorithm developed in [37] seems promising because it is also estimating the Doppler shift for uniform linear array as well as uniform rectangular array but it suffers from high computational complexity.

In this chapter, the contribution is multifold. In contrast to previous works, we consider a more realistic model where the target is moving. This adds the Doppler shift in the signal model that must be estimated for the accurate local-

ization of the target. Now, the estimation of DOA, DOD and Doppler shift is a three-dimensional search problem where computational complexity can be very high. To solve this problem, based on MPDR, new low complexity algorithms are derived. The cost function obtained with the derivation is a three-dimensional non-linear exhaustive search problem. To solve it, we derive a reduced complexity fast-Fourier-transform (FFT)-based algorithm for the DOA, DOD and Doppler shift parameter estimation in three-dimensions [86]. Furthermore, we carry out the derivation of each cost function to transform the three-dimensional search problems to two-dimensional search problems and then subsequently converting to one-dimensional searches. The conversion of three-dimensional problems into two-dimensional ones reduces the complexity significantly. Furthermore, with the use of generalized eigenvalues, the problem is solved by one dimensional search leading to low memory constraints.

3.1.1 Organization of the Chapter

The rest of the chapter is organized as follows: The bistatic MIMO radar signal model for DOA, DOD and Doppler estimation is presented in section 3.2. Section 3.3 presents the proposed parameter estimation algorithms for DOA, DOD and Doppler estimation and the derivations to reduce the dimensions. In section 3.4, we develop the FFT-based algorithm to estimate the parameters. The complexity analysis and its comparison with existing algorithms is shown in section 3.5. Simulation results are presented in section 3.6 and we conclude the chapter in section

3.2 Signal Model

Consider a bistatic MIMO radar setup with n_T colocated antennas at the transmitter and n_R antennas at the receiver. The transmitter and receiver are separated by a large distance as illustrated in Fig. 3.1. The antenna arrays at the transmitter and receiver are uniform and linear, the inter-element-spacing between any two adjacent antenna elements at the transmitter/receiver is half of the transmitted signal wavelength. Each antenna transmits a narrowband signal using a common carrier frequency. There is a possible point target present at (θ_k, ϕ_k) , where θ_k and ϕ_k are respectively the DOD from the transmitter to the target and DOA from the target to the receiver. (The notation (θ, ϕ) is not to be confused with azimuth and elevation. In this chapter, θ refers to the DOD or the angle of elevation from the transmitter and ϕ denotes the DOA or the angle of elevation at the receiver. Since linear arrays are assumed in this chapter, they are independent of azimuth.) Assume $\mathbf{s}(n) = [s_0(n), s_1(n), \dots, s_{L-1}(n)]^T$ is the vector of transmitted symbols (known at the receiver) at time index n , $\mathbf{y}(n) = [y_0(n), y_1(n), \dots, y_{L-1}(n)]^T$ is the vector of n_R baseband received samples for all antennas, and $\mathbf{z}(n) = [z_0(n), z_1(n), \dots, z_{L-1}(n)]^T$ is the vector of circularly symmetric white Gaussian noise samples at n_R receive antennas. The received

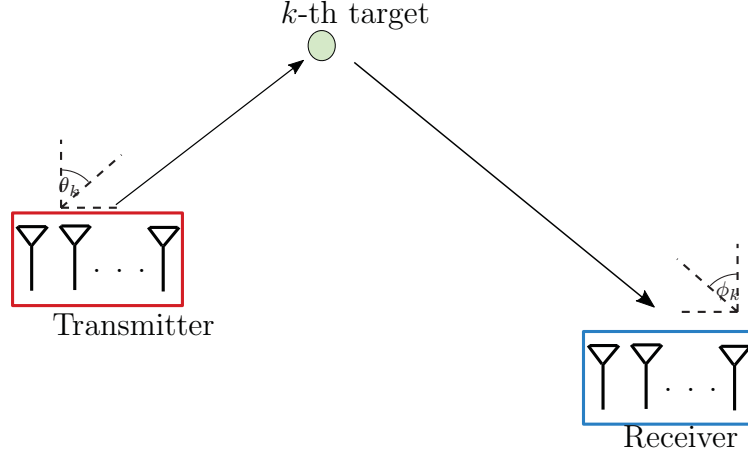


Figure 3.1: Bistatic radar geometry.

signal vector can be written as [87]

$$\mathbf{y}(n) = \beta_k e^{i(2\pi n f_{d_k})} \mathbf{a}_R(\phi_k) \mathbf{a}_T^T(\theta_k) \mathbf{s}(n) + \mathbf{z}(n), \quad n = 0, 1, \dots, L-1, \quad (3.1)$$

where

$$\mathbf{a}_T(\theta_k) = [1, e^{i\pi \sin(\theta_k)}, \dots, e^{i\pi(n_T-1) \sin(\theta_k)}]^T \quad (3.2)$$

$$\mathbf{a}_R(\phi_k) = [1, e^{i\pi \sin(\phi_k)}, \dots, e^{i\pi(n_R-1) \sin(\phi_k)}]^T, \quad (3.3)$$

β_k and f_{d_k} denotes the transmit steering vector, receive steering vector, reflection coefficient of the target and the Doppler shift of the target, respectively. The total number of snapshots is denoted by L . For different range bins, θ_k and ϕ_k will be different. In the following section, we propose low complexity algorithms to estimate these target parameters.

3.3 MPDR-based Reduced Dimension Estimation

The received signal vector in (3.1) can be multiplied by a weight vector $\mathbf{w}(\phi)$ to increase the signal-to-noise ratio, as follows

$$\mathbf{w}^H(\phi)\mathbf{y}(n) = \beta e^{j(2\pi n f_d)} \mathbf{w}^H(\phi) \mathbf{a}_R(\phi) \mathbf{a}_T^T(\theta) \mathbf{s}(n) + \mathbf{w}^H(\phi) \mathbf{z}(n) \quad (3.4)$$

There can be more than one approach to calculate the weight vector $\mathbf{w}(\phi)$. The first approach based on minimum power distortionless response (MPDR) is discussed in this chapter. In the majority of the literature, MPDR is also referred to as minimum variance distortionless response (MVDR) or Capon beamformer [8]. We use MPDR to emphasize that the estimated covariance matrix of the entire received signal is utilized instead of the noise covariance matrix [88].

The MPDR based beamforming weight vector [8] can be found by solving the following linearly-constrained optimization problem

$$\mathbf{w}_M(\phi) = \min_{\mathbf{w}(\phi)} \mathbf{w}^H(\phi) \hat{\mathbf{R}}_y \mathbf{w}(\phi) \quad \text{subject to} \quad \mathbf{w}^H(\phi) \mathbf{a}_R(\phi) = 1 \quad (3.5)$$

where

$$\hat{\mathbf{R}}_y = \frac{\mathbf{Y}\mathbf{Y}^H}{L} \quad (3.6)$$

is the estimated covariance matrix of the received samples with $\mathbf{Y} = [\mathbf{y}(0), \mathbf{y}(1), \dots, \mathbf{y}(L-1)]$

1)]. The solution of the constrained optimization problem in (3.5) yields

$$\mathbf{w}_M(\phi) = \frac{\hat{\mathbf{R}}_y^{-1} \mathbf{a}_R(\phi)}{\mathbf{a}_R^H(\phi) \hat{\mathbf{R}}_y^{-1} \mathbf{a}_R(\phi)} \quad (3.7)$$

The output of the filtered signal is found by putting (3.7) in (3.4)

$$\mathbf{w}_M^H(\phi) \mathbf{y}(n) = \beta e^{j(2\pi n f_d)} \mathbf{a}_T^T(\theta) \mathbf{s}(n) + \frac{\mathbf{a}_R^H(\phi) \hat{\mathbf{R}}_y^{-1} \mathbf{z}(n)}{\mathbf{a}_R^H(\phi) \hat{\mathbf{R}}_y^{-1} \mathbf{a}_R(\phi)}. \quad (3.8)$$

The spatial spectrum of the three unknown parameters ϕ, θ and f_d can be found by finding β . To find β , we need to minimize the following cost function

$$J_M(\beta, \phi, \theta, f_d) = \min_{\beta, \phi, \theta, f_d} \mathbb{E} |\mathbf{w}_M^H(\phi) \mathbf{y}(n) - \beta e^{j(2\pi n f_d)} \mathbf{a}_T^T(\theta) \mathbf{s}(n)|^2 \quad (3.9)$$

We can write the equivalent matrix form of (3.9)

$$J_M(\beta, \phi, \theta, f_d) = \min_{\beta, \phi, \theta, f_d} \frac{1}{L} \|\mathbf{w}_M^H(\phi) \mathbf{Y} - \beta \mathbf{a}_T^T(\theta) \mathbf{S} \mathbf{F}(f_d)\|_2^2 \quad (3.10)$$

where $\mathbf{F}(f_d) = \text{diag}([1 \ e^{j2\pi f_d} \ \dots \ e^{j2\pi(L-1)f_d}])$ and $\mathbf{S} = [\mathbf{s}(0), \mathbf{s}(1), \dots, \mathbf{s}(L-1)]$. The minimization of (3.10) with respect to β yields

$$\beta_M(\phi, \theta, f_d) = \frac{\mathbf{w}_M^H(\phi) \mathbf{Y} \mathbf{F}^H(f_d) \mathbf{d}(\theta)}{\|\mathbf{d}(\theta)\|^2} \quad (3.11)$$

where we have defined

$$\mathbf{d}(\theta) \triangleq \mathbf{S}^H \mathbf{a}_T^*(\theta) \quad (3.12)$$

for simplicity of notation. Note that in (3.7), $\hat{\mathbf{R}}_y^{-1}$ is positive-definite so that it can be factored as $\hat{\mathbf{R}}_y^{-1} = \hat{\mathbf{R}}_y^{-H/2} \hat{\mathbf{R}}_y^{-1/2}$. For simplicity of notation, we define the following vectors

$$\mathbf{b}(\phi) \triangleq \hat{\mathbf{R}}_y^{-1/2} \mathbf{a}_R(\phi) \quad (3.13)$$

$$\mathbf{c}(\theta, f_d) \triangleq \hat{\mathbf{R}}_y^{-1/2} \mathbf{Y} \mathbf{F}^H(f_d) \mathbf{d}(\theta) \quad (3.14)$$

By putting (3.7) in (3.11), we get

$$\beta_M(\phi, \theta, f_d) = \frac{\mathbf{b}^H(\phi) \mathbf{c}(\theta, f_d)}{\|\mathbf{b}(\phi)\|^2 \|\mathbf{d}(\theta)\|^2} \quad (3.15)$$

Since β is a function of ϕ , θ and f_d , to estimate these parameters substituting (3.11) in (3.10), we get

$$J_M(\phi, \theta, f_d) = \mathbf{w}_M^H(\phi) \hat{\mathbf{R}}_y \mathbf{w}_M(\phi) - \frac{|\mathbf{w}_M^H(\phi) \mathbf{Y} \mathbf{F}^H(f_d) \mathbf{d}(\theta)|^2}{L \|\mathbf{d}(\theta)\|^2} \quad (3.16)$$

By putting (3.7) in (3.16), we get

$$J_M(\phi, \theta, f_d) = \frac{1}{\|\mathbf{b}(\phi)\|^2} \left[1 - \frac{|\mathbf{b}^H(\phi) \mathbf{c}(\theta, f_d)|^2}{L \|\mathbf{b}(\phi)\|^2 \|\mathbf{d}(\theta)\|^2} \right] \quad (3.17)$$

The minimization of the cost function $J_M(\phi, \theta, f_d)$ in (3.17) gives us the estimates $\hat{\phi}_k, \hat{\theta}_k, \hat{f}_{d_k}$ of the unknown parameters of k -th target. The global minimum of $J_M(\phi, \theta, f_d)$ in (3.17) is difficult to find because this function is multimodal, highly non-linear and can have several local minima.

By treating the outside bracket as a constant (as shown in Appendix 3.8), the cost function can be minimized by minimizing the function inside the bracket given by

$$J'_M(\phi, \theta, f_d) = 1 - \frac{|\mathbf{b}^H(\phi)\mathbf{c}(\theta, f_d)|^2}{L\|\mathbf{b}(\phi)\|^2 \|\mathbf{d}(\theta)\|^2} \quad (3.18)$$

The minimization of $J'_M(\phi, \theta, f_d)$ is equivalent to maximizing

$$J''_M(\phi, \theta, f_d) = \frac{|\mathbf{b}^H(\phi)\mathbf{c}(\theta, f_d)|^2}{L\|\mathbf{b}(\phi)\|^2 \|\mathbf{d}(\theta)\|^2} \quad (3.19)$$

The expression of $J''_M(\phi, \theta, f_d)$ is similar to that of $\beta_M(\phi, \theta, f_d)$ in (3.15). It will give a three-dimensional spectrum from which $\hat{\phi}_k, \hat{\theta}_k$ and \hat{f}_{d_k} can be found by searching the peak. These estimates can be used to minimize $J_M(\phi, \theta, f_d)$. To estimate ϕ_k, θ_k and f_{d_k} using (3.19), a three-dimensional computationally expensive exhaustive search can be performed. We develop a faster three-dimensional FFT-based equivalent of the exhaustive search to solve (3.19). The details of the FFT-based evaluation are discussed in Section 3.4. We call this three-dimensional algorithm as MPDR-3D.

Next, we show the derivation to reduce the three-dimensional problem into

a combination of two-dimensional and one-dimensional problems. The function $J''_{\text{M}}(\phi, \theta, f_d)$ is a three-dimensional function and is computationally expensive. We try to reduce the complexity by reducing its dimension. We can make the vectors $\mathbf{b}(\phi)$ and $\mathbf{c}(\theta, f_d)$ unit-norm and write (3.19) as

$$J''_{\text{M}}(\phi, \theta, f_d) = \frac{|\tilde{\mathbf{b}}^{\text{H}}(\phi)\tilde{\mathbf{c}}(\theta, f_d)|^2 \|\mathbf{c}(\theta, f_d)\|^2}{L\|\mathbf{d}(\theta)\|^2} \quad (3.20)$$

where

$$\tilde{\mathbf{b}}(\phi) = \frac{\mathbf{b}(\phi)}{\|\mathbf{b}(\phi)\|} \quad (3.21)$$

and

$$\tilde{\mathbf{c}}(\theta, f_d) = \frac{\mathbf{c}(\theta, f_d)}{\|\mathbf{c}(\theta, f_d)\|} \quad (3.22)$$

We note that for uncorrelated waveforms $\|\mathbf{d}(\theta)\|^2 = Ln_T$ and $1/\|\mathbf{b}(\phi)\|^2$ is given by (3.42). Thus treating the denominator of $J''_{\text{M}}(\phi, \theta, f_d)$ in (3.20) as a constant, the cost function can be maximized by maximizing its numerator. Furthermore, the numerator will be maximized when the two unit norm vectors $\tilde{\mathbf{b}}(\phi)$ and $\tilde{\mathbf{c}}(\theta, f_d)$ are equal. In fact, both vectors cannot be equal in the presence of the noise. However, the fact that when $\phi = \phi_k$, $\theta = \theta_k$ and $f_d = f_{d_k}$, (3.20) will be maximized and $\tilde{\mathbf{b}}(\phi)$ will be approximately equal to $\tilde{\mathbf{c}}(\theta, f_d)$, can be exploited to convert the three-dimensional problem into a two-dimensional problem. Thus, replacing $\tilde{\mathbf{b}}(\phi)$

by $\tilde{\mathbf{c}}(\theta, f_d)$ in (3.20), we get the two-dimensional function given by

$$g_M(\theta, f_d) = \frac{\|\mathbf{c}(\theta, f_d)\|^2}{L\|\mathbf{d}(\theta)\|^2} \quad (3.23)$$

The estimates $\hat{\theta}_k$ and \hat{f}_{d_k} are found by searching the peak in two-dimensional spectrum of $g_M(\theta, f_d)$. The function in (3.23) can be solved by two-dimensional exhaustive search. To reduce the complexity, the numerator in (3.23) is converted into a 2D-FFT expression as shown in Appendix 3.9. The estimates $\hat{\theta}_k$ and \hat{f}_{d_k} obtained by $g_M(\theta, f_d)$ can be used to solve $J_M''(\phi, \theta, f_d)$. By using the estimates $\hat{\theta}_k$ and \hat{f}_{d_k} , $J_M''(\phi, \hat{\theta}_k, \hat{f}_{d_k})$ will be a one-dimensional function in ϕ . We call this two-dimensional (in θ and f_d) and one-dimensional (in ϕ) algorithm as MPDR-2D and its complete FFT-based evaluation is discussed in Section 3.4.

Next, we further reduce the two-dimensional problem of (3.23) into two one-dimensional problems. The function $g_M(\theta, f_d)$ is still two-dimensional which can be written as

$$g_M(\theta, f_d) = \frac{\mathbf{a}_T^T(\theta) \mathbf{A}(f_d) \mathbf{A}^H(f_d) \mathbf{a}_T^*(\theta)}{\mathbf{a}_T^T(\theta) \mathbf{S} \mathbf{S}^H \mathbf{a}_T^*(\theta)} \quad (3.24)$$

where

$$\mathbf{A}(f_d) \triangleq \mathbf{S} \mathbf{F}(f_d) \mathbf{Y}^H \hat{\mathbf{R}}_y^{-H/2} \quad (3.25)$$

which can be solved as a generalized eigenvalue problem. We can write

$$h_M(f_d) = \lambda_{\max}(f_d) \quad (3.26)$$

where $\lambda_{\max}(f_d)$ denote the generalized eigenvalue of $\mathbf{A}(f_d)\mathbf{A}^H(f_d)$ and $\mathbf{S}\mathbf{S}^H$. Thus, (3.23) can be written as a one-dimensional approximate function

$$g'_M(\theta) = \frac{\|\mathbf{c}(\theta, \hat{f}_d)\|^2}{L\|\mathbf{d}(\theta)\|^2} \quad (3.27)$$

Therefore, the reduced dimension functions in (3.26), (3.27) and $J''_M(\phi, \hat{\theta}_k, \hat{f}_{d_k})$ give the initial estimates of the unknown parameters in three one-dimensional searches which will be used to minimize the cost function in (3.17). We call this three one-dimensional search algorithm as MPDR-1D.

Therefore, the initial estimates obtained by $J''_M(\phi, \theta, f_d)$ can be used to solve $J_M(\phi, \theta, f_d)$. The global minimum of (3.17) will be located correctly.

3.4 Reduced Complexity FFT-based Solution

The evaluation of cost functions (3.19) derived in the previous section requires a three-dimensional search. To reduce the complexity and to accelerate the three-dimensional search, we can use FFT algorithm. In this section, FFT is exploited to evaluate all terms in the cost functions (3.19).

The terms that need to be evaluated can be separated as three-dimensional, two-dimensional and one-dimensional terms. In the following, we show the FFT-

based evaluation of each of them and present the resulting algorithm in Table 3.1.

3.4.1 Evaluation of Three-Dimensional Terms by FFT

The three-dimensional term in (3.19) is $\mathbf{b}^H(\phi)\mathbf{c}(\theta, f_d)$. This term has most of the computational load. Expanding $\mathbf{b}^H(\phi)\mathbf{c}(\theta, f_d)$, we can write

$$\mathbf{b}^H(\phi)\mathbf{c}(\theta, f_d) = \mathbf{a}_R^H(\phi)\hat{\mathbf{R}}_y^{-1}\mathbf{Y}\mathbf{F}^H(f_d)\mathbf{S}^H\mathbf{a}_T^*(\theta) \quad (3.28)$$

First, we define $\mathbf{X} = \mathbf{Y}\mathbf{F}^H(f_d)\mathbf{S}^H$ and show its solution by FFT as follows,

$$\text{vec}(\mathbf{X}) = \text{vec}(\mathbf{Y}\mathbf{F}^H(f_d)\mathbf{S}^H) \quad (3.29)$$

$$= [\mathbf{S}^* \otimes \mathbf{Y}]\text{vec}(\mathbf{F}^H(f_d)) \quad (3.30)$$

$$= [\mathbf{K}_{sy}]_{(n_T n_R \times L^2)} \text{vec}(\mathbf{F}^H(f_d)) \quad (3.31)$$

where $\mathbf{K}_{sy} = \mathbf{S}^* \otimes \mathbf{Y}$. Since $\mathbf{F}^H(f_d)$ is a diagonal matrix, $\text{vec}(\mathbf{F}^H(f_d))$ has at most L non-zero values. Therefore, by choosing non-zero entries in $\text{vec}(\mathbf{F}^H(f_d))$ and corresponding columns in \mathbf{K}_{sy} , we can write the equivalent of (3.31) as

$$\text{vec}(\mathbf{X}) = [\mathbf{K}'_{sy}]_{(n_T n_R \times L)} \mathbf{a}(f_d) \quad (3.32)$$

where $\mathbf{a}(f_d) = [1 \ e^{-j2\pi f_d} \ \dots \ e^{-j2\pi(L-1)f_d}]^\top$. The matrix \mathbf{K}'_{sy} is found by the operation of choosing the columns and is elaborated further as follows:

$$\begin{aligned} \mathbf{S}^* \otimes \mathbf{Y} &= \begin{bmatrix} s_1^*(0) & s_1^*(1) & \dots & s_1^*(L-1) \\ \vdots & \ddots & \dots & \dots \\ s_{n_T}^*(0) & s_1^*(1) & \dots & s_{n_T}^*(L-1) \end{bmatrix} \otimes \mathbf{Y} \\ &= \begin{bmatrix} s_1^*(0)\mathbf{Y} & s_1^*(1)\mathbf{Y} & \dots & s_1^*(L-1)\mathbf{Y} \\ \vdots & \ddots & \dots & \dots \\ s_{n_T}^*(0)\mathbf{Y} & s_1^*(1)\mathbf{Y} & \dots & s_{n_T}^*(L-1)\mathbf{Y} \end{bmatrix} \end{aligned} \quad (3.33)$$

Choosing the columns in the above matrix gives us:

$$\begin{aligned} \mathbf{K}'_{sy} &= \begin{bmatrix} s_1^*(0)\mathbf{y}(0) & s_1^*(1)\mathbf{y}(1) & \dots & s_1^*(L-1)\mathbf{y}(L-1) \\ \vdots & \ddots & \dots & \dots \\ s_{n_T}^*(0)\mathbf{y}(0) & s_1^*(1)\mathbf{y}(1) & \dots & s_{n_T}^*(L-1)\mathbf{y}(L-1) \end{bmatrix} \\ &= [\mathbf{s}^*(0) \otimes \mathbf{y}(0) \ \dots \ \mathbf{s}^*(L-1) \otimes \mathbf{y}(L-1)] \end{aligned} \quad (3.34)$$

Therefore, $\mathbf{K}_{sy} \text{vec}(\mathbf{F}^H(f_d))$ is nothing but $[\mathbf{S}^* \otimes \mathbf{Y}]\mathbf{a}(f_d)$. This equation shows that we have less entries to calculate by reducing the size of \mathbf{K}_{sy} from $(n_T n_R \times L^2)$ to the size of \mathbf{K}'_{sy} which is $(n_T n_R \times L)$. Now for m -th row vector \mathbf{k}_m^\top in \mathbf{K}'_{sy} ,

$$\mathbf{k}_m^\top \mathbf{a}(f_d) = \sum_{n=0}^{L-1} k_n e^{-j2\pi n f_d} \quad (3.35)$$

This is equivalent to evaluating the FFT of \mathbf{k}^\top , $\mathcal{F}[\mathbf{k}^\top]$. Thus (3.32) can be evaluated for all $f_d \in [-\frac{1}{2}, -\frac{1}{2}]$ for a given resolution by taking row-by-row N_{FFT} -point FFT of \mathbf{K}'_{sy} , i.e., $\mathcal{F}_r[\mathbf{K}'_{sy}]$. After evaluating $\mathcal{F}[\mathbf{K}'_{sy}]$, we get back $[\mathbf{X}]_{(n_R \times n_T)}$ by reshaping $[\text{vec}(\mathbf{X})]_{(n_T n_R \times 1)}$.

The next step is to evaluate $\mathbf{S}^H \mathbf{a}_T^*(\theta)$ which is the solution for the second dimension θ . It can be easily shown in a similar way to (3.35) that for any m -th row vector \mathbf{s}_m^\top in \mathbf{S} , we have

$$\begin{aligned} \mathbf{s}_m^\top \mathbf{a}_T^*(\theta) &= \sum_{p=0}^{n_T-1} s_m(p) e^{-j\pi p \sin(\theta)} \\ &= \sum_{p=0}^{n_T-1} s_m(p) e^{-j2\pi p f_\theta} \equiv \mathcal{F}[\mathbf{s}_m^\top] \end{aligned} \quad (3.36)$$

where $f_\theta = \frac{\sin(\theta)}{2} \in [-\frac{1}{2}, \frac{1}{2}]$.

The third step is to evaluate $\mathbf{a}_R^H(\phi) \hat{\mathbf{R}}_y^{-1}$ which is the third dimension ϕ . For n -th column vector $\mathbf{r}(n)$ in $\hat{\mathbf{R}}_y^{-1}$, we have

$$\begin{aligned} \mathbf{a}_R^H(\phi) \mathbf{r}(n) &= \sum_{m=0}^{n_R-1} r_m(n) e^{-j\pi m \sin(\phi)} \\ &= \sum_{m=0}^{n_R-1} r_m(n) e^{-j2\pi m f_\phi} \equiv \mathcal{F}[\mathbf{r}(n)] \end{aligned} \quad (3.37)$$

where $f_\phi = \frac{\sin(\phi)}{2} \in [-\frac{1}{2}, \frac{1}{2}]$. The three-dimensional term $\mathbf{a}_R^H(\phi) \hat{\mathbf{R}}_y^{-1} \mathbf{X} \mathbf{a}_T^*(\theta)$ can be solved by using above-mentioned three steps.

3.4.2 Evaluation of Two-Dimensional Terms by FFT

The two-dimensional term that appears in (3.23), as shown in Appendix 3.9, it can be represented by 2D-FFT. In more compact matrix form, (3.45) can be written as

$$\|\mathbf{c}(\theta, f_d)\|^2 \equiv \sum_{q=0}^{n_R-1} |\mathcal{F}_2[\mathbf{S}^* \otimes \mathbf{X}_q]|^2 \quad (3.38)$$

3.4.3 Evaluation of One-Dimensional Terms by FFT

The one-dimensional terms are $\mathbf{b}(\phi)$ and $\mathbf{d}(\theta)$. These terms are one-dimensional so there evaluation is straight forward by using (3.37) and (3.36).

3.4.4 Algorithms

The cost function derived in Section 3.3 can be solved efficiently by the above mentioned procedure using FFT for grid of size N_{FFT} -points. The minimum of the solution of (3.17) gives us the estimates of the unknown parameters \hat{f}_{θ_k} , \hat{f}_{ϕ_k} and \hat{f}_{d_k} . We can find $\hat{\theta}_k$ and $\hat{\phi}_k$ by using the relations $\hat{\theta}_k = \sin^{-1}(2\hat{f}_{\theta_k})$ and $\hat{\phi}_k = \sin^{-1}(2\hat{f}_{\phi_k})$. Using the above mentioned FFT-based evaluations, we can develop algorithms using the cost functions derived in Section 3.3. We write the three MPDR-based algorithms in pseudocode form in Table 3.1. MPDR-3D, MPDR-2D and MPDR-1D respectively are based on three-dimensional, two-dimensional and one-dimensional FFT.

The static target case is a special case of the above formulation when the Doppler shift is zero and $\mathbf{F}(f_{d_k}) = \mathbf{I}$. The static target case for comparison with 2D-MUSIC and RD-MUSIC is solved in the coming sections.

3.5 Complexity Analysis

We discuss the complexity of our proposed algorithm in comparison with 2D-MUSIC, RD-MUSIC algorithms [24] and the tensor decomposition based method of [37]. Since, 2D-MUSIC and RD-MUSIC do not estimate the Doppler shift, we make the complexity analysis for static target case only. The same analysis can be extended to the moving target case. The 2D-MUSIC algorithm requires $\mathcal{O}\{Ln_T^2n_R^2+n_T^3n_R^3+m^2[n_Tn_R(n_Tn_R-K)+n_Tn_R-K]\}$ for m searches and K targets (note that m represents number of grid points which is represented by N_{FFT} for our algorithm). The second algorithm used for comparison is RD-MUSIC which requires $\mathcal{O}\{L^2n_T^2n_R^2+n_T^3n_R^3+m[n_T^2n_R(n_Tn_R-K)+n_T^2(n_Tn_R-K)+n_T^2]\}$ where the complexity reduction is achieved by reducing m^2 factor to m by converting the 2D-search problem into two one-dimensional search problem. The tensor decomposition based algorithm requires $\mathcal{O}\{n(K^3 + Kn_Tn_RL) + (n_T^3 + n_R^3)K\}$ where n is the number of iterations required for the convergence of the algorithm [37]. The algorithm converges at an n of 83 on average and is also dependent on K . In contrast, our lowest complexity proposed algorithm (MPDR-2D) requires $\mathcal{O}\{N_{FFT}[n_R \log N_{FFT} + 3n_T \log N_{FFT} + 2M + L + 1] + L(2NL + 2N + LM)\}$ for the static target case. The complexity of our proposed algorithm is lower

Table 3.1: MPDR-based low complexity proposed algorithms

```

1: procedure MPDR-3D(Y)
2:   Compute  $\mathbf{R}_s = \frac{\mathbf{S}\mathbf{S}^H}{L}$ ,  $\hat{\mathbf{R}}_y = \frac{\mathbf{Y}\mathbf{Y}^H}{L}$  and  $\hat{\mathbf{R}}_y^{-1/2}$ 
3:   Compute  $\mathbf{K} = \mathbf{S}^* \circledast \mathbf{Y}$ 
4:   Compute  $\mathbf{K} = \mathcal{F}_r[\mathbf{K}]$ 
5:    $\mathbf{K} \leftarrow \text{reshape}(\mathbf{K})$ 
6:    $\mathbf{P} \leftarrow \mathcal{F}_r[\mathbf{K}]$ 
7:   Compute  $\hat{\mathbf{R}}_y^{-1/2} = \mathcal{F}_c[\hat{\mathbf{R}}_y^{-1/2}]$ 
8:   Get  $\hat{\mathbf{R}}_y^{-1} \leftarrow \hat{\mathbf{R}}_y^{-1}$ 
9:   Compute  $\mathbf{S}^H = \mathcal{F}[\mathbf{S}^H]$ 
10:  Compute  $\mathbf{X} \leftarrow \text{diag}(\hat{\mathbf{R}}_y^{-1/2} \times [\hat{\mathbf{R}}_y^{-H/2}])$ 
11:  Compute  $\mathbf{Y} \leftarrow \text{diag}([\mathbf{S}_s^{-1/2}]^T \times [\mathbf{S}_s^{-1/2}]^*)$ 
12:   $\{\hat{\phi}_k, \hat{\theta}_k, \hat{f}_{d_k}\} = \text{argmax} \frac{|\hat{\mathbf{R}}_y^{-1} \times \mathbf{P}|^{\circ 2}}{L^2 \times \mathbf{X} \circ \mathbf{Y}}$ 
13: end procedure

```

```

1: procedure MPDR-2D(Y)
2:   Compute  $\mathbf{R}_s = \frac{\mathbf{S}\mathbf{S}^H}{L}$ ,  $\hat{\mathbf{R}}_y = \frac{\mathbf{Y}\mathbf{Y}^H}{L}$  and  $\hat{\mathbf{R}}_y^{-1}$ 
3:    $\mathbf{X} = \mathbf{R}_y^{-1} \mathbf{Y}$ 
4:   Solve (3.23)
5:    $\{\hat{\phi}_k, \hat{f}_{d_k}\} \leftarrow \text{argmax} \text{ (3.27)}$ 
6:    $\{\hat{\phi}_k^i\} \leftarrow \text{argmax} \text{ (3.19) using } \{\hat{\phi}_k, \hat{f}_{d_k}\}$ 
7: end procedure

```

```

1: procedure MPDR-1D(Y)
2:   Compute  $\mathbf{R}_s = \frac{\mathbf{S}\mathbf{S}^H}{L}$ ,  $\hat{\mathbf{R}}_y = \frac{\mathbf{Y}\mathbf{Y}^H}{L}$  and  $\hat{\mathbf{R}}_y^{-1}$ 
3:    $\hat{f}_{d_k}^i \leftarrow \text{argmax} \text{ eig}(\mathbf{A}(f_d), L^2 \hat{\mathbf{R}}_y^{-1})$ 
4:    $\hat{\phi}_k^i \leftarrow \text{argmax} \text{ (3.27) using } \hat{f}_{d_k}^i$ 
5:    $\{\hat{\phi}_k, \hat{\theta}_k, \hat{f}_{d_k}\} \leftarrow \text{argmax} \text{ (3.19) using } \{\hat{\phi}_k, \hat{f}_{d_k}\}$ 
6: end procedure

```

than the three algorithms used for comparison in this complexity analysis. This reduced complexity is achieved because our algorithm exploits the low complexity of the FFT and is reduced dimension. The average runtime for the three above mentioned algorithms is independent of SNR.

3.6 Simulation Results and Discussion

We run some simulations to validate the algorithms proposed in this chapter. We assume multiple targets ($K = 3$) at $\phi_k = [10^\circ, 20^\circ, 30^\circ]$ and $\theta_k = [-10^\circ, 0^\circ, 10^\circ]$ with normalized Doppler shift $f_{d_k} = [-0.1, 0.1, 0.2]$. The grid search is varied from -90° to $+90^\circ$. For simplicity, we assume that the targets lie on some grid point which means they are on-grid targets. The transmitted signals are uncorrelated quadrature phase shift keying (QPSK) symbols. The noise is assumed to be uncorrelated Gaussian with zero mean and variance $\sigma_{\mathbf{z}}^2$. The noise variance $\sigma_{\mathbf{z}}^2$ was varied to control the SNR. For the simulations, SNR is defined as $\text{SNR} = 10 \log(1/\sigma_{\mathbf{z}}^2)$ where the power at each antenna is normalized so that total transmit power is unity. The number of antenna elements are $n_T = 8$ and $n_R = 8$, the number of snapshots L are 64, the number of grid points are 512 in most of the results and the MSE is averaged over 1000 iterations, otherwise the values are mentioned accordingly.

3.6.1 Static Target Comparison

We assume that a single target lies on the grid at (θ_k, ϕ_k) . The two parameters to be estimated (θ_k and ϕ_k) are generated randomly according to $[\theta_k, \phi_k] \sim \mathcal{U}(-10^\circ, 10^\circ)$. In Fig. 3.2 and Fig. 3.3, the MSE error performance for the DOA ($\hat{\phi}_k$) estimation and DOD ($\hat{\theta}_k$) estimation are plotted respectively, of the proposed algorithm for static target case. We also compare the performance of our algorithm with both 2D-MUSIC and RD-MUSIC algorithms. The number of antenna elements are $n_T = 10$ and $n_R = 10$, the number of snapshots L are 256 and the number of grid points are 512. The 2D-MUSIC and RD-MUSIC algorithms have almost the same performance. The results show that our proposed algorithm outperforms 2D-MUSIC and RD-MUSIC algorithms. The error floor that appears in the MSE of $\hat{\theta}_k$ for 2D-MUSIC and RD-MUSIC requires some explanation. The signal model used in 2D-MUSIC and RD-MUSIC assumes that the transmitted signals are fully uncorrelated and orthogonal, i.e. $\mathbf{E}[\mathbf{s}(n)\mathbf{s}^H(n)] = \mathbf{I}$ where \mathbf{I} is the identity matrix. If the transmitted signals are not fully uncorrelated, then 2D-MUSIC and RD-MUSIC algorithms fail to recover θ_k . Our approach utilizes $\mathbf{s}(n)$ and does not require the assumption $\mathbf{E}[\mathbf{s}(n)\mathbf{s}^H(n)] = \mathbf{I}$, therefore, it outperforms both 2D-MUSIC and RD-MUSIC algorithms in estimating θ_k .

3.6.2 MSE Performance of ϕ_k Estimation

First we show how the MSE performance is effected by reducing the dimensions.

Figure 3.4 shows the MSE performance of DOA ($\hat{\phi}_k$) obtained by all of the pro-

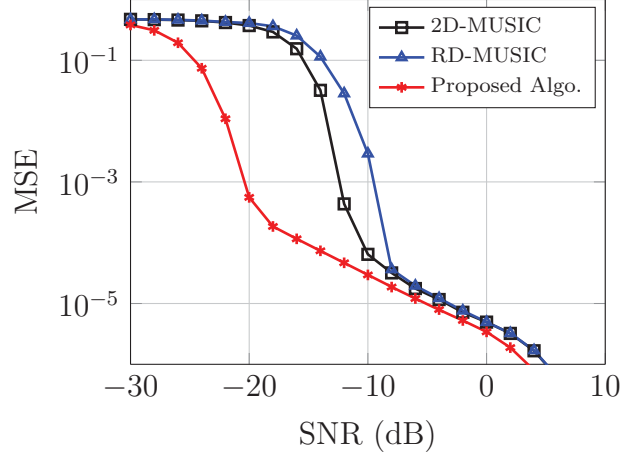


Figure 3.2: MSE performance for DOA estimation ($\hat{\phi}_k$) using $J_1(\phi_k, \theta_k)$. Simulation parameters: $L = 256$, $n_T = 10$, $n_R = 10$.

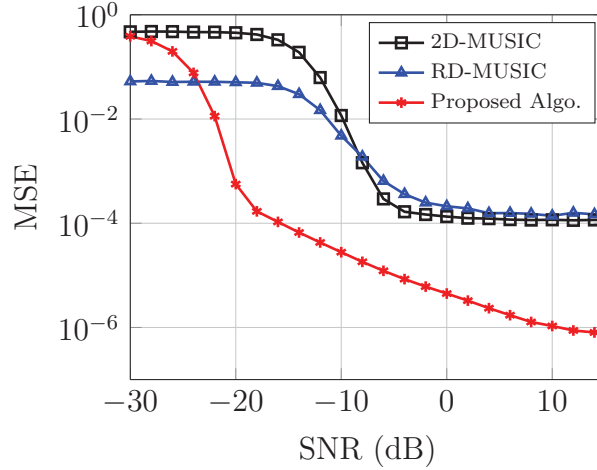


Figure 3.3: MSE performance for DOD estimation ($\hat{\theta}_k$) using $J_1(\phi_k, \theta_k)$. Simulation parameters: $L = 256$, $n_T = 10$, $n_R = 10$.

posed three algorithms. The results show that at an MSE of 10^{-2} , the SNR loss incurred in going from 3D to 2D is 1 dB whereas from 2D to 1D is 1.5 dB approximately. The performance loss that occurred in reducing the dimensions is due the assumptions that were made in the cost function simplification.

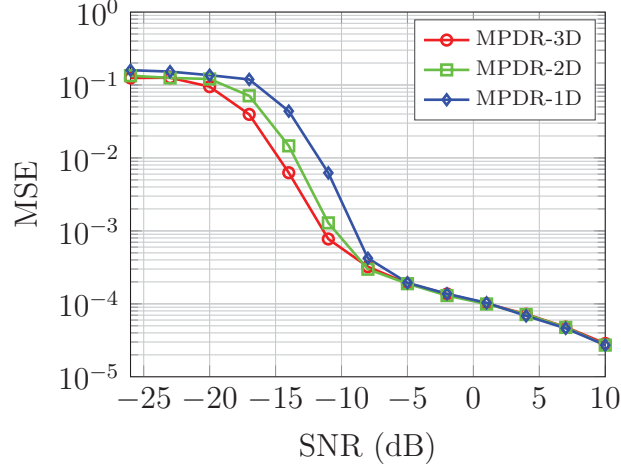


Figure 3.4: MSE performance of DOA ϕ_k for moving target. Simulation parameters: $L = 64$, $n_T = 8$, $n_R = 8$, $K = 3$.

3.6.3 MSE Performance of θ_k Estimation

The simulation results for θ_k estimation are shown in Fig. 3.5. The results show that both MPDR-1D outperforms the algorithms presented in [89], [84] and [90]. The algorithms of [89], [84] and [90] are all subspace methods and are unable to provide optimum results for multiple target parameter estimation. Only the method of [90] shows slightly better performance than [89] and [84] at high SNR. The two algorithms [89] and [84] reach an error floor while resolving multiple targets.

3.6.4 MSE Performance of f_{d_k} Estimation

The MSE performance results for Doppler shift estimation are shown in Fig. 3.6. The simulation results show that our proposed algorithms MPDR-1D outperforms the algorithms of [89], [84] and [90]. Only the algorithm of [84] shows slight improvement at high SNR.

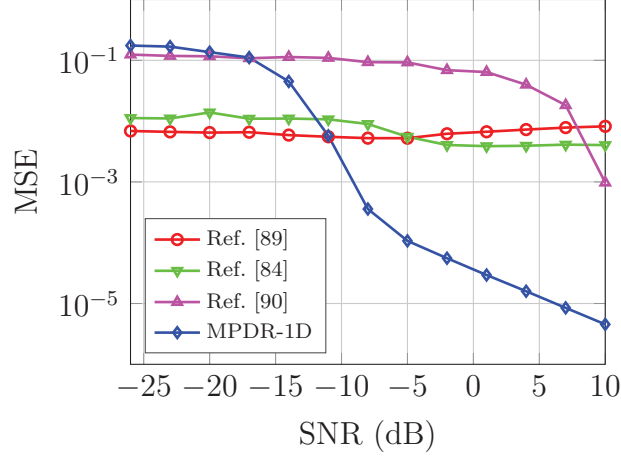


Figure 3.5: MSE performance of DOD θ_k for moving target. Simulation parameters: $L = 64$, $n_T = 8$, $n_R = 8$, $K = 3$.

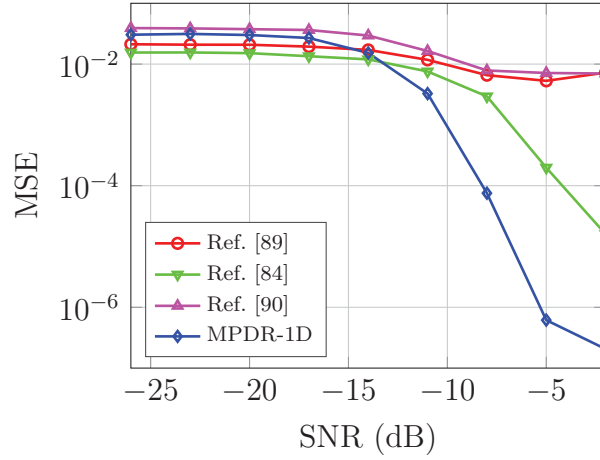


Figure 3.6: MSE performance of Doppler f_{dk} for moving target. Simulation parameters: $L = 64$, $n_T = 8$, $n_R = 8$, $K = 3$.

3.6.5 Complexity Comparison

The processing time for the proposed algorithms is shown in Table 3.2. Both the average runtime and memory required is shown for the discussed algorithms. It is evident from the results that the minimum processing time is achieved by 1D-FFT based algorithms for MPDR. Here, we will mention two more direction finding algorithms 2D-MUSIC and RD-MUSIC [24]. Both these algorithms cannot

Table 3.2: Complexity comparison.

Algorithm	Average Runtime (sec)	Memory requirements (MB)
MPDR-3D	7.33	-
MPDR-2D	0.13	61.84
MPDR-1D	0.09	1.01
Ref. [89]	2.02	4.56
Ref. [84]	0.53	673.99
Ref. [90]	0.33	0.81

estimate the Doppler shift. However, the average runtime per iteration is found to be 29.87 and 0.14 seconds for 2D-MUSIC and RD-MUSIC, respectively without estimating the Doppler shift for $n_T = n_R = 8$. The runtime for both algorithms is higher than our proposed 1D algorithms. In contrast, for the same number of antennas, MPDR-2D took 0.11 seconds with the Doppler estimation. The runtime is calculated using a machine with Xeon E5-2680 2.8 GHz dual-processors with maximum available RAM of 64 GB. Furthermore, for a same set of parameters, it is found by using the complexity analysis in section 3.5 that MPDR-2D is approximately 7 times faster than the tensor decomposition based algorithm of [37].

3.7 Concluding Remarks

In this chapter, a new FFT-based DOA, DOD and Doppler shift estimation algorithms using adaptive beamformer weight vector at the receiver for bistatic MIMO radar is proposed. We derive the reduced-dimension cost functions for MPDR es-

timators for the moving target case. The MPDR-based algorithms exhibit an error floor at high SNR. The MSE performance of MPDR-3D is shown to have better performance than 2D-MUSIC and RD-MUSIC.

As far as computational complexity is concerned, the MPDR-1D (with the Doppler shift estimation) beat 2D-MUSIC and RD-MUSIC (without the Doppler shift estimation). The reduced-dimension MPDR-1D algorithm have the lowest memory requirements because they are based on one-dimensional search. Since, FFT can be deployed easily on hardware, the approach presented here is also practical in radar applications.

3.8 APPENDIX A: Proof of Equation (3.18)

We need to evaluate the following expression

$$\frac{1}{\|\mathbf{b}(\phi)\|^2} = \frac{1}{\mathbf{a}_R^H(\phi)\mathbf{R}_y^{-1}\mathbf{a}_R(\phi)} \quad (3.39)$$

The received signal covariance matrix $\hat{\mathbf{R}}_y$ for k -th target is given by

$$\hat{\mathbf{R}}_y = n_T |\beta_k|^2 \mathbf{a}_R(\phi_k) \mathbf{a}_R^H(\phi_k) + \sigma_{\mathbf{z}}^2 \mathbf{I}_{n_R} \quad (3.40)$$

where we have assumed that $\mathbf{z}(n)$ is zero mean uncorrelated Gaussian noise with variance $\sigma_{\mathbf{z}}^2$ and is independent from the transmitted signal $\mathbf{s}(n)$. The inverse of

$\hat{\mathbf{R}}_y$ is found by using the matrix inversion lemma,

$$\hat{\mathbf{R}}_y^{-1} = \frac{1}{\sigma_{\mathbf{z}}^2} \mathbf{I}_{n_R} - \frac{n_T |\beta_k|^2 \mathbf{a}_R(\phi_k) \mathbf{a}_R^H(\phi_k)}{\sigma_{\mathbf{z}}^4 + \sigma_{\mathbf{z}}^2 n_T n_R |\beta_k|^2} \quad (3.41)$$

Using (3.41), the expression of (3.39) is given by

$$\frac{1}{\|\mathbf{b}(\phi)\|^2} = \frac{\sigma_{\mathbf{z}}^4 + \sigma_{\mathbf{z}}^2 n_T n_R |\beta_k|^2}{\sigma_{\mathbf{z}}^2 n_R + n_T |\beta_k|^2 [n_R^2 - |\mathbf{a}_R^H(\phi_k) \mathbf{a}_R(\phi)|^2]} \quad (3.42)$$

The result obtained in (3.42) depends on β_k . For the case when $\phi = \phi_k$, β_k will have a non-zero value (target is present) but for the case when $\phi \neq \phi_k$, β_k will be zero (target is absent). Thus, we can interpret the relation in (3.42) as the following

$$\frac{1}{\|\mathbf{b}(\phi)\|^2} = \begin{cases} n_T |\beta_k|^2 + \frac{\sigma_{\mathbf{z}}^2}{n_R}, & \phi = \phi_k \\ \frac{\sigma_{\mathbf{z}}^2}{n_R}, & \phi \neq \phi_k \end{cases} \quad (3.43)$$

Therefore, the last result in (3.43) shows that the expression in (3.39) can be treated as constant.

3.9 APPENDIX B: Proof of Equation (3.38)

The two-dimensional term is given by

$$\|\mathbf{c}(\theta, f_d)\|^2 = \mathbf{a}_T^T(\theta) \mathbf{S} \mathbf{F}(f_d) \mathbf{Y}^H \hat{\mathbf{R}}_y^{-1} \mathbf{Y} \mathbf{F}^H(f_d) \mathbf{S}^H \mathbf{a}_T^*(\theta)$$

$$= \mathbf{a}_T^T(\theta) \mathbf{S} \mathbf{F}(f_d) \mathbf{X}^H \mathbf{X} \mathbf{F}^H(f_d) \mathbf{S}^H \mathbf{a}_T^*(\theta) \quad (3.44)$$

where $\mathbf{X} = \hat{\mathbf{R}}_y^{-1/2} \mathbf{Y}$. First we solve $\mathbf{S}^H \mathbf{a}_T^*(\theta)$ by opening the matrices,

$$\begin{aligned} \mathbf{S}^H \mathbf{a}_T^*(\theta) &= \begin{bmatrix} s_0^*(0) & s_1^*(0) & \dots & s_{n_T-1}^*(0) \\ s_0^*(1) & s_1^*(1) & \dots & s_{n_T-1}^*(1) \\ \vdots & \ddots & \dots & \vdots \\ s_0^*(L-1) & s_1^*(L-1) & \dots & s_{n_T-1}^*(L-1) \end{bmatrix} \begin{bmatrix} 1 \\ e^{-j2\pi f_\theta} \\ \vdots \\ e^{-j2\pi(n_T-1)f_\theta} \end{bmatrix} \\ &= \begin{bmatrix} \sum_{m=0}^{n_T-1} s_m^*(0) e^{-j2\pi m f_\theta}, & \sum_{m=0}^{n_T-1} s_m^*(1) e^{-j2\pi m f_\theta}, & \dots, \\ & \sum_{m=0}^{n_T-1} s_m^*(L-1) e^{-j2\pi m f_\theta} \end{bmatrix}^T \end{aligned}$$

Then, we solve $\mathbf{X} \mathbf{F}^H(f_d)$

$$\begin{aligned} &\mathbf{X} \mathbf{F}^H(f_d) \\ &= \begin{bmatrix} x_0(0) & x_0(1) & \dots & x_0(L-1) \\ x_1(0) & x_1(1) & \dots & x_1(L-1) \\ \vdots & \ddots & \dots & \vdots \\ x_{n_R-1}(0) & x_{n_R-1}(1) & \dots & x_{n_R-1}(L-1) \end{bmatrix} \begin{bmatrix} 1 & 0 & \dots & 0 \\ 0 & e^{-j2\pi f_d} & \dots & 0 \\ \vdots & \ddots & \dots & \vdots \\ 0 & 0 & \dots & e^{-j2\pi(L-1)f_d} \end{bmatrix} \end{aligned}$$

Multiplying the above two results of $\mathbf{S}^H \mathbf{a}_T^*(\theta)$ and $\mathbf{X} \mathbf{F}^H(f_d)$, we get

$$\mathbf{X} \mathbf{F}^H(f_d) \mathbf{S}^H \mathbf{a}_T^*(\theta)$$

$$\begin{aligned}
&= \begin{bmatrix} x_0(0) & \dots & x_0(L-1)e^{-j2\pi(L-1)f_d} \\ x_1(0) & \dots & x_1(L-1)e^{-j2\pi(L-1)f_d} \\ \vdots & \dots & \vdots \\ x_{n_R-1}(0) & \dots & x_{n_R-1}(L-1)e^{-j2\pi(L-1)f_d} \end{bmatrix} \begin{bmatrix} \sum_{m=0}^{n_T-1} s_m^*(0)e^{-j2\pi mf_\theta} \\ \sum_{m=0}^{n_T-1} s_m^*(1)e^{-j2\pi mf_\theta} \\ \vdots \\ \sum_{m=0}^{n_T-1} s_m^*(L-1)e^{-j2\pi mf_\theta} \end{bmatrix} \\
&= \begin{bmatrix} \sum_{m=0}^{n_T-1} \sum_{p=0}^{L-1} s_m^*(p)x_0(p)e^{-j2\pi mf_\theta}e^{-j2\pi pf_d}, \\ \sum_{m=0}^{n_T-1} \sum_{p=0}^{L-1} s_m^*(p)x_1(p)e^{-j2\pi mf_\theta}e^{-j2\pi pf_d}, \dots, \\ \sum_{m=0}^{n_T-1} \sum_{p=0}^{L-1} s_m^*(p)x_{n_R-1}(p)e^{-j2\pi mf_\theta}e^{-j2\pi pf_d} \end{bmatrix}
\end{aligned}$$

The term $\mathbf{a}_T^\top(\theta)\mathbf{S}\mathbf{F}(f_d)\mathbf{X}^\mathbf{H}$ is the Hermitian of $\mathbf{X}\mathbf{F}^\mathbf{H}(f_d)\mathbf{S}^\mathbf{H}\mathbf{a}_T^*(\theta)$. Thus, multiplying the vector above with its Hermitian gives,

$$\begin{aligned}
&\mathbf{a}_T^\top(\theta)\mathbf{S}\mathbf{F}(f_d)\mathbf{X}^\mathbf{H}\mathbf{X}\mathbf{F}^\mathbf{H}(f_d)\mathbf{S}^\mathbf{H}\mathbf{a}_T^*(\theta) \\
&= \left| \sum_{m=0}^{n_T-1} \sum_{p=0}^{L-1} s_m^*(p)x_0(p)e^{-j2\pi mf_\theta}e^{-j2\pi pf_d} \right|^2 \\
&\quad + \left| \sum_{m=0}^{n_T-1} \sum_{p=0}^{L-1} s_m^*(p)x_1(p)e^{-j2\pi mf_\theta}e^{-j2\pi pf_d} \right|^2 + \dots \\
&\quad + \left| \sum_{m=0}^{n_T-1} \sum_{p=0}^{L-1} s_m^*(p)x_{n_R-1}(p)e^{-j2\pi mf_\theta}e^{-j2\pi pf_d} \right|^2 \\
&= \sum_{q=0}^{n_R-1} \left| \sum_{m=0}^{n_T-1} \sum_{p=0}^{L-1} s_m^*(p)x_q(p)e^{-j2\pi mf_\theta}e^{-j2\pi pf_d} \right|^2 \tag{3.45}
\end{aligned}$$

This evaluated term is equivalent to 2D-FFT expression. Its FFT-based solution is further discussed in Section 3.4.

CHAPTER 4

APES-BASED REDUCED COMPLEXITY DOA AND DOD ESTIMATION FOR MOVING TARGET IN BISTATIC MIMO RADAR

4.1 Introduction

In this chapter, we propose another reduced dimension and low complexity algorithm to estimate DOA, DOD and the Doppler shift of a moving target for a MIMO radar. We derive the cost function based on APES objective function. First, we solve each cost function with a low complexity FFT-based solution in three dimen-

sions. We further carry out a derivation to reduce the three-dimensional search to two-dimensional search and solve it with a 2D-FFT. Another reduced dimension algorithm is derived using the generalized eigen value method which finds the estimate of unknown parameters in one dimension with less memory constraints. This way, we propose three algorithms based on the cost function simplification. We show simulation results for a static target case and a moving target case. Also, we have considered the scenarios of on-grid targets and off-grid targets. We compare the MSE performance and computational complexity of our proposed algorithms with existing algorithms as well. We show that our proposed algorithms have better MSE performance than existing algorithms and achieves the CRLB for all unknown target parameters. The proposed algorithms exhibit lower computational complexity than the existing ones and also provide an estimate for the Doppler shift.

4.1.1 Organization of the Chapter

The rest of the chapter is organized as follows: The bistatic MIMO radar signal model for DOA, DOD and Doppler estimation is the same as presented in Chapter 3 Section 3.2. Section 4.2 presents the proposed parameter estimation algorithms for DOA, DOD and Doppler estimation and the derivations to reduce the dimensions. In section 4.3, we develop the FFT-based algorithm to estimate the parameters. The complexity analysis and its comparison with existing algorithms is shown in section 4.4. In section 4.5, we show the necessary calculations

to find CRLB for both cases of static target and moving target. Simulation results are presented in section 4.6 and we conclude the chapter in section 4.7.

4.2 APES-based Reduced Dimension Estimation

The received signal vector in (3.1) can be multiplied by a weight vector $\mathbf{w}(\phi)$ to increase the SNR, as follows

$$\mathbf{w}^H(\phi)\mathbf{y}(n) = \beta e^{j(2\pi n f_d)} \mathbf{w}^H(\phi) \mathbf{a}_R(\phi) \mathbf{a}_T^T(\theta) \mathbf{s}(n) + \mathbf{w}^H(\phi) \mathbf{z}(n) \quad (4.1)$$

There can be another approach to calculate the weight vector $\mathbf{w}(\phi)$. The first approach is based on MPDR as discussed in Chapter 3. The second approach is called APES and is discussed here.

In this section, the parameters are estimated on the basis of APES algorithm [91]. In APES, we want to choose the weight vector \mathbf{w} such that the filter output is as close as possible in least-squares (LS) sense to $\beta_k e^{j(2\pi n f_{d_k})} \mathbf{a}_T^T(\theta_k) \mathbf{s}(n)$ while keeping the desired signal undistorted. Therefore, we need to solve the following linearly-constrained optimization problem,

$$\begin{aligned} \{\mathbf{w}_A(\phi), \beta_A\} &= \min_{\mathbf{w}(\phi), \beta} \mathbf{E} |\mathbf{w}^H(\phi) \mathbf{y}(n) - \beta e^{j(2\pi n f_d)} \mathbf{a}_T^T(\theta) \mathbf{s}(n)|^2 \\ \text{subject to} \quad & \mathbf{w}^H(\phi) \mathbf{a}_R(\phi) = 1 \end{aligned} \quad (4.2)$$

which can be re-written in equivalent matrix form as

$$\begin{aligned} \{\mathbf{w}_A(\phi), \beta_A\} &= \min_{\mathbf{w}(\phi), \beta} \frac{1}{L} \|\mathbf{w}^H(\phi) \mathbf{Y} - \beta \mathbf{a}_T^T(\theta) \mathbf{S} \mathbf{F}(f_d)\|_2^2 \\ \text{subject to} \quad &\mathbf{w}^H(\phi) \mathbf{a}_R(\phi) = 1 \end{aligned} \quad (4.3)$$

The objective function in the above equation can be simplified as,

$$\begin{aligned} &\frac{1}{L} \|\mathbf{w}^H(\phi) \mathbf{Y} - \beta \mathbf{a}_T^T(\theta) \mathbf{S} \mathbf{F}(f_d)\|_2^2 \\ &= \mathbf{w}^H(\phi) \hat{\mathbf{R}}_y \mathbf{w}(\phi) - \frac{\mathbf{w}^H(\phi) \mathbf{Y} \mathbf{F}^H(f_d) \mathbf{S}^H \mathbf{a}_T^*(\theta) \mathbf{a}_T^T(\theta) \mathbf{S} \mathbf{F}(f_d) \mathbf{Y}^H \mathbf{w}(\phi)}{L \mathbf{a}_T^T(\theta) \mathbf{S} \mathbf{S}^H \mathbf{a}_T^*(\theta)} \\ &= \mathbf{w}^H(\phi) \left[\hat{\mathbf{R}}_y - \frac{\mathbf{Y} \mathbf{F}^H(f_d) \mathbf{S}^H \mathbf{a}_T^*(\theta) \mathbf{a}_T^T(\theta) \mathbf{S} \mathbf{F}(f_d) \mathbf{Y}^H}{L \mathbf{a}_T^T(\theta) \mathbf{S} \mathbf{S}^H \mathbf{a}_T^*(\theta)} \right] \mathbf{w}(\phi) \\ &= \mathbf{w}^H(\phi) \hat{\mathbf{Q}} \mathbf{w}(\phi) \end{aligned} \quad (4.4)$$

$$(4.5)$$

where

$$\hat{\mathbf{Q}} \triangleq \hat{\mathbf{R}}_y - \frac{\mathbf{Y} \mathbf{F}^H(f_d) \mathbf{d}(\theta) \mathbf{d}^H(\theta) \mathbf{F}(f_d) \mathbf{Y}^H}{L \|\mathbf{d}(\theta)\|^2}. \quad (4.6)$$

Using the above result, equation (4.5) can be re-written as

$$\min_{\mathbf{w}(\phi)} \mathbf{w}^H(\phi) \hat{\mathbf{Q}} \mathbf{w}(\phi) \quad \text{subject to } \mathbf{w}^H(\phi) \mathbf{a}_R(\phi) = 1 \quad (4.7)$$

which yields [91]

$$\mathbf{w}_{\text{APES}}(\phi) = \frac{\hat{\mathbf{Q}}^{-1} \mathbf{a}_R(\phi)}{\mathbf{a}_R^H(\phi) \hat{\mathbf{Q}}^{-1} \mathbf{a}_R(\phi)} \quad (4.8)$$

Using (4.8) to solve (4.5), we denote

$$J_A(\phi, \theta, f_d) = \frac{1}{\mathbf{a}_R^H(\phi) \hat{\mathbf{Q}}^{-1} \mathbf{a}_R(\phi)} \quad (4.9)$$

and use the matrix inversion lemma to find the inverse of $\hat{\mathbf{Q}}$, given by

$$\hat{\mathbf{Q}}^{-1} = \hat{\mathbf{R}}_y^{-1} + \frac{\hat{\mathbf{R}}_y^{-H/2} \mathbf{c}(\theta, f_d) \mathbf{c}^H(\theta, f_d) \hat{\mathbf{R}}_y^{-1/2}}{L \|\mathbf{d}(\theta)\|^2 - \|\mathbf{c}(\theta, f_d)\|^2} \quad (4.10)$$

By putting $\hat{\mathbf{Q}}^{-1}$ in (4.9) and taking the factor $1/\|\mathbf{b}(\theta)\|^2$ common, we express (4.9) as,

$$J_A(\phi, \theta, f_d) = \frac{1}{\|\mathbf{b}(\phi)\|^2} \times \frac{1}{1 + \frac{|\mathbf{b}^H(\phi) \mathbf{c}(\theta, f_d)|^2}{\|\mathbf{b}(\phi)\|^2 [L \|\mathbf{d}(\theta)\|^2 - \|\mathbf{c}(\theta, f_d)\|^2]}} \quad (4.11)$$

The cost function in (4.11) is non-convex, non-linear and can have local minima. By using the proof in Section 3.8 of Chapter 3, we can minimize (4.11) by minimizing $J'_A(\phi, \theta, f_d)$ as follows

$$J'_A(\phi, \theta, f_d) = \frac{1}{1 + \frac{|\mathbf{b}^H(\phi) \mathbf{c}(\theta, f_d)|^2}{\|\mathbf{b}(\phi)\|^2 [L \|\mathbf{d}(\theta)\|^2 - \|\mathbf{c}(\theta, f_d)\|^2]}} \quad (4.12)$$

which is equivalent to the maximization of

$$J''_A(\phi, \theta, f_d) = \frac{|\mathbf{b}^H(\phi) \mathbf{c}(\theta, f_d)|^2}{\|\mathbf{b}(\phi)\|^2 [L \|\mathbf{d}(\theta)\|^2 - \|\mathbf{c}(\theta, f_d)\|^2]} \quad (4.13)$$

The maximization of the cost function in (4.13) gives us the initial estimates

$\hat{\phi}_k, \hat{\theta}_k, \hat{f}_{d_k}$ of the unknown parameters of the target to minimize (4.11). The cost function in (4.13) is a three-dimensional function and its global minimum can be found by exhaustive search. We propose a fast algorithm to solve this exhaustive search by using three-dimensional FFT in Section 4.3. We call this proposed algorithm as APES-1.

In the following, we show the derivation to reduce the dimensions of the three-dimensional search of (4.13). By using the definitions

$$\mathbf{b}(\phi) \triangleq \hat{\mathbf{R}}_y^{-1/2} \mathbf{a}_R(\phi) \quad (4.14)$$

$$\mathbf{c}(\theta, f_d) \triangleq \hat{\mathbf{R}}_y^{-1/2} \mathbf{Y} \mathbf{F}^H(f_d) \mathbf{d}(\theta) \quad (4.15)$$

we can express (4.13) as the following

$$J_A''(\phi, \theta, f_d) = \frac{|\tilde{\mathbf{b}}^H(\phi) \tilde{\mathbf{c}}(\theta, f_d)|^2 \|\mathbf{c}(\theta, f_d)\|^2}{L \|\mathbf{d}(\theta)\|^2 - \|\mathbf{c}(\theta, f_d)\|^2} \quad (4.16)$$

Replacing $\tilde{\mathbf{b}}(\phi)$ by $\tilde{\mathbf{c}}(\theta, f_d)$, we get

$$g_A(\theta, f_d) = \frac{\|\mathbf{c}(\theta, f_d)\|^2}{L \|\mathbf{d}(\theta)\|^2 - \|\mathbf{c}(\theta, f_d)\|^2} \quad (4.17)$$

The function $g_A(\theta, f_d)$ can be solved by 2D-FFT as shown in Section 3.9 of Chapter 3. The estimates $\hat{\theta}_k$ and \hat{f}_{d_k} can be found by searching the peak in the two-dimensional function $g_A(\theta, f_d)$. Using the initial estimates $\hat{\theta}_k$ and \hat{f}_{d_k} , (4.13) will be a one-dimensional function in ϕ . Thus, we have reduced the three-dimensional

search problem into a combination of two-dimensional and one-dimensional search.

We name this algorithm as APES-2D.

Next, we convert the two-dimensional search into two one-dimensional searches.

The function $\hat{\theta}_k$ and \hat{f}_{d_k} can be written as

$$g_A(\theta, f_d) = \frac{\mathbf{a}_T^T(\theta) [\mathbf{A}(f_d)\mathbf{A}^H(f_d)] \mathbf{a}_T^*(\theta)}{\mathbf{a}_T^T(\theta) [L\mathbf{S}\mathbf{S}^H - \mathbf{A}(f_d)\mathbf{A}^H(f_d)] \mathbf{a}_T^*(\theta)} \quad (4.18)$$

where we have used the definition

$$\mathbf{A}(f_d) \triangleq \mathbf{S}\mathbf{F}(f_d)\mathbf{Y}^H\hat{\mathbf{R}}_y^{-H/2} \quad (4.19)$$

for the matrix $\mathbf{A}(f_d)$. The function in (4.18) can be seen as a generalized eigen

value problem. The maximum generalized eigen value of the two matrices $\mathbf{A}(f_d)\mathbf{A}^H(f_d)$

and $L\mathbf{S}\mathbf{S}^H - \mathbf{A}(f_d)\mathbf{A}^H(f_d)$,

$$h_A(f_d) = \lambda_{\max}(f_d) \quad (4.20)$$

where $\lambda_{\max}(f_d)$ denote the maximum generalized eigen value of the matrices

$\mathbf{A}(f_d)\mathbf{A}^H(f_d)$ and $L\mathbf{S}\mathbf{S}^H - \mathbf{A}(f_d)\mathbf{A}^H(f_d)$ for a given f_d . The estimate \hat{f}_{d_k} can be

found by searching the peak in the one-dimensional function (4.20). The estimate

\hat{f}_{d_k} is substituted in (4.17) to get

$$g'_A(\theta) = \frac{\|\mathbf{c}(\theta, \hat{f}_{d_k})\|^2}{L\|\mathbf{d}(\theta)\|^2 - \|\mathbf{c}(\theta, \hat{f}_{d_k})\|^2} \quad (4.21)$$

The reduced dimension functions in (4.20), (4.18) and $J_A''(\phi, \hat{\theta}, \hat{f}_{d_k})$ gives the initial estimates of the unknown parameters in three one-dimensional searches which will be used to minimize the cost function in (4.11). We name this algorithm as APES-1D.

4.3 Reduced Complexity FFT-based Solution

The evaluation of cost functions (4.13) derived in the previous section requires a three-dimensional search. To reduce the complexity and to accelerate the three-dimensional search, we can use FFT algorithm. In this section, FFT is exploited to evaluate all terms in the cost functions (4.13).

The terms that need to be evaluated can be separated as three-dimensional, two-dimensional and one-dimensional terms. In the following, we show the FFT-based evaluation of each of them and present the resulting algorithm in Table 4.1.

4.3.1 Evaluation of Three-Dimensional Terms by FFT

The three-dimensional term that is same in both (3.19) and (4.13) is $\mathbf{b}^H(\phi)\mathbf{c}(\theta, f_d)$. This term has most of the computational load. Expanding $\mathbf{b}^H(\phi)\mathbf{c}(\theta, f_d)$, we can write

$$\mathbf{b}^H(\phi)\mathbf{c}(\theta, f_d) = \mathbf{a}_R^H(\phi)\hat{\mathbf{R}}_y^{-1}\mathbf{Y}\mathbf{F}^H(f_d)\mathbf{S}^H\mathbf{a}_T^*(\theta) \quad (4.22)$$

First, we define $\mathbf{X} = \mathbf{Y}\mathbf{F}^H(f_d)\mathbf{S}^H$ and show its solution by FFT as follows,

$$\text{vec}(\mathbf{X}) = \text{vec}(\mathbf{Y}\mathbf{F}^H(f_d)\mathbf{S}^H) \quad (4.23)$$

$$= [\mathbf{S}^* \otimes \mathbf{Y}] \text{vec}(\mathbf{F}^H(f_d)) \quad (4.24)$$

$$= [\mathbf{K}_{sy}]_{(n_T n_R \times L^2)} \text{vec}(\mathbf{F}^H(f_d)) \quad (4.25)$$

where $\mathbf{K}_{sy} = \mathbf{S}^* \otimes \mathbf{Y}$. Since $\mathbf{F}^H(f_d)$ is a diagonal matrix, $\text{vec}(\mathbf{F}^H(f_d))$ has at most L non-zero values. Therefore, by choosing non-zero entries in $\text{vec}(\mathbf{F}^H(f_d))$ and corresponding columns in \mathbf{K}_{sy} , we can write the equivalent of (4.25) as

$$\text{vec}(\mathbf{X}) = [\mathbf{K}'_{sy}]_{(n_T n_R \times L)} \mathbf{a}(f_d) \quad (4.26)$$

where $\mathbf{a}(f_d) = [1 \ e^{-j2\pi f_d} \ \dots \ e^{-j2\pi(L-1)f_d}]^T$. The matrix \mathbf{K}'_{sy} is found by the operation of choosing the columns and is elaborated further as follows:

$$\begin{aligned} \mathbf{S}^* \otimes \mathbf{Y} &= \begin{bmatrix} s_1^*(0) & s_1^*(1) & \dots & s_1^*(L-1) \\ \vdots & \ddots & \dots & \dots \\ s_{n_T}^*(0) & s_{n_T}^*(1) & \dots & s_{n_T}^*(L-1) \end{bmatrix} \otimes \mathbf{Y} \\ &= \begin{bmatrix} s_1^*(0)\mathbf{Y} & s_1^*(1)\mathbf{Y} & \dots & s_1^*(L-1)\mathbf{Y} \\ \vdots & \ddots & \dots & \dots \\ s_{n_T}^*(0)\mathbf{Y} & s_{n_T}^*(1)\mathbf{Y} & \dots & s_{n_T}^*(L-1)\mathbf{Y} \end{bmatrix} \end{aligned} \quad (4.27)$$

Choosing the columns in the above matrix gives us:

$$\begin{aligned} \mathbf{K}'_{sy} &= \begin{bmatrix} s_1^*(0)\mathbf{y}(0) & s_1^*(1)\mathbf{y}(1) & \cdots & s_1^*(L-1)\mathbf{y}(L-1) \\ \vdots & \ddots & \cdots & \cdots \\ s_{n_T}^*(0)\mathbf{y}(0) & s_{n_T}^*(1)\mathbf{y}(1) & \cdots & s_{n_T}^*(L-1)\mathbf{y}(L-1) \end{bmatrix} \\ &= [\mathbf{s}^*(0) \otimes \mathbf{y}(0) \quad \cdots \quad \mathbf{s}^*(L-1) \otimes \mathbf{y}(L-1)] \end{aligned} \quad (4.28)$$

Therefore, $\mathbf{K}_{sy} \text{vec}(\mathbf{F}^H(f_d))$ is nothing but $[\mathbf{S}^* \otimes \mathbf{Y}] \mathbf{a}(f_d)$. This equation shows that we have less entries to calculate by reducing the size of \mathbf{K}_{sy} from $(n_T n_R \times L^2)$ to the size of \mathbf{K}'_{sy} which is $(n_T n_R \times L)$. Now for m -th row vector \mathbf{k}_m^T in \mathbf{K}'_{sy} ,

$$\mathbf{k}_m^T \mathbf{a}(f_d) = \sum_{n=0}^{L-1} k_n e^{-j2\pi n f_d} \quad (4.29)$$

This is equivalent to evaluating the FFT of \mathbf{k}^T , $\mathcal{F}[\mathbf{k}^T]$. Thus (4.26) can be evaluated for all $f_d \in [-\frac{1}{2}, \frac{1}{2}]$ for a given resolution by taking row-by-row N_{FFT} -point FFT of \mathbf{K}'_{sy} , i.e., $\mathcal{F}_r[\mathbf{K}'_{sy}]$. After evaluating $\mathcal{F}[\mathbf{K}'_{sy}]$, we get back $[\mathbf{X}]_{(n_R \times n_T)}$ by reshaping $[\text{vec}(\mathbf{X})]_{(n_T n_R \times 1)}$.

The next step is to evaluate $\mathbf{S}^H \mathbf{a}_T^*(\theta)$ which is the solution for the second dimension θ . It can be easily shown in a similar way to (4.29) that for any m -th row vector \mathbf{s}_m^T in \mathbf{S} , we have

$$\begin{aligned} \mathbf{s}_m^T \mathbf{a}_T^*(\theta) &= \sum_{p=0}^{n_T-1} s_m(p) e^{-j\pi p \sin(\theta)} \\ &= \sum_{p=0}^{n_T-1} s_m(p) e^{-j2\pi p f_\theta} \equiv \mathcal{F}[\mathbf{s}_m^T] \end{aligned} \quad (4.30)$$

where $f_\theta = \frac{\sin(\theta)}{2} \in [-\frac{1}{2}, \frac{1}{2}]$.

The third step is to evaluate $\mathbf{a}_R^H(\phi)\hat{\mathbf{R}}_y^{-1}$ which is the third dimension ϕ . For n -th column vector $\mathbf{r}(n)$ in $\hat{\mathbf{R}}_y^{-1}$, we have

$$\begin{aligned}\mathbf{a}_R^H(\phi)\mathbf{r}(n) &= \sum_{m=0}^{n_R-1} r_m(n)e^{-j\pi m \sin(\phi)} \\ &= \sum_{m=0}^{n_R-1} r_m(n)e^{-j2\pi m f_\phi} \equiv \mathcal{F}[\mathbf{r}(n)]\end{aligned}\tag{4.31}$$

where $f_\phi = \frac{\sin(\phi)}{2} \in [-\frac{1}{2}, \frac{1}{2}]$. The three-dimensional term $\mathbf{a}_R^H(\phi)\hat{\mathbf{R}}_y^{-1}\mathbf{X}\mathbf{a}_T^*(\theta)$ can be solved by using above-mentioned three steps.

4.3.2 Evaluation of two-dimensional terms by FFT

The two-dimensional term that appears in (4.13) and (4.17). As shown in Section 3.9 of Chapter 3, it can be represented by 2D-FFT. In more compact matrix form, (3.45) can be written as

$$\|\mathbf{c}(\theta, f_d)\|^2 \equiv \sum_{q=0}^{n_R-1} |\mathcal{F}_2[\mathbf{S}^* \otimes \mathbf{X}_q]|^2\tag{4.32}$$

where \otimes represents Khatri-Rao product.

4.3.3 Evaluation of one-dimensional terms by FFT

The one-dimensional terms are $\mathbf{b}(\phi)$ and $\mathbf{d}(\theta)$. These terms are one-dimensional so there evaluation is straight forward by using (4.31) and (4.30).

4.3.4 Algorithms

The cost function derived in Section 4.2 can be solved efficiently by the above mentioned procedure using FFT for grid of size N_{FFT} -points. The minimum of the solution of (4.11) gives us the estimates of unknown parameters \hat{f}_{θ_k} , \hat{f}_{ϕ_k} and \hat{f}_{d_k} . We can find $\hat{\theta}_k$ and $\hat{\phi}_k$ by using the relations $\hat{\theta}_k = \sin^{-1}(2\hat{f}_{\theta_k})$ and $\hat{\phi}_k = \sin^{-1}(2\hat{f}_{\phi_k})$. Using the above mentioned FFT-based evaluations, we can develop algorithms using the cost functions derived in Section 4.2. We write the three APES-based algorithms in pseudocode form in Table 4.1. APES-3D, APES-2D and APES-1D respectively are based on three-dimensional, two-dimensional and one-dimensional FFT.

The static target case is a special case of the above formulation when the Doppler shift is zero and $\mathbf{F}(f_{d_k}) = \mathbf{I}$. We solve the static target case for comparison with 2D-MUSIC and RD-MUSIC in the coming sections.

4.4 Complexity Analysis

We discuss the complexity of our proposed algorithm in comparison with 2D-MUSIC, RD-MUSIC algorithms [24] and tensor decomposition based method of [37]. Since, 2D-MUSIC and RD-MUSIC do not estimate the Doppler shift, we make the complexity analysis for static target case only. The same analysis can be extended to the moving target case. The 2D-MUSIC algorithm requires $\mathcal{O}\{Ln_T^2n_R^2+n_T^3n_R^3+m^2[n_Tn_R(n_Tn_R-K)+n_Tn_R-K]\}$ for m searches and K targets (Note that m represents number of grid points which is represented by N_{FFT} for

Table 4.1: APES-based Low complexity proposed algorithm

1:	procedure APES-3D(\mathbf{Y})
2:	Compute $\mathbf{R}_s = \frac{\mathbf{S}\mathbf{S}^H}{L}$, $\hat{\mathbf{R}}_y = \frac{\mathbf{Y}\mathbf{Y}^H}{L}$ and $\hat{\mathbf{R}}_y^{-1}$
3:	Compute $\mathbf{K} = \mathbf{S}^* \otimes \mathbf{Y}$
4:	Compute $\mathcal{K} = \mathcal{F}[\mathbf{K}]$
5:	$\mathcal{K} \leftarrow \text{reshape}(\mathcal{K})$
6:	$\mathcal{P} \leftarrow \mathcal{F}[\mathcal{K}]$
7:	Compute $\hat{\mathcal{R}}_y^{-1} = \mathcal{F}[\hat{\mathbf{R}}_y^{-1}]$
8:	Get $\hat{\mathcal{R}}_y^{-1} \leftarrow \hat{\mathcal{R}}_y^{-1}$
9:	Compute $\mathcal{R}_s^{-1/2} = \mathcal{F}[\mathbf{R}_s^{-1/2}]^T$
10:	Compute $\mathcal{X} \leftarrow \text{diag}([\mathcal{R}_s^{-1/2}]^T \times [\mathcal{R}_s^{-1/2}]^*)$
11:	Compute $\mathcal{Y} \leftarrow \text{diag}(\hat{\mathcal{R}}_y^{-1/2} \times [\hat{\mathcal{R}}_y^{-H/2}])$
12:	Compute $\mathcal{Z} \leftarrow \mathcal{P}^H \times \hat{\mathcal{R}}_y^{-1} \times \mathcal{P}$
13:	$\{\hat{\phi}_k, \hat{\theta}_k, \hat{f}_{d_k}\} = \text{argmax} \frac{ \hat{\mathcal{R}}_y^{-1} \times \mathcal{P} ^{\circ 2}}{\mathcal{Y} \circ [L^2 \times \mathcal{X} \circ \mathcal{Z}]}$
14:	end procedure

1:	procedure APES-2D(\mathbf{Y})
2:	Compute $\mathbf{R}_s = \frac{\mathbf{S}\mathbf{S}^H}{L}$, $\hat{\mathbf{R}}_y = \frac{\mathbf{Y}\mathbf{Y}^H}{L}$ and $\hat{\mathbf{R}}_y^{-1}$
3:	$\mathbf{X} = \hat{\mathbf{R}}_y^{-1} \mathbf{Y}$
4:	Solve (3.45)
5:	$\{\hat{\phi}_k, \hat{f}_{d_k}\} \leftarrow \text{argmax} \text{ (3.45)}$
6:	$\{\hat{\phi}_k, \hat{\theta}_k, \hat{f}_{d_k}\} \leftarrow \text{argmax} \text{ (4.13) using } \{\hat{\phi}_k, \hat{f}_{d_k}\}$
7:	end procedure

1:	procedure APES-1D(\mathbf{Y})
2:	Compute $\mathbf{R}_s = \frac{\mathbf{S}\mathbf{S}^H}{L}$, $\hat{\mathbf{R}}_y = \frac{\mathbf{Y}\mathbf{Y}^H}{L}$ and $\hat{\mathbf{R}}_y^{-1}$
3:	$\hat{f}_{d_k} \leftarrow \text{argmax} \text{ eig}(\mathbf{B}(f_d), \mathbf{C}(f_d))$
4:	$\hat{\phi}_k \leftarrow \text{argmax} \text{ (4.17) using } \hat{f}_{d_k}$
5:	$\hat{\theta}_k \leftarrow \text{argmax} \text{ (4.13) using } \{\hat{\phi}_k, \hat{f}_{d_k}\}$
6:	end procedure

our algorithm). The second algorithm used for comparison is RD-MUSIC which requires $\mathcal{O}\{L^2 n_T^2 n_R^2 + n_T^3 n_R^3 + m[n_T^2 n_R(n_T n_R - K) + n_T^2(n_T n_R - K) + n_T^2]\}$ where the complexity reduction is achieved by reducing m^2 factor to m by converting the 2D-search problem into two one-dimensional search problem. The tensor decomposition based algorithm requires $\mathcal{O}\{n(K^3 + K n_T n_R L) + (n_T^3 + n_R^3)K\}$ where n is the number of iterations required for the convergence of the algorithm [37]. The algorithm converges at an n of 83 on average and is also dependent on K . In contrast, our lowest complexity proposed algorithm (APES-1D) requires $\mathcal{O}\{N_{FFT}[n_R \log N_{FFT} + 3n_T \log N_{FFT} + 2M + N + 1] + N(2NL + 2N + LM)\}$ for the static target case. The complexity of our proposed algorithm is lower than the three algorithms used for comparison in this complexity analysis. This reduced complexity is achieved because our algorithm exploits the low complexity of the FFT and is reduced dimension. The average runtime for the three above mentioned algorithms is independent of SNR.

4.5 Cramér-Rao Lower Bound

In the following subsections, the CRLB for the static target and moving target scenarios are discussed.

4.5.1 CRLB for Static Target

Let's define,

$$\boldsymbol{\eta} = \begin{bmatrix} \mathcal{R}(\beta_k) & \mathcal{I}(\beta_k) & \theta_k & \phi_k \end{bmatrix} \quad (4.33)$$

The FIM for the unknown parameters assuming that the noise samples are uncorrelated is given by the Slepian-Bang's formula

$$\mathbf{F}(\boldsymbol{\eta}) = \frac{2}{\sigma_z^2} \mathcal{R} \left[\sum_{n=0}^{N-1} \left(\frac{\partial \mathbf{u}^H(n)}{\partial \boldsymbol{\eta}} \frac{\partial \mathbf{u}(n)}{\partial \boldsymbol{\eta}^T} \right) \right] \quad (4.34)$$

where

$$\mathbf{u}(n) = \beta_k \mathbf{a}_R(\phi_k) \mathbf{a}_T^T(\theta_k) \mathbf{s}(n), \quad (4.35)$$

$$\frac{\partial \mathbf{u}^H(n)}{\partial \boldsymbol{\eta}} = \begin{bmatrix} \frac{\partial \mathbf{u}^H(n)}{\partial \mathcal{R}(\beta_k)} \\ \frac{\partial \mathbf{u}^H(n)}{\partial \mathcal{I}(\beta_k)} \\ \frac{\partial \mathbf{u}^H(n)}{\partial \theta_k} \\ \frac{\partial \mathbf{u}^H(n)}{\partial \phi_k} \end{bmatrix}_{4 \times n_R}, \quad (4.36)$$

and

$$\frac{\partial \mathbf{u}^H(n)}{\partial \boldsymbol{\eta}^T} = \left[\frac{\partial \mathbf{u}(n)}{\partial \mathcal{R}(\beta_k)} \quad \frac{\partial \mathbf{u}(n)}{\partial \mathcal{I}(\beta_k)} \quad \frac{\partial \mathbf{u}(n)}{\partial \theta_k} \quad \frac{\partial \mathbf{u}(n)}{\partial \phi_k} \right]_{n_R \times 4}. \quad (4.37)$$

The evaluation of (4.36) requires the evaluation of the four partial derivatives involved in the equation. These four partial derivatives are found as

$$\frac{\partial \mathbf{u}(n)}{\partial \mathcal{R}(\beta_k)} = \mathbf{a}_R(\phi_k) \mathbf{a}_T^\top(\theta_k) \mathbf{s}(n), \quad (4.38)$$

$$\frac{\partial \mathbf{u}(n)}{\partial \mathcal{I}(\beta_k)} = j \mathbf{a}_R(\phi_k) \mathbf{a}_T^\top(\theta_k) \mathbf{s}(n), \quad (4.39)$$

$$\frac{\partial \mathbf{u}(n)}{\partial \theta_k} = \beta_k (j\pi \cos(\theta_k)) \mathbf{a}_R(\phi_k) \mathbf{a}_T^\top(\theta_k) \mathbf{A}_T \mathbf{s}(n), \quad (4.40)$$

$$\frac{\partial \mathbf{u}(n)}{\partial \phi_k} = \beta_k (j\pi \cos(\phi_k)) \mathbf{A}_R \mathbf{a}_R(\phi_k) \mathbf{a}_T^\top(\theta_k) \mathbf{s}(n), \quad (4.41)$$

where

$$\mathbf{A}_T = \text{diag}([0 \ 1 \ \dots \ n_T - 1]) \quad (4.42)$$

and

$$\mathbf{A}_R = \text{diag}([0 \ 1 \ \dots \ n_R - 1]). \quad (4.43)$$

The other four partial derivatives in (4.37) can be found by using the identity

$\partial \mathbf{x}^H = (\partial \mathbf{x})^H$. Therefore, the FIM in (4.34) can be found using (4.38) – (4.41).

The CRLB is found by inverting the FIM $\mathbf{F}(\boldsymbol{\eta})$.

4.5.2 CRLB for Moving Target

For the moving target case, we have the additional parameter f_{d_k} . Let's define the vector $\boldsymbol{\alpha}$ of unknown parameters as the following,

$$\boldsymbol{\alpha} = \begin{bmatrix} \mathcal{R}(\beta_k) & \mathcal{I}(\beta_k) & \theta_k & \phi_k & f_{d_k} \end{bmatrix} \quad (4.44)$$

The FIM for the unknown parameters is again given by the Slepian-Bang's formula assuming that the noise samples are uncorrelated.

$$\mathbf{F}(\boldsymbol{\alpha}) = \frac{2}{\sigma_{\mathbf{z}}^2} \mathcal{R} \left[\sum_{n=0}^{N-1} \left(\frac{\partial \mathbf{v}^H(n)}{\partial \boldsymbol{\alpha}} \frac{\partial \mathbf{v}(n)}{\partial \boldsymbol{\alpha}^T} \right) \right] \quad (4.45)$$

where

$$\mathbf{v}(n) = \beta_k e^{j2\pi n f_{d_k}} \mathbf{a}_R(\phi_k) \mathbf{a}_T^T(\theta_k) \mathbf{s}(n), \quad (4.46)$$

$$\frac{\partial \mathbf{v}^H(n)}{\partial \boldsymbol{\alpha}} = \begin{bmatrix} \frac{\partial \mathbf{v}^H(n)}{\partial \mathcal{R}(\beta_k)} \\ \frac{\partial \mathbf{v}^H(n)}{\partial \mathcal{I}(\beta_k)} \\ \frac{\partial \mathbf{v}^H(n)}{\partial \theta_k} \\ \frac{\partial \mathbf{v}^H(n)}{\partial \phi_k} \\ \frac{\partial \mathbf{v}^H(n)}{\partial f_{d_k}} \end{bmatrix}_{5 \times n_R} \quad (4.47)$$

and

$$\frac{\partial \mathbf{v}^H(n)}{\partial \boldsymbol{\alpha}^T} = \begin{bmatrix} \frac{\partial \mathbf{v}(n)}{\partial \mathcal{R}(\beta_k)} & \frac{\partial \mathbf{v}(n)}{\partial \mathcal{I}(\beta_k)} & \frac{\partial \mathbf{v}(n)}{\partial \theta_k} & \frac{\partial \mathbf{v}(n)}{\partial \phi_k} & \frac{\partial \mathbf{v}(n)}{\partial f_{d_k}} \end{bmatrix}_{n_R \times 5} \quad (4.48)$$

The evaluation of (4.47) requires the evaluation of the five partial derivatives involved in the equation. These five partial derivatives are found as the following

$$\frac{\partial \mathbf{v}(n)}{\partial \mathcal{R}(\beta_k)} = e^{j2\pi n f_{d_k}} \mathbf{a}_R(\phi_k) \mathbf{a}_T^T(\theta_k) \mathbf{s}(n) \quad (4.49)$$

$$\frac{\partial \mathbf{v}(n)}{\partial \mathcal{I}(\beta_k)} = j e^{j2\pi n f_{d_k}} \mathbf{a}_R(\phi_k) \mathbf{a}_T^T(\theta_k) \mathbf{s}(n) \quad (4.50)$$

$$\frac{\partial \mathbf{v}(n)}{\partial \theta_k} = j \pi \cos(\theta_k) \beta_k e^{j2\pi n f_{d_k}} \mathbf{a}_R(\phi_k) \mathbf{a}_T^T(\theta_k) \mathbf{A}_T \mathbf{s}(n) \quad (4.51)$$

$$\frac{\partial \mathbf{v}(n)}{\partial \phi_k} = j \pi \cos(\phi_k) \beta_k e^{j2\pi n f_{d_k}} \mathbf{A}_R \mathbf{a}_R(\phi_k) \mathbf{a}_T^T(\theta_k) \mathbf{s}(n) \quad (4.52)$$

$$\frac{\partial \mathbf{v}(n)}{\partial f_{d_k}} = j 2\pi n \beta_k e^{j2\pi n f_{d_k}} \mathbf{a}_R(\phi_k) \mathbf{a}_T^T(\theta_k) \mathbf{s}(n) \quad (4.53)$$

where \mathbf{A}_T and \mathbf{A}_R are the same as defined in (4.42) and (4.43) respectively. The other five partial derivatives in (4.48) can be found by using the identity $\partial \mathbf{x}^H = (\partial \mathbf{x})^H$. Therefore, the FIM in (4.45) can be found using (4.49) – (4.53). The CRLB is found by inverting the FIM $\mathbf{F}(\boldsymbol{\alpha})$.

4.6 Simulation Results and Discussion

We run several simulations to validate the algorithms proposed in this chapter. We assume multiple targets ($K = 3$) at $\phi_k = \{10^\circ, 20^\circ, 30^\circ\}$ and $\theta_k = \{-10^\circ, 0^\circ, 10^\circ\}$

with normalized Doppler shift $f_{d_k} = \{-0.1, 0.1, 0.2\}$. The grid search is varied from -90° to $+90^\circ$. For simplicity, we assume that the all targets lie on some grid point which means on-grid targets. The transmitted signals are uncorrelated quadrature phase shift keying (QPSK) symbols. The noise is assumed to be uncorrelated Gaussian with zero mean and variance $\sigma_{\mathbf{z}}^2$. The noise variance $\sigma_{\mathbf{z}}^2$ was varied to control the SNR. For the simulations, SNR is defined as $\text{SNR} = 10 \log(1/\sigma_{\mathbf{z}}^2)$ where the power at each antenna is normalized so that total transmit power is unity. The number of antenna elements are $n_T = 8$ and $n_R = 8$, the number of snapshots L are 64, the number of grid points are 512 in most of the results and the MSE is averaged over 1000 iterations, otherwise mentioned accordingly.

4.6.1 MSE Performance of ϕ_k Estimation

First we show how the MSE performance is effected by reducing the dimensions. Figure 4.1 shows the MSE performance of DOA ($\hat{\phi}_k$) obtained by all of the proposed six algorithms. The CRLB is also plotted for comparison. The results show that at an MSE of 10^{-2} , the SNR loss incurred in going from 3D to 2D is 1 dB whereas from 2D to 1D is 1.5 dB approximately. The performance loss that occurred in reducing the dimensions is due the assumptions that were made in the cost function simplification. Since it is suboptimal solution, that is why it is away from the CRLB. Although MPDR and APES algorithms are derived from two different cost functions but they have almost the same MSE performance.

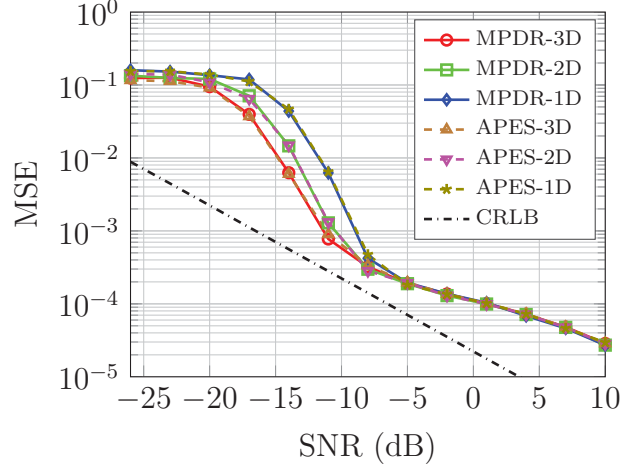


Figure 4.1: MSE performance of DOA ϕ_k for moving target. Simulation parameters: $L = 64$, $n_T = 8$, $n_R = 8$, $K = 3$.

4.6.2 MSE Performance of θ_k Estimation

The simulation results for θ_k estimation are shown in Fig. 4.2. The results show that both MPDR-1D and APES-1D outperforms the algorithms presented in [89], [84] and [90]. The algorithms of [89], [84] and [90] are all subspace methods and are unable to provide optimum results for multiple target parameter estimation. Only the method of [90] shows slightly better performance than [89] and [84] at high SNR. The two algorithms [89] and [84] reach an error floor while resolving multiple targets. The performance of our proposed algorithms is close to CRLB.

4.6.3 MSE Performance of f_{d_k} Estimation

The MSE performance results for Doppler shift estimation are shown in Fig. 4.3. The simulation results show that our proposed algorithms MPDR-1D and APES-1D outperforms the algorithms of [89], [84] and [90]. Only the algorithm of [84] shows slight improvement at high SNR. Our proposed algorithm approach the

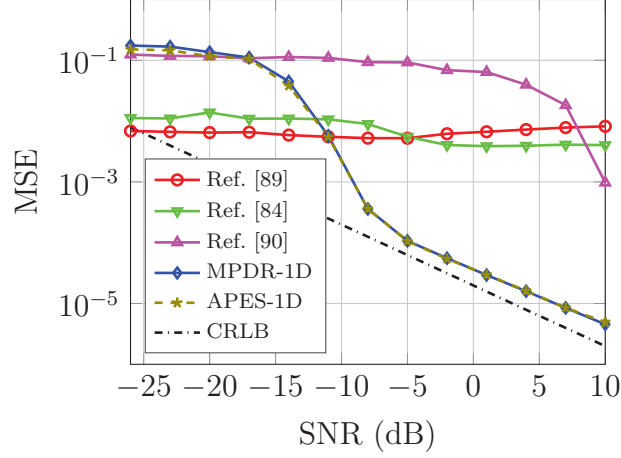


Figure 4.2: MSE performance of DOD θ_k for moving target. Simulation parameters: $L = 64$, $n_T = 8$, $n_R = 8$, $K = 3$.

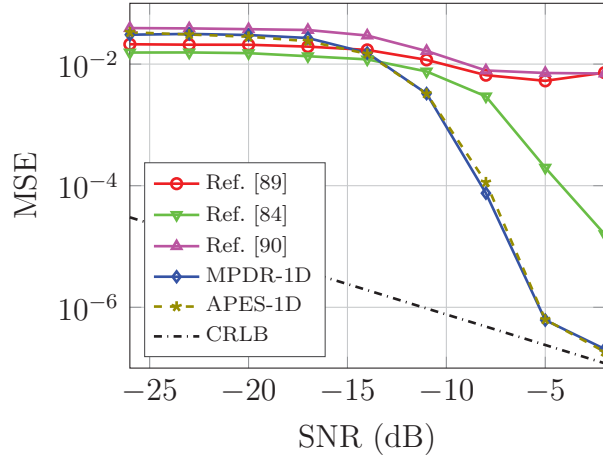


Figure 4.3: MSE performance of Doppler f_{d_k} for moving target. Simulation parameters: $L = 64$, $n_T = 8$, $n_R = 8$, $K = 3$.

CRLB at SNR greater than -5 dB.

4.6.4 Complexity Comparison

The processing time for the proposed algorithms is shown in Table 4.2. Both the average runtime and memory required is shown for the discussed algorithms. It is evident from the results that the minimum processing time is achieved by 1D-FFT

Table 4.2: Complexity comparison

Algorithm	Average Runtime (sec)	Memory requirements (MB)
MPDR-3D	7.33	$> 10^3$
MPDR-2D	0.13	61.84
MPDR-1D	0.09	1.01
APES-3D	11.79	$> 10^3$
APES-2D	0.12	63.80
APES-1D	0.09	1.01
Ref. [89]	2.02	4.56
Ref. [84]	0.53	673.99
Ref. [90]	0.33	0.81

based algorithms for both MPDR and APES methods. Here, we will mention two more direction finding algorithms 2D-MUSIC and RD-MUSIC [24]. Both these algorithms cannot estimate Doppler shift. However, the average runtime per iteration is found to be 29.87 and 0.14 seconds for 2D-MUSIC and RD-MUSIC, respectively without estimating the Doppler shift for $n_T = n_R = 8$. The runtime for both algorithms is higher than our proposed 1D algorithms. In contrast, for the same number of antennas, APES-2D took 0.12 seconds with the Doppler estimation. The runtime is calculated using a machine with Xeon E5-2680 2.8 GHz dual-processors with maximum available RAM of 64 GB. Furthermore, for a same set of parameters, it is found by using the complexity analysis in section 4.4 that APES-1D is approximately 7 times faster than the tensor decomposition based algorithm of [37].

4.7 Concluding Remarks

In this chapter, we present new FFT-based DOA, DOD and Doppler shift estimation algorithms using two adaptive beamformer weight vectors at the receiver for bistatic MIMO radar. We derive the reduced-dimension cost function for APES estimator for the moving target case. We show that the APES-based algorithms achieve the CRLB for the estimation performance of DOA, DOD, Doppler shift and reflection coefficient.

As far as computational complexity is concerned, the 1D-FFT-based APES-1D (with the Doppler shift estimation) beat the compared algorithms. The reduced-dimension 1D-FFT-based APES-Algorithm-1D have the lowest memory requirements because it is based on one-dimensional search. Since, FFT can be deployed easily on hardware, the approach presented here is also practical in radar applications.

CHAPTER 5

DOA ESTIMATION BY REGULARIZED LEAST-SQUARES

In the widely discussed approaches for direction of arrival (DOA) estimation in literature (and also in previous chapters), the covariance matrix of the received signal is full rank and the sources are assumed to be uncorrelated. If the covariance matrix of received signal is rank deficient, then we cannot find the inverse of the covariance matrix. Also, if the sources are coherent, then some of the algorithms fail to recover the estimate of the DOA. Regularized least-squares algorithms deal with ill-conditioned matrices and rank deficient matrices. In this chapter, we solve the DOA problem by using regularized least-squares algorithms when the covariance matrix of received signal is rank deficient and the sources are coherent.

5.1 Introduction

The DOA algorithms often face the scenario of coherent (or fully correlated) sources. The coherent source problem in DOA estimation may arise due to multipath reflections or intentional jamming. Some of the DOA algorithms are not able to resolve coherent sources such as Capon [8] and MUSIC [92]. The ESPRIT algorithm [19] and the root-MUSIC algorithm [93] can resolve coherent sources.

In most of the DOA problems discussed in literature, the covariance matrix of received signal snapshots is assumed to be full rank. The techniques which require the inversion of covariance matrix do not work if the covariance matrix is rank deficient. The ESPRIT algorithm [19] and the root-MUSIC algorithm [93] can resolve coherent sources but they suffer from performance degradation when the number of samples is low or the covariance matrix of received signal is rank deficient.

In order to tackle both problems of coherent sources and rank deficiency in the covariance matrix, we propose regularized least-squares (RLS) algorithms to solve the DOA problem. The RLS algorithms are designed to solve the linear system of equations $\mathbf{y} = \mathbf{A}\mathbf{x} + \mathbf{z}$ when the matrix \mathbf{A} is ill-conditioned or rank deficient. By ill-conditioned matrix, we mean that the condition number of the matrix is high. There are many algorithms available in literature that solves the RLS problem. They include the L-curve [94], normalized cumulative periodogram (NCP) [95] and perturbation-based regularization (PBR) [96] etc. These algorithms differ mainly in the approach of finding the regularization parameter.

In this chapter, we will use the existing RLS algorithms to solve the DOA estimation problem. We will address the problem under the scenario when the sources are fully correlated and the covariance matrix is rank deficient.

5.1.1 Organization of the Chapter

The DOA problem is formulated in Section 5.2 and its solution with RLS is discussed in Section 5.3. Section 5.4 presents the simulation results and Section 5.5 concludes this chapter.

5.1.2 Regularized Least-Squares

Regularized least-squares (RLS) is a variation of standard least-squares problem.

In RLS, we seek a vector $\hat{\mathbf{w}}$ that solves

$$\min_{\mathbf{w}} [(\mathbf{w} - \bar{\mathbf{w}})^H \Pi (\mathbf{w} - \bar{\mathbf{w}}) + \|\mathbf{y} - \mathbf{H}\mathbf{w}\|^2] \quad (5.1)$$

The term $(\mathbf{w} - \bar{\mathbf{w}})^H \Pi (\mathbf{w} - \bar{\mathbf{w}})$ is the regularization term where Π is positive-definite matrix, usually $\Pi = \delta \mathbf{I}$ for $\delta > 0$ and $\bar{\mathbf{w}}$ is usually 0.

The solution to the regularized LS can be found by following methods

- Geometric argument
- Completion-of-squares argument
- Differentiation argument

The differentiation argument is discussed here. (For the geometric argument and completion-of-squares argument, the reader is referred to [97]). Let's denote the cost function that we want to minimize by $\mathcal{J}(\mathbf{w})$,

$$\mathcal{J}(\mathbf{w}) \triangleq (\mathbf{w} - \bar{\mathbf{w}})^H \Pi (\mathbf{w} - \bar{\mathbf{w}}) + \|\mathbf{y} - \mathbf{H}\mathbf{w}\|^2 \quad (5.2)$$

$$\begin{aligned} &= \mathbf{w}^H \Pi \mathbf{w} - \mathbf{w}^H \Pi \bar{\mathbf{w}} - \bar{\mathbf{w}}^H \Pi \mathbf{w} + \bar{\mathbf{w}}^H \Pi \bar{\mathbf{w}} \\ &+ \mathbf{y}^H \mathbf{y} - \mathbf{y}^H \mathbf{H} \mathbf{w} - \mathbf{w}^H \mathbf{H}^H \mathbf{y} + \mathbf{w}^H \mathbf{H}^H \mathbf{H} \mathbf{w} \end{aligned} \quad (5.3)$$

Differentiating with respect to \mathbf{w} to find the gradient vector, we get

$$\nabla_{\mathbf{w}^H} \mathcal{J}(\mathbf{w}) = \Pi \mathbf{w} - \Pi \bar{\mathbf{w}} - \mathbf{H}^H \mathbf{y} + \mathbf{H}^H \mathbf{H} \mathbf{w} \quad (5.4)$$

The gradient evaluates to zero at all $\hat{\mathbf{w}}$ that satisfy

$$\Pi \hat{\mathbf{w}} - \Pi \bar{\mathbf{w}} - \mathbf{H}^H \mathbf{y} + \mathbf{H}^H \mathbf{H} \hat{\mathbf{w}} = 0 \quad (5.5)$$

$$[\Pi + \mathbf{H}^H \mathbf{H}] \hat{\mathbf{w}} - \Pi \bar{\mathbf{w}} - \mathbf{H}^H \mathbf{y} = 0 \quad (5.6)$$

$$[\Pi + \mathbf{H}^H \mathbf{H}] \hat{\mathbf{w}} - \Pi \bar{\mathbf{w}} - \mathbf{H}^H \mathbf{H} \bar{\mathbf{w}} = \mathbf{H}^H \mathbf{y} - \mathbf{H}^H \mathbf{H} \bar{\mathbf{w}} \quad (5.7)$$

$$[\Pi + \mathbf{H}^H \mathbf{H}] (\hat{\mathbf{w}} - \bar{\mathbf{w}}) = \mathbf{H}^H (\mathbf{y} - \mathbf{H} \bar{\mathbf{w}}) \quad (5.8)$$

Therefore, the solution of regularized LS is given by

$$\hat{\mathbf{w}} = \bar{\mathbf{w}} + [\Pi + \mathbf{H}^H \mathbf{H}]^{-1} \mathbf{H}^H (\mathbf{y} - \mathbf{H} \bar{\mathbf{w}}) \quad (5.9)$$

when \mathbf{H} is full column rank.

The solution(s) $\hat{\mathbf{w}}$ so obtained correspond to minima of $\mathcal{J}(\mathbf{w})$ since its Hessian matrix is non-negative

$$\nabla_{\mathbf{w}}^2 \mathcal{J}(\mathbf{w}) = \Pi + \mathbf{H}^H \mathbf{H} \geq 0 \quad (5.10)$$

for regularization $\Pi > 0$.

For the case of $\bar{\mathbf{w}} = 0$ and $\Pi = \delta \mathbf{I}$, we have the simplified RLS solution given by

$$\hat{\mathbf{w}} = [\delta \mathbf{I} + \mathbf{H}^H \mathbf{H}]^{-1} \mathbf{H}^H \mathbf{y} \quad (5.11)$$

The advantage of COPRA algorithm [96] is that it optimally chooses the regularization parameter δ .

5.2 Problem Formulation

The DOA problem for a uniform linear array is formulated as the following. The received signal vector at an antenna array is given by

$$\mathbf{y} = \mathbf{h}s(t) + \mathbf{v} \quad (5.12)$$

where

$$\mathbf{h} = \begin{bmatrix} 1 & e^{j\frac{2\pi}{\lambda}d \cos \phi} & e^{j\frac{4\pi}{\lambda}d \cos \phi} & \dots & e^{j\frac{(M-1)\pi}{\lambda}d \cos \phi} \end{bmatrix}_{M \times 1}^T \quad (5.13)$$

This is *linearly-constrained minimum-variance* problem or *minimum-variance distortionless-response* problem, given by

$$\min_{\mathbf{k}} \mathbf{k}^H \mathbf{R}_v \mathbf{k} \quad \text{subject to} \quad \mathbf{k}^H \mathbf{h} = 1 \quad (5.14)$$

The minimum mean-square estimator for $s(t)$ is given by

$$\hat{s}(t) = [\mathbf{h}^H \mathbf{R}_v^{-1} \mathbf{h}]^{-1} \mathbf{h}^H \mathbf{R}_v^{-1} \mathbf{y} \quad (\text{MVDR}) \quad (5.15)$$

If $\mathbf{R}_v = \sigma_v^2 \mathbf{I}$, then

$$\hat{s}(t) = [\mathbf{h}^H \mathbf{h}]^{-1} \mathbf{h}^H \mathbf{y} \quad (\text{LS}) \quad (5.16)$$

$$= \frac{1}{M} \sum_{n=0}^{M-1} y_n e^{-j \frac{2\pi n}{\lambda} d \cos \phi} \quad (5.17)$$

which is the least-squares solution of this problem.

For the signal model

$$\mathbf{y} = \mathbf{h}s(t) + \mathbf{v} \quad (5.18)$$

we seek a weighting vector \mathbf{w} such that $\mathbf{w}^H \mathbf{y} = s(t)$. The weighting vector \mathbf{w} for minimum-power distortionless-response (MPDR) is given by

$$\mathbf{w} = \frac{\mathbf{R}_y^{-1} \mathbf{h}}{\mathbf{h}^H \mathbf{R}_y^{-1} \mathbf{h}} \quad (5.19)$$

The beamformer output is given by

$$\mathbf{w}^H \mathbf{y} = \frac{\mathbf{h}^H \mathbf{R}_y^{-1}}{\mathbf{h}^H \mathbf{R}_y^{-1} \mathbf{h}} \mathbf{y} \quad (5.20)$$

The power of the beamformer output is given by

$$P_{BF} = \mathbb{E} [|\mathbf{w}^H \mathbf{y}|^2] \quad (5.21)$$

$$= \mathbf{w}^H \mathbf{R}_y \mathbf{w} \quad (5.22)$$

$$= \frac{1}{\mathbf{h}^H \mathbf{R}_y^{-1} \mathbf{h}} \quad (5.23)$$

Re-writing above using the relation $\mathbf{A}^{-1} = \mathbf{A}^{-H/2} \mathbf{A}^{-1/2}$

$$P_{BF} = \frac{1}{\mathbf{h}^H \mathbf{R}_y^{-H/2} \mathbf{R}_y^{-1/2} \mathbf{h}} \quad (5.24)$$

$$= \frac{1}{\mathbf{b}^H \mathbf{b}} \quad (5.25)$$

where $\mathbf{b} \triangleq \mathbf{R}_y^{-1/2} \mathbf{h}$. Thus, we can solve $\mathbf{h} = \mathbf{R}_y^{1/2} \mathbf{b}$ to find \mathbf{b} using standard LS if the covariance matrix \mathbf{R}_y is full rank. But if the covariance matrix \mathbf{R}_y is rank deficient, the standard LS will not work. Thus, RLS can solve (5.25) if the matrix \mathbf{R}_y is rank deficient. The rank deficiency in the covariance matrix \mathbf{R}_y occurs when the number of snapshots are less than the number of antennas.

5.3 DOA estimation by RLS

In this section, we propose the approach to use RLS for DOA estimation. It should be noted from the definition of \mathbf{h} that (5.25) is a function of ϕ . We re-write (5.25) showing the dependence on ϕ as follows

$$P_{BF}(\phi) = \frac{1}{\mathbf{b}^H(\phi)\mathbf{b}(\phi)} \quad (5.26)$$

where

$$\mathbf{b}(\phi) \triangleq \mathbf{R}_y^{-1/2}\mathbf{h}(\phi) \quad (5.27)$$

which implies

$$\mathbf{h}(\phi) = \mathbf{R}_y^{1/2}\mathbf{b}(\phi) \quad (5.28)$$

The equation (5.26) is a spectrum as a function of ϕ and its peaks give us the location of the targets. Next, we show the validity of (5.28).

Suppose a k -th single target is located at ϕ_k . The theoretical covariance matrix \mathbf{R}_y is given by

$$\mathbf{E} \mathbf{y} \mathbf{y}^H = \mathbf{E} [\mathbf{h}(\phi_k)s(t) + \mathbf{v}][\mathbf{h}(\phi_k)s(t) + \mathbf{v}]^H \quad (5.29)$$

$$= \mathbf{E} [\mathbf{h}(\phi_k)s(t) + \mathbf{v}][s^*(t)\mathbf{h}^H(\phi_k) + \mathbf{v}^H] \quad (5.30)$$

$$= \mathbf{E} \mathbf{h}(\phi_k) s(t) s^*(t) \mathbf{h}^H(\phi_k) + \mathbf{E} \mathbf{v} \mathbf{v}^H + \mathbf{E} \mathbf{h}(\phi_k) s(t) \mathbf{v} + \mathbf{E} \mathbf{v} s^*(t) \mathbf{h}^H(\phi_k) \quad (5.31)$$

Assuming independence between the noise and source waveform and assuming the noise to be uncorrelated, we have

$$\mathbf{R}_y = \mathbf{h}(\phi_k) [\mathbf{E} s(t) s^*(t)] \mathbf{h}^H(\phi_k) + \mathbf{E} \mathbf{v} \mathbf{v}^H \quad (5.32)$$

$$= \sigma_k^2 \mathbf{h}(\phi_k) \mathbf{h}^H(\phi_k) + \mathbf{R}_v \quad (5.33)$$

where $\sigma_k^2 = \mathbf{E} s(t) s^*(t)$ is the power of the source signal and $\mathbf{R}_v = \mathbf{E} \mathbf{v} \mathbf{v}^H$ is the covariance matrix of the noise. The estimated covariance matrix $\hat{\mathbf{R}}_y$ obtained from N number of time samples will be approximately equal to (5.33). In the presence of a source, \mathbf{R}_y is given by (5.33) but in the absence of source $\mathbf{R}_y = \mathbf{R}_v$. In order to get a solution of (5.28), we need the initial estimate of ϕ_k , say $\hat{\phi}_k^i$.

We initialize the algorithm using correlation by solving

$$\Psi = \mathbf{y}^H \mathbf{H} \quad (5.34)$$

where \mathbf{H} is the matrix of all possibilities of ϕ . By searching the peaks in Ψ , we find the initial estimate $\hat{\phi}_k^i$. Then, using RLS algorithms we solve (5.28). The pseudocode form of the algorithm is shown in Table 5.1.

Table 5.1: DOA estimation by RLS

1:	procedure DOA-RLS(\mathbf{Y})
2:	Compute $\mathbf{\Psi} = \mathbf{Y}^H \mathbf{H}$ from the observation matrix \mathbf{Y}
3:	Calculate mean of rows of $\mathbf{\Psi}$ and find peak locations as DOA estimates $\{\hat{\phi}_1^i, \dots, \hat{\phi}_K^i\}$
4:	Estimate $\hat{\mathbf{R}}_y = \frac{\mathbf{Y}\mathbf{Y}^H}{N}$ and calculate $\hat{\mathbf{R}}_y^{1/2}$
5:	Solve (5.28) by RLS around each $\hat{\phi}_k^i$
6:	Find the maximum in the spectrum obtained in step 5 which gives $\hat{\phi}_k$.
7:	end procedure

5.4 Simulation Results

We shown some simulation results to benchmark the performance of the proposed algorithm. We assume two coherent source located at $\phi_1 = -10^\circ, \phi_2 = 10^\circ$. The grid search is varied from -90° to $+90^\circ$ with a resolution of 0.1° . We also assume that the source location falls on some grid point. The waveform of the two sources is fully correlated, i.e. $s_2(t) = 2s_1(t)$ where $s_1(t)$ is QPSK waveform. The noise is assumed to be uncorrelated Gaussian with zero mean and variance $\sigma_{\mathbf{z}}^2$. For the simulations, SNR is defined as $\text{SNR} = 10 \log(1/\sigma_{\mathbf{z}}^2)$ where the power at each antenna element is normalized so that the total transmit power is unity. The spacing between antenna elements is assumed to be half-wavelength of the source waveform. The number of iterations for averaging the results is 10^4 .

Fig. 5.1 shows the RMSE performance of the proposed method compared with MUSIC and root-MUSIC. We assume uncorrelated sources with the waveform of the two sources as uncorrelated and we choose $s_1(t)$ and $s_2(t)$ to be a QPSK waveform. The simulation results show that MUSIC and root-MUSIC can resolve

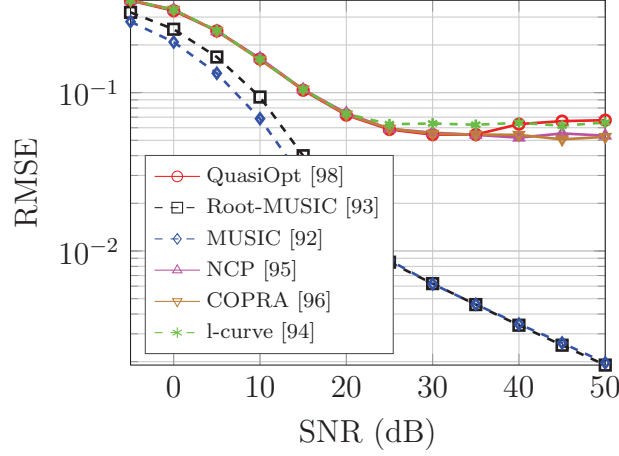


Figure 5.1: RMSE performance. Simulation parameters: $N = 8$, $n_R = 10$, $K = 2$ uncorrelated sources.

the uncorrelated sources. MUSIC gives the best RMSE performance with the compared algorithms. All the RLS algorithms reach an error floor. This error floor requires some explanation. The regularization parameter diverges as we go away from the true location of the target. Therefore, slight mismatch in the actual location and estimated location can cause big divergence in the regularization parameter. That is why the performance of RLS algorithms is limited to an error floor.

Fig. 5.2 shows the RMSE performance of the proposed method. The number of antenna elements are $n_R = 10$ and the number of snapshots are $N = 8$ so that the covariance matrix of the received signal is rank deficient. The waveform of the two sources is fully correlated, i.e. $s_2(t) = 2s_1(t)$ where $s_1(t)$ is QPSK waveform. The simulation results show that MUSIC and root-MUSIC are not able to recover the DOAs of the two coherent sources. Root-MUSIC suffers due to low number of snapshots. The proposed RLS-based algorithm is able to recover the coher-

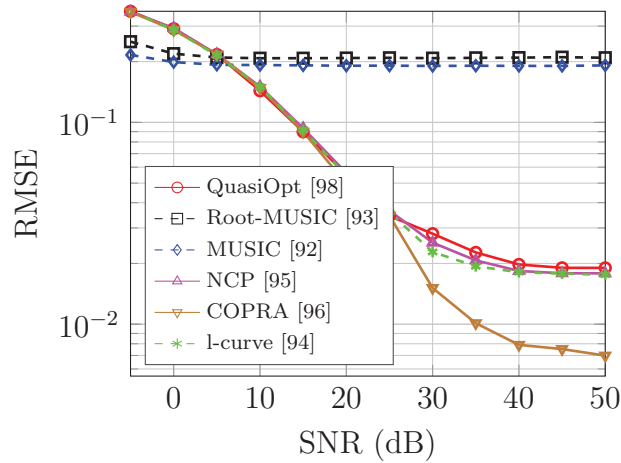


Figure 5.2: RMSE performance. Simulation parameters: $N = 8$, $n_R = 10$, $K = 2$ coherent sources.

Table 5.2: Complexity comparison.

Algorithm	MUSIC	QuasiOpt	COPRA
Average runtime (sec)	0.05	0.12	0.36
Algorithm	NCP	L-curve	Root-MUSIC
Average runtime (sec)	0.37	0.34	0.02

ent sources with rank deficient covariance matrix. The best RMSE performance among the RLS algorithms used is shown by the RLS approach of COPRA.

The complexity comparison is shown in Table 5.2. Although root-MUSIC has lowest complexity but its MSE performance deteriorates at low number of snapshots. Among the RLS algorithms that are able to recover the coherent sources, l-curve algorithm has the lowest complexity and the COPRA algorithm has the second lowest complexity.

5.5 Concluding Remarks

In this work, we proposed the RLS algorithms to solve the DOA problem for rank deficient covariance matrix and coherent sources. The state-of-art RLS algorithm called COPRA shows the best performance with very low complexity.

CHAPTER 6

CONCLUSIONS AND FUTURE WORK

6.1 Concluding Remarks

The dissertation has addressed the problem of target parameter estimation for MIMO radars. For the case of monostatic MIMO radar, we show that the CS algorithms show some improvement in certain parameter estimation but at the expense of high complexity. The CS algorithms are not generally designed for structured sensing matrices. If the structured matrices are used to recover sparse signals, the number of sparse unknown element to be recovered becomes limited due to coherence in the columns of the sensing matrix. That is why, the SABMP algorithm performed good at high SNR but suffered a lot at low SNR levels. The only improvement that is obtained using SABMP algorithm was for the case of reflection coefficient estimation. SABMP algorithm, like any other CS algorithm,

is a matching pursuit algorithm that requires some search space. That is why, no matter how good the SABMP algorithm is, its computational complexity cannot be reduced from a certain level.

In bistatic MIMO radar, we conclude that CRLB can be achieved by the proposed algorithms in this work. Reduced complexity algorithms provide performance near to CRLB but the complexity is shown to be low due to reduction in search dimensions. The reduced dimension algorithms show remarkable performance and exhibits near optimal performance by achieving CRLB, especially in single target case. For multiple target case, the performance is still better than latest published algorithms. The computational time for the one-dimensional search algorithm was the lowest.

The algorithms proposed for bistatic radar has the condition on its covariance matrix that it must be full rank. This condition is addressed using RLS where the problem of DOA is addressed with rank deficient covariance matrix.

6.2 Future Work

Some parts that have some extended work are:

- The CS algorithms has some limitations with structured matrices. Since in most radar problems, the transformation matrix has Vandermonde structure, they are not suitable candidates for radar problems. The main reason of this limitation is the coherence among the columns of the sensing matrix.
- The bistatic radar model suffers from synchronization issues. This factor

needs to be incorporated in the radar model.

- The proposed model needs to be tested for strong interference and jamming conditions. Also colored noise model can be added.
- The proposed model assumes isotropic antenna elements. These model can be extended to more realistic non-isotropic/directional antenna models.
- The bistatic algorithms proposed depend on the inversion of covariance matrix of the received snapshots. If the covariance matrix is ill-conditioned or rank deficient, the proposed algorithm will not work.
- More investigation is required for the use of regularized least-squares in radar problems.

REFERENCES

- [1] D. Bliss and K. Forsythe, “Multiple-input multiple-output (MIMO) radar and imaging: degrees of freedom and resolution,” in *Thrity-Seventh Asilomar Conf. Signals, Syst. Comput. 2003*. IEEE, pp. 54–59.
- [2] J. Li and P. Stoica, “MIMO radar diversity means superiority,” in *Proc. 14th Annu. Work. Adapt. Sens. Array Process. MIT Lincoln Lab. Lexington, MA*, 2006.
- [3] E. Fishler, A. Haimovich, R. Blum, J. Cimini, L.J., D. Chizhik, and R. Valenzuela, “Spatial diversity in radars-models and detection performance,” *IEEE Trans. Signal Process.*, vol. 54, no. 3, pp. 823–838, 2006.
- [4] J. Li and P. Stoica, “MIMO radar with colocated antennas,” *IEEE Signal Process. Mag.*, vol. 24, no. 5, pp. 106–114, Sep. 2007.
- [5] A. Haimovich, R. Blum, and L. Cimini, “MIMO radar with widely separated antennas,” *IEEE Signal Process. Mag.*, vol. 25, no. 1, pp. 116–129, 2008.

- [6] P. Stoica, "Target detection and parameter estimation for MIMO radar systems," *IEEE Trans. Aerosp. Electron. Syst.*, vol. 44, no. 3, pp. 927–939, Jul. 2008.
- [7] J. Li and P. Stoica, *MIMO Radar Signal Processing*. John Wiley & Sons, 2009.
- [8] J. Capon, "High-resolution frequency-wavenumber spectrum analysis," *Proc. IEEE*, vol. 57, no. 8, pp. 1408–1418, 1969.
- [9] P. Stoica, "An adaptive filtering approach to spectral estimation and SAR imaging," *IEEE Trans. Signal Process.*, vol. 44, no. 6, pp. 1469–1484, Jun. 1996.
- [10] A. Jakobsson and P. Stoica, "Combining Capon and APES for estimation of spectral lines," *Circuits, Syst. Signal Process.*, vol. 19, no. 2, pp. 159–169, 2000.
- [11] P. Stoica, "A diagonal growth curve model and some signal-processing applications," *IEEE Trans. Signal Process.*, vol. 54, no. 9, pp. 3363–3371, Sep. 2006.
- [12] W. Roberts, P. Stoica, J. Li, T. Yardibi, and F. A. Sadjadi, "Iterative adaptive approaches to mimo radar imaging," *IEEE J. Sel. Top. Signal Process.*, vol. 4, no. 1, pp. 5–20, Feb. 2010.

- [13] G.-o. Glentis and A. Jakobsson, “Efficient implementation of iterative adaptive approach spectral estimation techniques,” *IEEE Trans. Signal Process.*, vol. 59, no. 9, pp. 4154–4167, Sep. 2011.
- [14] J. Scheer and W. Holm, *Principles of Modern Radar: Advanced Techniques*. Edison, NJ, USA: SciTech Publishing, 2013.
- [15] J. Lipor, S. Ahmed, and M. S. Alouini, “Fourier-based transmit beampattern design using MIMO radar,” *IEEE Trans. Signal Process.*, vol. 62, no. 9, pp. 2226–2235, May 2014.
- [16] S. Ahmed and M.-S. Alouini, “MIMO radar transmit beampattern design without synthesising the covariance matrix,” *IEEE Trans. Signal Process.*, vol. 62, no. 9, pp. 2278–2289, May 2014.
- [17] S. Jardak, S. Ahmed, and M.-S. Alouini, “Low complexity joint estimation of reflection coefficient, spatial location, and Doppler shift for MIMO-radar by exploiting 2D-FFT,” in *2014 Int. Radar Conf.* IEEE, Oct. 2014, pp. 1–5.
- [18] ———, “Low complexity parameter estimation for off-the-grid targets,” in *2015 Sens. Signal Process. Def.*, no. 1. IEEE, Sep. 2015, pp. 1–5.
- [19] R. Roy and T. Kailath, “ESPRIT-estimation of signal parameters via rotational invariance techniques,” *IEEE Trans. Acoust.*, vol. 37, no. 7, pp. 984–995, Jul. 1989.
- [20] C. Duofang, C. Baixiao, and Q. Guodong, “Angle estimation using ESPRIT in MIMO radar,” *Electron. Lett.*, vol. 44, no. 12, p. 770, 2008.

- [21] C. Jinli, G. Hong, and S. Weimin, "Angle estimation using ESPRIT without pairing in MIMO radar," *Electron. Lett.*, vol. 44, no. 24, pp. 1422–1423, 2008.
- [22] M. Jin, G. Liao, and J. Li, "Joint DOD and DOA estimation for bistatic MIMO radar," *Signal Processing*, vol. 89, no. 2, pp. 244–251, Feb. 2009.
- [23] J. Chen, H. Gu, and W. Su, "A new method for joint DOD and DOA estimation in bistatic MIMO radar," *Signal Processing*, vol. 90, no. 2, pp. 714–718, Feb. 2010.
- [24] X. Zhang, L. Xu, and D. Xu, "Direction of departure (DOD) and direction of arrival (DOA) estimation in MIMO radar with reduced-dimension MUSIC," *IEEE Commun. Lett.*, vol. 14, no. 12, pp. 1161–1163, Dec. 2010.
- [25] M. L. Bencheikh, Y. Wang, and H. He, "Polynomial root finding technique for joint DOA DOD estimation in bistatic MIMO radar," *Signal Processing*, vol. 90, no. 9, pp. 2723–2730, Sep. 2010.
- [26] X. Liu and G. Liao, "Reduced-dimensional angle estimation in bistatic MIMO radar system," in *Proc. IEEE CIE Int. Conf. Radar*, Oct. 2011, pp. 67–70.
- [27] J. Wang, "Angle estimation of coherent targets for bistatic MIMO radar," in *Proc. IEEE CIE Int. Conf. Radar*, no. 2, Oct. 2011, pp. 989–992.
- [28] H. Yan, J. Li, and G. Liao, "Multitarget identification and localization using bistatic MIMO radar systems," *EURASIP J. Adv. Signal Process.*, vol. 2008, no. ID 283483, 2008.

- [29] R. Xie, Z. Liu, and J.-x. Wu, “Direction finding with automatic pairing for bistatic MIMO radar,” *Signal Processing*, vol. 92, no. 1, pp. 198–203, Jan. 2012.
- [30] W. Wang, X. Wang, and X. Li, “Propagator method for angle estimation of non-circular sources in bistatic MIMO radar,” in *IEEE Radar Conf.*, Apr. 2013, pp. 1–5.
- [31] B. Tang, J. Tang, Y. Zhang, and Z. Zheng, “Maximum likelihood estimation of DOD and DOA for bistatic MIMO radar,” *Signal Processing*, vol. 93, no. 5, pp. 1349–1357, May 2013.
- [32] T. Q. Xia, “Joint diagonalization based DOD and DOA estimation for bistatic MIMO radar,” *Signal Processing*, vol. 108, pp. 159–166, Mar. 2015.
- [33] J. Li and X. Zhang, “Improved joint DOD and DOA estimation for MIMO array with velocity receive sensors,” *IEEE Signal Process. Lett.*, vol. 18, no. 12, pp. 717–720, Dec. 2011.
- [34] J. He, M. N. S. Swamy, and M. O. Ahmad, “Joint DOD and DOA estimation for mimo array with velocity receive sensors,” *IEEE Signal Process. Lett.*, vol. 18, no. 7, pp. 399–402, Jul. 2011.
- [35] B. Yao, W. Wang, and Q. Yin, “DOD and DOA estimation in bistatic non-uniform multiple-input multiple-output radar systems,” *IEEE Commun. Lett.*, vol. 16, no. 11, pp. 1796–1799, Nov. 2012.

- [36] W. Shi, J. Huang, C. He, and J. Han, “Joint direction-of-departure and direction-of-arrival estimation in MIMO array,” in *IEEE Int. Conf. IEEE Reg. 10 (TENCON 2013)*, Oct. 2013, pp. 1–4.
- [37] Y. Cheng, H. Gu, and W. Su, “Joint 4-D angle and Doppler shift estimation via tensor decomposition for MIMO array,” *Commun. Lett. IEEE*, vol. 16, no. 6, pp. 917–920, 2012.
- [38] D. Donoho, “Compressed sensing,” *IEEE Trans. Inf. Theory*, vol. 52, no. 4, pp. 1289–1306, Apr. 2006.
- [39] E. J. Candes and P. A. Randall, “Highly robust error borrection by convex programming,” *IEEE Trans. Inf. Theory*, vol. 54, no. 7, pp. 2829–2840, Jul. 2008.
- [40] Y. Pati, R. Rezaiifar, and P. Krishnaprasad, “Orthogonal matching pursuit: recursive function approximation with applications to wavelet decomposition,” in *Proc. 27th Asilomar Conf. Signals, Syst. Comput.* IEEE Comput. Soc. Press, 1993, pp. 40–44.
- [41] D. Needell and R. Vershynin, “Uniform uncertainty principle and signal recovery via regularized orthogonal matching pursuit,” *Found. Comput. Math.*, vol. 9, no. 3, pp. 317–334, Jun. 2008.
- [42] D. Donoho, Y. Tsaig, I. Drori, and J.-L. Starck, “Sparse solution of under-determined systems of linear equations by stagewise orthogonal matching pursuit,” *IEEE Trans. Inf. Theory*, vol. 58, no. 2, pp. 1094–1121, Feb. 2012.

- [43] D. Needell and J. Tropp, “Cosamp: Iterative signal recovery from incomplete and inaccurate samples,” *Appl. Comput. Harmon. Anal.*, vol. 26, no. 3, pp. 301–321, May 2009.
- [44] M. Tipping, “Sparse bayesian learning and the relevance vector machine,” *J. Mach. Learn. Res.*, vol. 1, 2001.
- [45] S. Ji, Y. Xue, and L. Carin, “Bayesian compressive sensing,” *IEEE Trans. Signal Process.*, vol. 56, no. 6, pp. 2346–2356, Jun. 2008.
- [46] P. Schniter, L. Potter, and J. Ziniel, “Fast Bayesian matching pursuit,” in *2008 Inf. Theory Appl. Work.* IEEE, Jan. 2008, pp. 326–333.
- [47] A. Quadeer and T. Al-Naffouri, “Structure-based Bayesian sparse reconstruction,” *IEEE Trans. Signal Process.*, vol. 60, no. 12, pp. 6354–6367, Dec. 2012.
- [48] M. Masood and T. Al-Naffouri, “Sparse reconstruction using distribution agnostic Bayesian matching pursuit,” *IEEE Trans. Signal Process.*, vol. 61, no. 21, pp. 5298–5309, Nov. 2013.
- [49] E. Candès and C. Fernandez-Granda, “Super-resolution from noisy data,” *J. Fourier Anal. Appl.*, vol. 19, no. 6, pp. 1229–1254, Aug. 2013.
- [50] G. Tang, B. Bhaskar, P. Shah, and B. Recht, “Compressed sensing off the grid,” *IEEE Trans. Inf. Theory*, vol. 59, no. 11, pp. 7465–7490, Nov. 2013.

- [51] E. Candès and C. Fernandez-Granda, “Towards a mathematical theory of super-resolution,” *Commun. Pure Appl. Math.*, vol. 67, no. 6, pp. 906–956, Jun. 2014.
- [52] K. Mishra, M. Cho, A. Kruger, and W. Xu, “Off-the-grid spectral compressed sensing with prior information,” in *2014 IEEE Int. Conf. Acoust. Speech Signal Process.* IEEE, May 2014, pp. 1010–1014.
- [53] —, “Super-resolution line spectrum estimation with block priors,” *arXiv Prepr. arXiv1404.7041*, 2014.
- [54] Z. Yang and L. Xie, “Continuous compressed sensing with a single or multiple measurement vectors,” in *arXiv Prepr. arXiv1405.6544*, 2014, pp. 2–5.
- [55] J. Ender, “On compressive sensing applied to radar,” *Signal Processing*, vol. 90, no. 5, pp. 1402–1414, May 2010.
- [56] Y. Yu, A. Petropulu, and H. Poor, “MIMO radar using compressive sampling,” *IEEE J. Sel. Top. Signal Process.*, vol. 4, no. 1, pp. 146–163, Feb. 2010.
- [57] P. Stoica, P. Babu, and J. Li, “SPICE: a sparse covariance-based estimation method for array processing,” *IEEE Trans. Signal Process.*, vol. 59, no. 2, pp. 629–638, Feb. 2011.
- [58] M. Rossi, A. M. Haimovich, and Y. C. Eldar, “Spatial compressive sensing for MIMO radar,” *IEEE Trans. Signal Process.*, vol. 62, no. 2, pp. 419–430, Jan. 2014.

- [59] Z. Tan, Y. C. Eldar, and A. Nehorai, “Direction of arrival estimation using co-prime arrays: A super resolution viewpoint,” *IEEE Trans. Signal Process.*, vol. 62, no. 21, pp. 5565–5576, Nov. 2014.
- [60] L. Hu, Z. Shi, J. Zhou, and Q. Fu, “Compressed sensing of complex sinusoids: An approach based on dictionary refinement,” *IEEE Trans. Signal Process.*, vol. 60, no. 7, pp. 3809–3822, Jul. 2012.
- [61] J. Fang, J. Li, Y. Shen, H. Li, S. Member, and S. Li, “Super-resolution compressed sensing: An iterative reweighted algorithm for joint parameter learning and sparse signal recovery,” *IEEE Signal Process. Lett.*, vol. 21, no. 6, pp. 761–765, Jun. 2014.
- [62] N. Rao, P. Shah, S. Wright, and R. Nowak, “A greedy forward-backward algorithm for atomic norm constrained minimization,” in *2013 IEEE Int. Conf. Acoust. Speech Signal Process.* IEEE, May 2013, pp. 5885–5889.
- [63] O. Teke, A. C. Gurbuz, and O. Arikan, “A robust compressive sensing based technique for reconstruction of sparse radar scenes,” *Digit. Signal Process.*, vol. 27, pp. 23–32, Apr. 2014.
- [64] Z. Yang, L. Xie, and C. Zhang, “Off-grid direction of arrival estimation using sparse Bayesian inference,” *IEEE Trans. Signal Process.*, vol. 61, no. 1, pp. 38–43, Jan. 2013.

- [65] Y. Yu, S. Sun, R. N. Madan, and A. Petropulu, “Power allocation and waveform design for the compressive sensing based MIMO radar,” *IEEE Trans. Aerosp. Electron. Syst.*, vol. 50, no. 2, pp. 898–909, Apr. 2014.
- [66] T. Huang, Y. Liu, H. Meng, and X. Wang, “Adaptive matching pursuit with constrained total least squares,” *EURASIP J. Adv. Signal Process.*, vol. 2012, no. 1, p. 252, Dec. 2012.
- [67] K. V. Mishra, M. Cho, A. Kruger, and W. Xu, “Spectral super-resolution with prior knowledge,” *IEEE Trans. Signal Process.*, vol. 63, no. 20, pp. 5342–5357, Oct. 2015.
- [68] E. J. Candès, J. K. Romberg, and T. Tao, “Stable signal recovery from incomplete and inaccurate measurements,” *Commun. Pure Appl. Math.*, vol. 59, no. 8, pp. 1207–1223, Aug. 2006.
- [69] H. Jiang, J.-K. Zhang, and K. M. Wong, “Joint DOD and DOA estimation for bistatic MIMO radar in unknown correlated noise,” *IEEE Trans. Veh. Technol.*, vol. 64, no. 11, pp. 5113–5125, Nov. 2015.
- [70] E. Candes and T. Tao, “Decoding by linear programming,” *IEEE Trans. Inf. Theory*, vol. 51, no. 12, pp. 4203–4215, Dec. 2005.
- [71] N. Yu and Y. Li, “Deterministic construction of fourier-based compressed sensing matrices using an almost difference set,” *EURASIP J. Adv. Signal Process.*, vol. 2013, no. 1, p. 155, 2013.

- [72] H. Ali, S. Ahmed, T. Al-Naffouri, and M.-S. Alouini, “Reduction of snapshots for MIMO radar detection by block/group orthogonal matching pursuit,” in *Int. Radar Conf.*, 2014, pp. 1–4.
- [73] M. Masood and T. Al-Naffouri, “Support agnostic Bayesian matching pursuit for block sparse signals,” in *2013 IEEE Int. Conf. Acoust. Speech Signal Process.* IEEE, May 2013, pp. 4643–4647.
- [74] D. L. Donoho and M. Elad, “Optimally sparse representation in general (nonorthogonal) dictionaries via ℓ_1 minimization,” *Proc. Natl. Acad. Sci.*, vol. 100, no. 5, pp. 2197–2202, Mar. 2003.
- [75] R. Gribonval and M. Nielsen, “Sparse representations in unions of bases,” *IEEE Trans. Inf. Theory*, vol. 49, no. 12, pp. 3320–3325, Dec. 2003.
- [76] P. Stoica and R. Moses, *Spectral Analysis of Signals*. Upper Saddle River, NJ, USA: Prentice-Hall, Inc., 2005.
- [77] R. G. Baraniuk, V. Cevher, M. F. Duarte, and C. Hegde, “Model-based compressive sensing,” *IEEE Trans. Inf. Theory*, vol. 56, no. 4, pp. 1982–2001, Apr. 2010.
- [78] S. Fortunati, R. Grasso, F. Gini, M. S. Greco, and K. LePage, “Single-snapshot DOA estimation by using compressed sensing,” *EURASIP J. Adv. Signal Process.*, vol. 2014, no. 1, p. 120, 2014.

- [79] M. S. Davis, G. A. Showman, and A. D. Lanterman, “Coherent MIMO radar: The phased array and orthogonal waveforms,” *IEEE Aerosp. Electron. Syst. Mag.*, vol. 29, no. 8, pp. 76–91, 2014.
- [80] X. Gao, X. Zhang, G. Feng, Z. Wang, and D. Xu, “On the MUSIC-derived approaches of angle estimation for bistatic MIMO radar,” in *2009 Int. Conf. Wirel. Networks Inf. Syst.* IEEE, Dec. 2009, pp. 343–346.
- [81] D. Nion and N. D. Sidiropoulos, “A PARAFAC-based technique for detection and localization of multiple targets in a MIMO radar system,” in *2009 IEEE Int. Conf. Acoust. Speech Signal Process.* IEEE, Apr. 2009, pp. 2077–2080.
- [82] X. Zhang, Z. Xu, L. Xu, and D. Xu, “Trilinear decomposition-based transmit angle and receive angle estimation for multiple-input multiple-output radar,” *Radar, Sonar Navig. IET*, vol. 5, no. 6, pp. 626–631, 2011.
- [83] Z. Zheng and J. Zhang, “Fast method for multi-target localisation in bistatic MIMO radar,” *Electron. Lett.*, vol. 47, no. 2, p. 138, 2011.
- [84] C. Yunhe, “Joint estimation of angle and Doppler frequency for bistatic MIMO radar,” *Electron. Lett.*, vol. 46, no. 2, p. 170, 2010.
- [85] D. Nion and N. D. Sidiropoulos, “Tensor algebra and multidimensional harmonic retrieval in signal processing for MIMO radar,” *IEEE Trans. Signal Process.*, vol. 58, no. 11, pp. 5693–5705, 2010.
- [86] H. Ali, S. Ahmed, T. Y. Al-Naffouri, and M.-S. Alouini, “Reduced complexity FFT-based DOA and DOD estimation for moving target in bistatic MIMO

- radar,” in *2016 IEEE Int. Conf. Acoust. Speech Signal Process.* IEEE, Mar. 2016, pp. 3021–3025.
- [87] B. Friedlander, “On signal models for MIMO radar,” *IEEE Trans. Aerosp. Electron. Syst.*, vol. 48, no. 4, pp. 3655–3660, 2012.
- [88] H. L. Van Trees, *Optimum Array Processing*. New York, USA: John Wiley & Sons, Inc., Mar. 2002.
- [89] J. Li and X. Zhang, “Sparse representation-based joint angle and Doppler frequency estimation for MIMO radar,” *Multidimens. Syst. Signal Process.*, vol. 26, no. 1, pp. 179–192, Jan. 2015.
- [90] S. Yang, Y. Li, K. Zhang, and W. Tang, “Multiple-parameter estimation method based on spatio-temporal 2-D processing for bistatic MIMO radar,” *Sensors*, vol. 15, no. 12, pp. 31 442–31 452, 2015.
- [91] P. Stoica, “A new derivation of the APES filter,” *IEEE Signal Process. Lett.*, vol. 6, no. 8, pp. 205–206, Aug. 1999.
- [92] R. O. Schmidt, “Multiple emitter location and signal parameter estimation,” *IEEE Trans. Antennas Propag.*, vol. 34, no. 3, pp. 276–280, Mar. 1986.
- [93] A. Barabell, “Improving the resolution performance of eigenstructure-based direction-finding algorithms,” in *ICASSP ’83. IEEE Int. Conf. Acoust. Speech, Signal Process.*, vol. 8. Institute of Electrical and Electronics Engineers, 1983, pp. 336–339.

- [94] P. C. Hansen and D. P. O’Leary, “The use of the L-curve in the regularization of discrete ill-posed problems,” *SIAM J. Sci. Comput.*, vol. 14, no. 6, pp. 1487–1503, Nov. 1993.
- [95] P. C. Hansen, M. E. Kilmer, and R. H. Kjeldsen, “Exploiting residual information in the parameter choice for discrete ill-posed problems,” *BIT Numer. Math.*, vol. 46, no. 1, pp. 41–59, Mar. 2006.
- [96] M. Suliman, T. Ballal, and T. Y. Al-Naffouri, “Perturbation-based regularization for signal estimation in linear discrete ill-posed problems,” *CoRR*, vol. 1611.09742, Nov. 2016.
- [97] A. H. Sayed, *Adaptive Filters*. Hoboken, NJ, USA: John Wiley & Sons, Inc., Mar. 2008.
- [98] P. C. Hansen, “Regularization tools – a Matlab package for analysis and solution of discrete ill-posed problems,” *Numer. Algorithms*, vol. 6, no. March, pp. 1–35, 1998.

Vitae

- Hussain Ali
- Nationality: Pakistani
- Current Address: P.O. Box 8247, King Fahd University of Petroleum and Minerals, Dhahran 31261, Saudi Arabia.
- Permanent Address: House 5, Block 8, Shah Faisal Colony, Chaklala, Rawalpindi, Pakistan.
- Telephone: (+966) 501 694 872
- Email: *hussainali85@gmail.com*
- Received Bachelor of Engineering (B.E.) in Electrical (Telecommunications) Engineering from Military College of Signals, National University of Sciences & Technology, Rawalpindi, Pakistan in 2007.
- Received M.S. in Telecommunication Engineering from King Fahd University of Petroleum and Minerals, Dhahran, Saudi Arabia in December 2012.
- Completed Ph.D. in Electrical Engineering from King Fahd University of Petroleum and Minerals, Dhahran, Saudi Arabia in December 2017.

LIST OF PUBLICATIONS

- H. Ali, S. Ahmed, T. Y. Al-Naffouri, M. S. Sharawi, and M.-S. Alouini, “Target parameter estimation for spatial and temporal formulations in MIMO radars using compressive sensing,” *EURASIP J. Adv. Signal Process.*, vol. 2017, no. 1, pp. 1–11, 2017.
- H. Ali, S. Ahmed, T. Y. Al-Naffouri and M. S. Alouini, “Reduced complexity FFT-based DOA and DOD estimation for moving target in bistatic MIMO radar,” 2016 IEEE International Conference on Acoustics, Speech and Signal Processing (ICASSP), Shanghai, 2016, pp. 3021–3025.
- H. Ali, S. Ahmed T. Y. Al-Naffouri and S. Alouini, “Reduction of Snapshots for MIMO radar detection by Block/Group Orthogonal Matching Pursuit,” International Radar Conference 2014, Lille, France, 13–17 October 2014.